JOURNAL OF MATERIALS SCIENCE 28 (1993) 569–610

Fibre–matrix adhesion and its relationship to composite mechanical properties

L. T. DRZAL
Composite Materials and Structures Center, Michigan State University, East Lansing, MI, 48824, USA

M. MADHUKAR
Department of Engineering Science and Mechanics, The University of Tennessee, Knoxville, TN 37996, USA

Two major areas of enquiry exist in the field of fibre–matrix adhesion in composite materials. One is the fundamental role that fibre–matrix adhesion plays on composite mechanical properties. The other is what is the "best" method used to measure fibre–matrix adhesion in composite materials. Results of an attempt to provide an experimental foundation for both areas are reported here. A well-characterized experimental system consisting of an epoxy matrix and carbon fibres was selected in which only the fibre surface chemistry was altered to produce three different degrees of adhesion. Embedded single-fibre fragmentation tests were conducted to quantify the level of fibre–matrix adhesion. Observation of the events occurring at the fibre breaks led to the documentation of three distinct failure modes coincident with the three levels of adhesion. The lowest level produced a frictional debonding, the intermediate level produced interfacial crack growth and the highest level produced radial matrix fracture. High fibre volume fraction composites made from the same material were tested for on- and off-axis, as well as fracture, properties. Results indicate that composite results can be explained if both differences in adhesion and failure mode are considered. It will be further demonstrated that fibre–matrix adhesion is an "optimum" condition which has to be selected for the stress state that the interface will experience. The embedded single-fibre fragmentation test is both a valuable measurement tool for quantifying fibre–matrix adhesion as well as the one method which provides fundamental information about the failure mode necessary for understanding the role of adhesion on composite mechanical properties.

1. Background

As composite materials have moved to the forefront of activity in the materials community in the last two decades, there has been an increasing interest in being able to understand the physical and chemical mechanisms responsible for fibre–matrix adhesion as well as the role of fibre–matrix adhesion on composite properties. Early mechanical analyses have shown that when composites are fabricated and the applied load is coincident with the fibre direction, a simple rule of mixtures expression can be used to predict composite properties from the properties of the constituents. The resulting model has limited utility in practice because structural applications for composite materials rarely allow for the applied loads to be in the fibre direction only. There is almost always a component of the structural loads that is in a direction at an angle to the fibre axis. In these situations, fibre–matrix adhesion is important to ensure that a maximum stress level can be maintained across the interface and from fibre to matrix without disruption. At less than optimum levels of adhesion, the load-bearing capacity of the composite has to be reduced to compensate for the reduced adhesion at the interface or the structural component has to be increased in size by increasing ply thickness. Either option is undesirable because it negates a significant portion of the weight and cost advantage of the composite structural component over an equivalent monolithic material.

Most early work on the development of composite materials considered fibre–matrix adhesion to be a necessary condition to ensure good composite properties. The majority of effort was concentrated on increasing fibre–matrix adhesion through the use of surface treatments and coatings. The patent literature on carbon-fibre surface treatments and a large portion of the silane literature on finishes for glass fibres contain descriptions of processes for improving fibre–matrix adhesion.

It is very desirable to have a testing method to measure the adhesion between fibre and matrix which can provide a reproducible, reliable method for investigating and measuring fibre–matrix adhesion. Composite testing of unidirectional composite specimens with loads applied to place the fibre–matrix interface under shear or under a tensile load perpendicular to the fibre axis were commonly used methods. Because the majority of early composite research was

0022–2461

done on glass fibres, these approaches were satisfactory from an engineering sense. However, once different reinforcing fibres (e.g. carbon and boron fibres, polymeric fibres and different glass fibres) were introduced, fabrication of large samples of composites made from experimental runs of new materials tended to be costly.

Several testing methods were developed for measuring fibre–matrix adhesion using single fibres or groups of fibres. The goal was to measure fibre–matrix adhesion in a way that would be a predictor of composite fibre–matrix adhesion, as well as to understand the fundamental physics and chemistry of adhesion itself. Although there has been a wide variety of methods proposed in recent years, most can be reduced to three basic measurement methods. They are fibre pull-out methods, fibre fragmentation methods, and fibre micro-compression methods [1].

In the pull-out experiments, one end of a single fibre is embedded in a block of matrix (Fig. 1). The free end is gripped and an increasing load is applied as the fibre is pulled out of the matrix while the load and displacement are measured. The maximum load, F, measured before detachment of the fibre from the matrix is related to the average value of the fibre–matrix shear strength, τ, through the equation.

$$F = \tau \pi l d \quad (1)$$

where πd is the fibre circumference and l is the embedded length. In principle, this is a direct measurement method, but closer inspection shows that the state of stress at the juncture of the fibre and the matrix creates a normal tensile interfacial force not encountered in an actual composite. The normal tensile force can act on the interface to reduce the measured shear strength. If the length of fibre embedded in the block of matrix is longer than the critical transfer length for that fibre–matrix combination, the fibre will fracture within the block. This requires the fabrication of thin discs of matrix or very precise control of the depth of the fibre end, because fibre length to diameter ratios of 50–100 are typical. For 10 μm diameter fibres, this means that the matrix thickness or fibre-end location in a matrix block must not exceed 500 μm to avoid fibre fracture. Recent developments have been made to overcome this fabrication difficulty by advocating the use of microdroplets less than 500 μm in size [2] or by using half-droplets formed on surfaces [3].

An alternative single-fibre method relies on using the shear stress transfer process to produce fragmentation in a continuous fibre (Fig. 2). In this technique, the fibre is totally encapsulated in a matrix coupon, a tensile load is applied to the coupon, and an interfacial shear stress-transfer mechanism is relied upon to transfer the coupon tensile forces to the encapsulated fibre through the interface [4]. As the load is increased on the specimen, shear forces are transmitted to the fibre along the interface. The fibre tensile stress increases to the point where the fracture strength, σ_f, is exceeded and the fibre breaks inside the matrix. This fragmentation process is repeated as the sample strain is increased producing shorter and shorter fibre fragments within the coupon until the remaining fragment lengths are no longer sufficient in size to produce further fracture through this stress-transfer mechanism. The final fibre fragment length-to-diameter ratio, l/d, is measured. A shear-lag analysis is conducted on the fragments in order to calculate an interfacial shear strength, τ.

$$\tau = \left(\frac{\sigma_f}{2}\right)\left(\frac{d}{l_c}\right) \quad (2)$$

In practice, there is a distribution of critical lengths and Weibull statistics are used to fit the data as shown

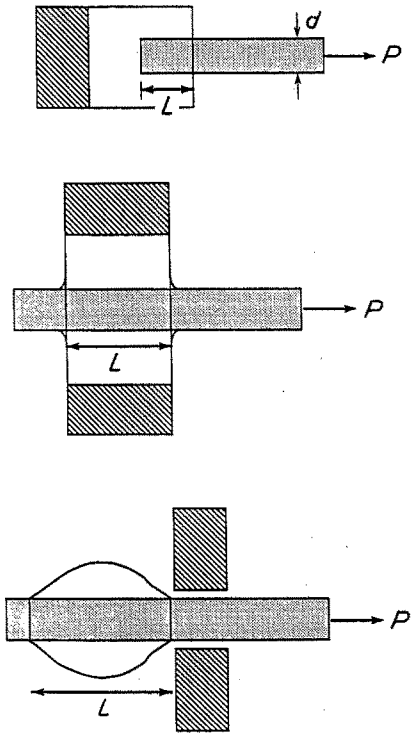

$$\tau = \frac{\sigma_f}{2}\frac{d}{l_c}$$

Advantages

Any reinforcing fibre may be used
Any matrix may be used
Direct measurement of load

Disadvantages

Embedment length is important
External meniscus is important
Clamping of the disc is important
Must be able to grip the fibre mechanically
State of stress at the exit creates a tensile interfacial force
No information about failure mode
Interface may not be the same as composite interface
1–3 data points per specimen

Figure 1 Schematic diagram of the single-fibre pull-out method for measuring fibre–matrix adhesion.

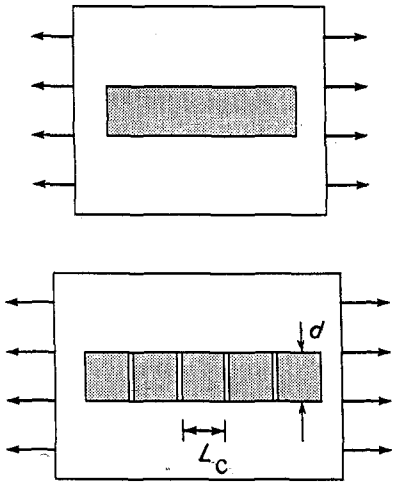

Advantages

State of stress is similar to that in the composite
Many data points with few specimens
Sensitive to interfacial conditions
Considers the interfacial shear strength as being composed of a fibre surface and interface component
Direct observation of interfacial events
Qualitative assessment of the stresses and failure modes

Disadvantages

Samples are time-consuming to prepare
Samples are not actual composites
Requires assumptions about materials
Requires assumptions about state of stress
Need fibre strength-length data to avoid misinterpretation
Matrix $\varepsilon_f > 3 \times$ fibre ε_f
Matrix fracture toughness

Figure 2 Schematic diagram of the single-fibre critical length method for measuring fibre–matrix adhesion.

$$\tau = \left(\frac{\sigma_f}{2\beta}\right)\Gamma\left(1 - \frac{1}{\alpha}\right) \quad (3)$$

where α and β are the scale and shape parameters from the Weibull distribution, Γ is the gamma function and the other terms have the same meaning as before. Although this method assumes that the interfacial stresses are uniform along the fibre length, the state of stress produced on the fibre does closely resemble the state of stress encountered in a high fibre volume fraction composite. Poisson's effect on the matrix coupon also serves to introduce a net compressive interfacial state of stress.

The embedded single-fibre technique also has one significant advantage. The failure process itself can be observed in transmitted polarized light (i.e. frictional debonding, interfacial crack growth parallel to the fibre–matrix interface and matrix crack growth perpendicular to the fibre axis) and the locus of failure can be identified while the process replicates the *in situ* events in the actual composite itself. A limitation is that the strain to failure of the matrix must exceed that of the fibre by at least a factor of three. A transparent matrix is very useful for the *in situ* observation of the fragment lengths as well as the failure modes but recent developments in acoustic emission have shown that this is no longer a limitation [5].

Both single-fibre methods discussed are specially fabricated for each test. The desire to conduct a measurement on an actual composite has given rise to the microindentation method (Fig. 3) [6]. Here a high fibre volume fraction composite is sectioned perpendicular to the fibre axis and a probe approximately 75% of the fibre diameter is placed on the end of a single fibre and a force is applied. Upon detection of debonding, the applied force is recorded and the interfacial shear strength is calculated. Several questions still remain as to the nature of the events taking place below the fibre surface and how they influence the measured debonding force.

A recent review contains a detailed literature survey of different single-fibre methods and a comparison of the assumptions and limitations which are inherent in each one [1]. In addition, numerous other papers included in this volume go into details of each of the methods.

The ultimate purpose of this research was to deduce the mechanisms and principles responsible for fibre–matrix adhesion. Achievement of this goal required that a sensitive, reproducible method must be used for measuring fibre–matrix adhesion and the relationship between the interfacial properties measured by this method with actual composite properties must be shown. The single embedded fibre fragmentation test was selected for evaluation of fibre–matrix adhesion in this experimental program because of its ability to not only measure fibre–matrix adhesion but also to identify the interfacial failure mode associated with different levels of adhesion.

2. Materials

In order to serve as the experimental system to explore the relationships between fibre–matrix adhesion, the embedded single-fibre fragmentation test method and composite mechanical properties, a carbon fibre–epoxy system was selected as a standard composite material system. One carbon fibre with three different surface treatments combined with a low-temperature

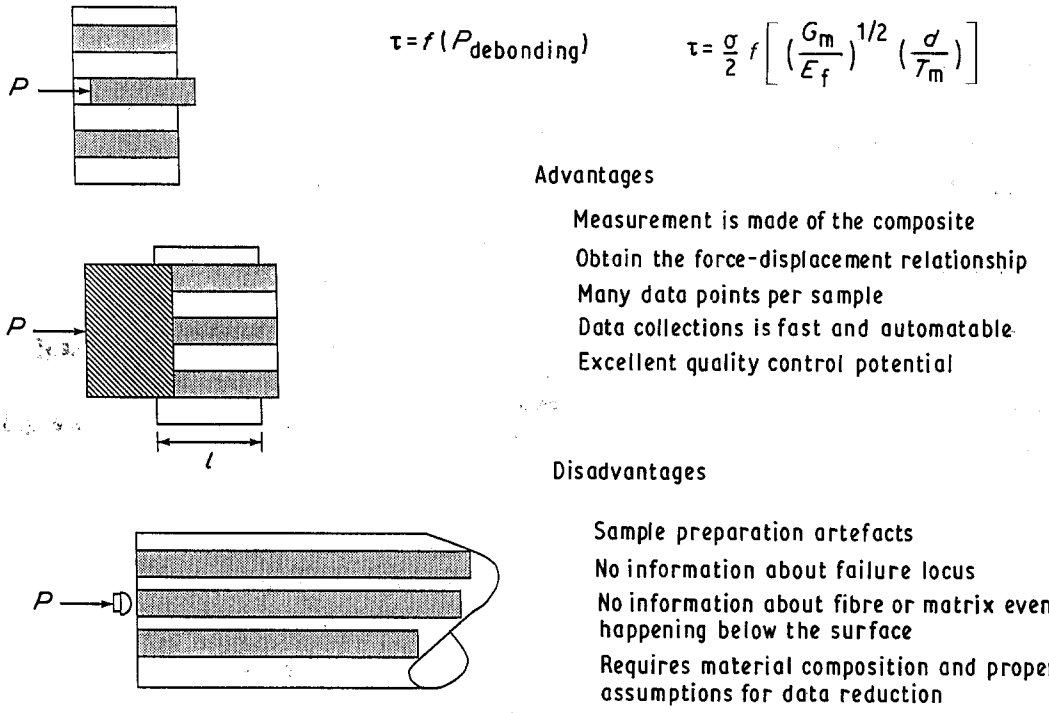

Figure 3 Schematic diagram of the micro-indentation method whereby a single fibre is compressed for measuring fibre–matrix adhesion.

amine-cured epoxy has been the object of a detailed interfacial and composite property research program.

2.1. Polymeric matrix

An epoxy–amine matrix system was selected for this study. This chemistry is representative of the majority of composite applications [7]. The reactants can be processed at low temperatures and the properties of the resultant matrix are typical for a high-performance matrix. A di-functional epoxy, diglycidyl ether of bis-phenol-A (DGEBA) at stoichiometric conditions (14.5 p.h.r. meta-phenylene diamine) was mixed, debulked and processed for 2 h at 75°C and 2 h at 125°C for both single-fibre and composite coupons.

2.2. Reinforcing fibres

The "A"-type carbon fibres used in this study were produced by high-temperature inert gas graphitization of polyacrylonitrile fibre. The resulting carbon fibre was composed of turbostratic graphitic layers which are formed into lamellar ribbons oriented nearly parallel to the fibre axis as well as varying in orientation across the fibre diameter. The surface of these fibres has seen the catastrophic molecular rearrangement associated with graphitization. Adhesion of these fibres in their untreated state to a typical amine-cured epoxy results in very low interfacial shear strength. Many surface treatments for improving the adhesion to carbon fibres have been proposed and various commercial ones are described in the patent literature [8]. The polyacrylonitrile-based carbon fibres chosen for this study were the A-4 fibres (Hercules, Inc.) having a fibre tensile modulus of about 234 GPa and tensile strength of 3.6 GPa when measured at a 25 mm gauge length. The fibres were provided with three different surface conditions. "AU4" fibres were "as-received" that is, removed from the heat treatment ovens without any further surface treatment. "AS4" fibres were surface treated with an electrochemical oxidation step which optimizes the adhesion to epoxy matrices and "AS4C" fibres were coated with a 100–200 nm layer of epoxy applied from an organic solvent directly on to the surface-treated AS-4 fibres. These fibres were circular in cross-section.

2.3. Composite specimens

Unidirectional composite prepregs were fabricated from the three batches of carbon fibres, i.e. AU-4, AS-4, and AS-4C. The impregnation was done using a hot-melt prepregger with a slit die (Research Tool Corporation). Resin temperature was maintained at 52° C (125° F) while the fibre tow was drawn through a narrow outlet die that formed a thin impregnated layer of composite that was wound on to a cylindrical mandrel at a rate of about 9 linear ft min^{-1}. Approximately 2 lb (~0.9 kg) tension was maintained on the tow during processing. Single-layer tapes of fixed fibre volume content were prepared in this manner. Sections of dimensions 279 mm × 305 mm (11 in × 12 in) were cut from the tape and manually stacked in the desired sequence for consolidation using standard autoclave techniques. The curing cycle was 0.69 MPa (100 p.s.i.) for 2 h at 75 °C (167 °F) followed by 2 h at 125 °C (257 °F). Vacuum was vented for 15 min into the 75 °C (167 °F) soak. The laminate was cooled to ambient temperature before removal from the autoclave. The composite panels made from the three fibre types were designated AU-4/Epoxy, AS-4/Epoxy, and AS-4C/Epoxy. Approximately 12.7 mm (0.5 in.) wide strips were cut from all sides of the plate and discarded. Rectangular specimens of dimensions shown

in Fig. 4, were cut from the remaining plate using a diamond-coated wheel. Cross-ply glass/epoxy end-tabs were applied using epoxy glue to those specimens that required gripping by hydraulic wedge grips.

Fibre volume fraction and void content of unidirectional specimens were determined by optical numeric volume fraction analysis (Onvfa) which is described in detail in [9]. This technique has been shown to provide results that agree with those obtained by ASTM acid digestion technique to within 2%. The Onvfa method measures the fibre volume fraction by multiplying the number of fibres per unit area in digitized microscope images of composite cross-sections by the average cross-sectional area of a single fibre. One sample from each panel was analysed and measurements were obtained by averaging 15 images per sample, each containing approximately 1500 fibres. The results are summarized in Table I.

In the case of $\pm 45°$ panels, the Onvfa method was used only to determine the void content. The fibre volume fractions of these panels were calculated from the density measurements (according to ASTM D-792 specifications) of samples from $[\pm 45]_{3s}$ panels. For calculating the fibre volume fraction from the density measurements, the following equation was used

$$\rho_c = \rho_f V_f + \rho_m(1 - V_f) \quad (4)$$

where ρ_c, ρ_f ρ_m are the densities of composite, fibre and matrix, respectively, and V_f is the volume fraction of fibres. The void content was not included in Equation 4 because it was assumed that during the immersion of samples under water for the density measurement, the water penetrated in the voids, thus the volume displaced by the specimens was the actual specimen volume minus the volume occupied by voids. Results for all the $\pm 45°$ panels are summarized in Table I.

3. Methods

The mechanical characterization test conducted in this study were 0° and 90° tension (ASTM D-3039), 0° compression (ASTM D-3410), 0° and 90° three-point flexure (ASTM D-790), $\pm 45°$ tension (ASTM D-3518) and Iosipescu shear test for in-plane shear characterization, short-beam shear test (ASTM D-2344) for interlaminar shear characterization, and double cantilever beam (DCB) and end-notched flexure (ENF) for Mode I and Mode II interlaminar fracture toughness, respectively. The geometries and dimensions of specimens are shown in Fig. 4. Cross-ply glass/epoxy end-tabs were applied to all the tension and compression specimens. Strain measurements during the tensile tests were made using strain gauges as well as a biaxial axial extensometer. The aspect ratio (span/thickness) for all the three-point flexure tests were chosen to be 60. It has been shown that as the aspect ratio increases, the apparent flexural modulus asymptotically approaches the tensile modulus.

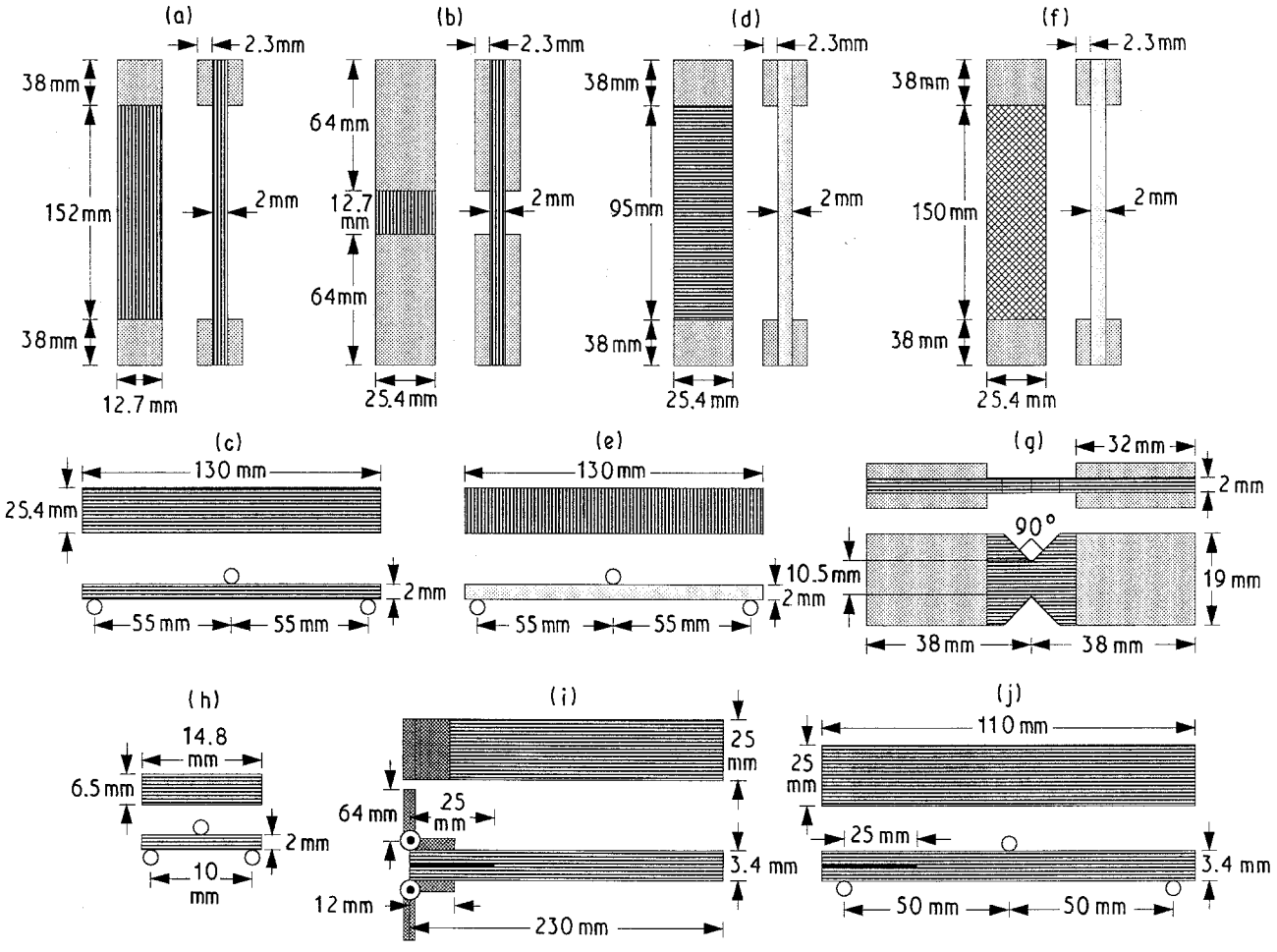

Figure 4 Geometries and dimensions of (a) $[0]_{12}$ tension, (b) $[0]_{12}$ compression, (c) $[0]_{12}$ three-point flexure, (d) $[90]_{12}$ tension, (e) $[90]_{12}$ three-point flexure, (f) $[\pm 45]_{3s}$ tension, (g) Iosipescu shear, (h) short-beam shear, (i) $[0]_{24}$ DCB, and (j) $[0]_{24}$ ENF composite specimens.

TABLE I Numerical volume fraction analysis results

Material	Lay-up	No. of panels	Fibre V_f (%)	Void V_f (%)
AU-4/Epoxy	$[0]_{12}$	6	67 ± 4	0.9 ± 0.9
AS-4/Epoxy	$[0]_{12}$	6	68 ± 6	0.4 ± 0.4
AS-4C/Epoxy	$[0]_{12}$	5	67 ± 5	1.0 ± 0.8
AU-4/Epoxy	$[\pm 45]_{3S}$	2	74 ± 2	3.6 ± 1.6
AS-4/Epoxy	$[\pm 45]_{3S}$	2	67 ± 1	1.8 ± 0.3
AS-4C/Epoxy	$[\pm 45]_{3S}$	2	69 ± 2	2.0 ± 0.1
AU-4/Epoxy	$[0]_{24}$	2	61 ± 8	0.6 ± 0.6
AS-4/Epoxy	$[0]_{24}$	2	69 ± 6	0.1 ± 0.0
AS-4C/Epoxy	$[0]_{24}$	2	68 ± 5	0.2 ± 0.0

For Kevlar and glass-fibre reinforced epoxy composites, the aspect ratio at which the flexural modulus approaches the tensile modulus has been shown to be about 60 [10]. The compression tests were conducted on an Illinois Institute of Technology Research Institute (IITRI) compression fixture. The longitudinal and compressive stress–strain curves were generated from the back-to-back strain gauges to detect specimen bending during the applied compressive loading. The data for the specimens where significant bending was observed were discarded. The Iosipescu shear tests were performed according to the procedure outlined in [11]. Glass/epoxy end tabs were applied to all the Iosipescu specimens. Untabbed specimens caused specimen crushing under the loading points resulting in shear strength values that were lower than those obtained from the tabbed specimens. The shear strain was determined from the $\pm 45°$ strain gauges that were bonded between the notch roots. The DCB and ENF testings were performed according to the procedure outlined in [12]. At least ten specimens were tested for each type of test. All the tests were performed on a closed-loop servohydraulic MTS testing machine and the data was acquired on an IBM PS/2 Model 30 computer. The fracture surfaces of failed specimens were examined using scanning electron microscopy (SEM) and the effect of fibre–matrix adhesion on the major failure modes was determined.

4. Results and discussion

4.1. Previous work

A starting point for any investigation into adhesion is an examination of the chemical and physical condition of the surface of the adherend (in this case the reinforcement) and any changes made during the surface preparation procedures.

The surface chemical and topographical features of these reinforcing fibres have been characterized using a variety of techniques and the results reported in detail elsewhere [13–15]. The fibres, whether surface-treated or untreated, have the same surface area as measured by gas adsorption. They differ in their surface chemistry primarily in the amount of surface oxygen groups and nitrogen groups present. Wettability measurements on these fibres show that the surface free energy is greater than that of the matrix ensuring thermodynamic compatibility.

It is important to determine the type and extent of chemical bonding between the matrix and the reinforcing fibre. Solid-state analysis of the actual fibre–epoxy matrix interface is impossible. However, reaction with appropriate model compounds has been very useful in defining the upper bounds on the extent of chemical interaction between fibre and matrix under normal processing conditions.

In a series of experiments, monofunctional epoxy compounds, amines and epoxy–amine adducts were dissolved in an inert aromatic solvent and placed in contact with carbon fibres under the same temperature conditions experienced in the solid-state processing of the composite [16]. Afterwards, the fibres were extracted in the pure solvent, dried and then their surface composition was determined with XPS analysis. Comparison of the carbon fibre spectra before and after this exposure to the matrix constituents confirmed that chemical adsorption had taken place (Table II). Both the epoxy group and the amine group can chemically react with the surface oxygen groups. Chemical bonding would be expected to create a stronger interaction than physical bonding. On an absolute basis less than 5% of the surface sites of the carbon fibre are involved in chemical bonding.

4.1.1. Surface Treatment

The embedded single-fibre fragmentation test was used to provide a measure of the level of fibre–matrix adhesion for this fibre–matrix combination. Table III shows the value of the interfacial shear strength from this measurement calculated according to Equation 3. There is a doubling of the interfacial shear strength with surface treatment (AS4) and a further increase with the application of the fibre finish (AS4C). The concurrent observation of the fibre photoelastic stress pattern and microtoming of the resultant interphase provide an explanation for the changes observed with surface treatment (Figs 5 and 6).

The explanation for this behaviour comes from the realization that there is a two-part process associated with the electrolytic surface anodization used with carbon fibres (Fig. 7). Not only are surface oxygens

TABLE II Per cent functional groups chemisorbed on to AS4 carbon fibre surface during thermal processing

Fibre	Epoxy	Amine	Hydroxyl
AS4	3%	3%	0%

TABLE III Properties of the fibres and matrix, interfacial shear strengths and failure modes

Material	Tensile modulus (GPa)	Tensile strength (GPa)	Interfacial shear strength (MPa)	Interfacial failure Mechanism
AU4	234.4	3.58	37.2	Poor interfacial
AS4	234.4	3.58	68.3	Moderate interfacial
AS4C	234.4	3.58	81.4	Strong matrix
Epoxy	3.6	0.09	–	–

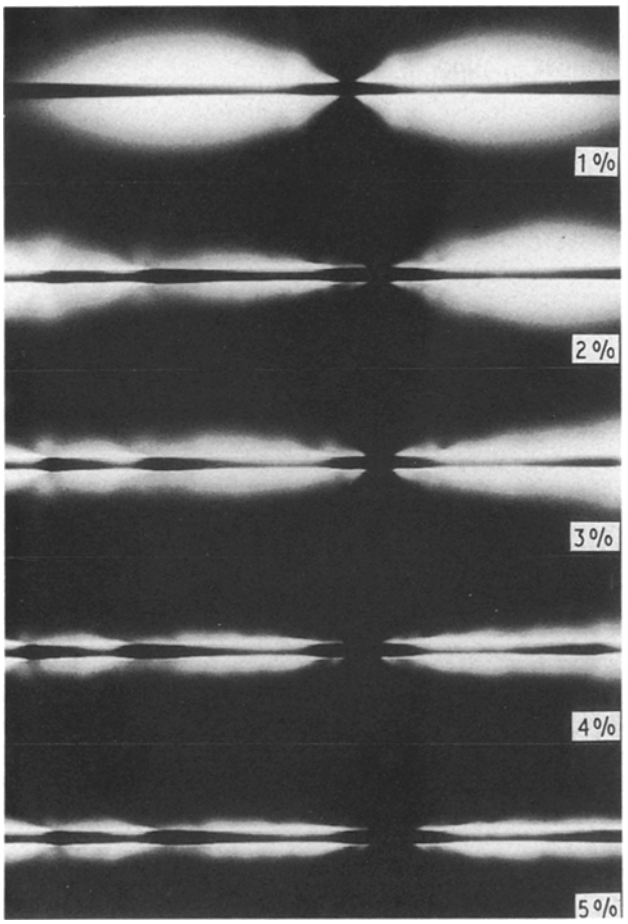

Figure 5 Transmitted polarized light micrographs of a single AU carbon fibre under increasing strain in an epoxy matrix showing the fibre break and the photoelastic stress pattern characteristic of frictional debonding ×450.

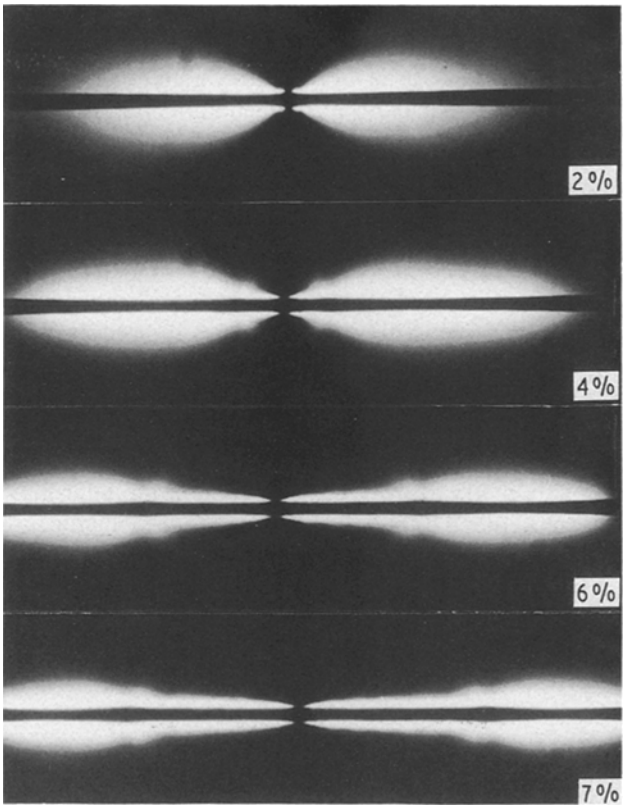

Figure 6 Transmitted polarized light micrographs of a single AS carbon fibre under increasing strain in an epoxy matrix showing the fibre break and the photoelastic stress pattern characteristic of interfacial crack growth ×450.

and other species added in the surface treatment process, but the native fibre surface that has undergone the graphitization step during the conversion of the polyacrylonitrile to graphite is removed by the surface treatment. The etching away of the native fibre surface and the addition of surface oxygen groups increase the concentration to about twice the level initially present on the fibre surface before surface treatment. Ultramicrotome sectioning and TEM examination of the failed fibre–matrix interface have detected the failure path before and after surface treatment. Failure of the "as-received" AU4 interface is through the outer layer of the carbon fibre while pure interfacial failure results after surface treatment. This result shows that the main function of the fibre surface treatment is to remove the initial defect-laden surface and leave behind a structurally sound surface, i.e. one which is capable of sustaining high mechanical loads without failure. This increase in structural integrity is responsible for the majority of the improvement in adhesion. The addition of the surface chemical oxygen groups is responsible for only 10% of the increase in adhesion.

4.1.2. Surface finishes

In addition to the use of surface treatments which are primarily chemical in nature, surface finishes or coatings are also used to affect fibre–matrix adhesion. The surface-treated carbon fibres coated with 100 nm epoxy resin without any curing agent (AS4C) were processed as usual and the level of adhesion was measured with the embedded single-fibre critical length test [15]. The level of interfacial shear stress

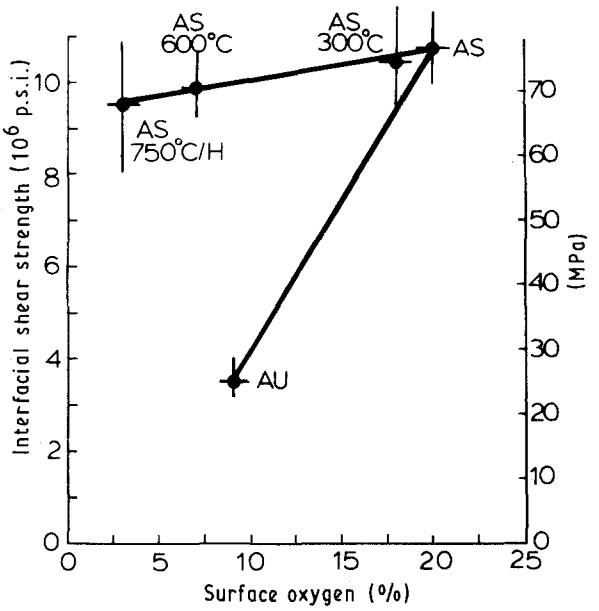

Figure 7 A plot of the single fibre interfacial shear strength against the number of oxygen groups present on a carbon fibre surface as a function of various surface treatments. AU, untreated fibre; AS, the fibre after surface treatment; AS, fibres with treatment conditions in parentheses.

that the interface could withstand increased by about 25%. The mechanism by which this surface finish increases the level of fibre–matrix adhesion as measured by the single-fibre fragmentation test is fundamentally different than the surface-treatment mechanism.

The finish layer interacts with the bulk matrix and causes a local change in properties in the fibre–matrix interphase. The properties of this *in situ* finish layer itself are imparted to the interphase and can control adhesion. Because the local structure and properties of these "finish" layers which are hundreds of nanometres thick and most likely contain a gradient in amine concentration which cannot be analytically probed directly, model compounds prepared of epoxy stoichiometry known to be possible in the interphase were prepared and processed in a manner identical to the composite. Measurements of strength, stiffness and fracture toughness of variable epoxy/amine stoichiometries with the amine to epoxy ratio less than stoichiometric, combined with optical micrographs of the fibre–matrix interface under stress show that the increase in the adhesion level is due to better stress transfer between fibre and matrix. The modulus of epoxy-rich stoichiometries increases but the material also becomes more brittle. Because of the more brittle interface, matrix cracking is detected at fibre breaks instead of fibre–matrix interfacial failure, as seen in other interfacial conditions (Fig. 8).

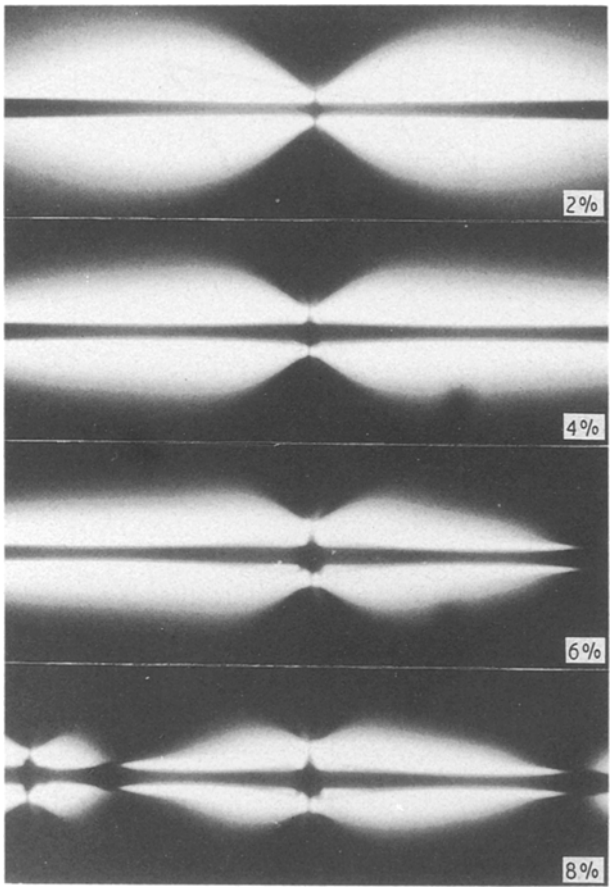

Figure 8 Transmitted polarized light micrographs of a single ASC carbon fibre under increasing strain in an epoxy matrix showing the fibre break and the photoelastic stress pattern characteristic of matrix crack growth × 450.

4.2. Composite mechanical properties

The set of three fibres, AU-4, AS-4 and AS-4C, combined with the amine-cured epoxy matrix, provides the quantitative basis for developing structure–property relationships between fibre–matrix adhesion and composite mechanical properties. The data in Table III show that there are significant changes in adhesion as measured by the embedded single-fibre test while the properties of the fibre are unchanged by the different surface treatments. It is also important to note that the change in the level of adhesion brings about an accompanying change in the interfacial failure mode (Fig. 9). Conventional models for prediction of composite properties incorporate constituent properties and would predict identical properties for composites made from these combinations of fibre and matrix. Conventional wisdom also would suggest that any changes in composite properties caused by changes in the level of fibre–matrix adhesion would manifest themselves primarily in the off-axis properties (e.g. transverse (90°) tensile and shear) but not in fibre-dominated properties (e.g. 0° tension or 0° compression). In order to test this hypothesis, both types of test have been conducted.

The summary of results obtained from different test methods is given below. The discussion is divided into three parts, on-axis properties, off-axis properties, and interlaminar fracture toughness characterization. The on-axis properties (such as longitudinal tensile, compressive, and flexural properties) are dominated by fibre properties, whereas the off-axis properties (such as transverse tensile and flexural, inplane and interlaminar shear) and interlaminar fracture toughness

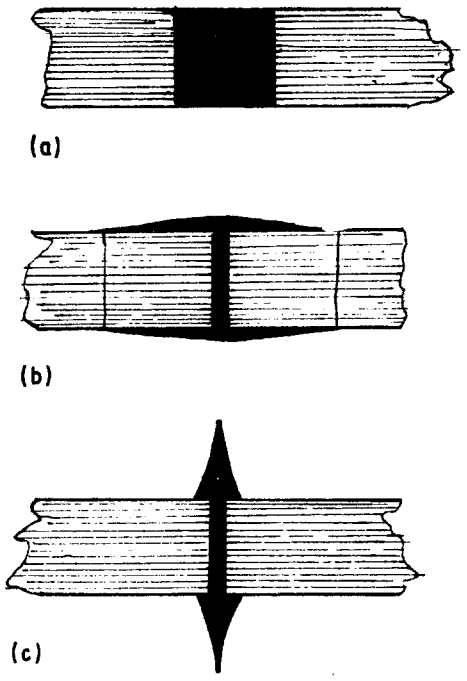

Figure 9 Schematic diagrams illustrating the three failure modes detected with increasing fibre–matrix adhesion. The drawings represent a single fibre in the epoxy matrix and subjected to shear causing the fibre to fracture (a) at low levels of adhesion – frictional debonding, (b) at intermediate levels – interfacial crack growth, and (c) at the highest levels matrix cracking perpendicular to the fibre axis.

are dominated by matrix and interfacial properties. The sensitivity of composite properties to fibre–matrix adhesion will be governed by how matrix and fibres are connected and how the applied load is transferred and distributed in the composite. For example, in the case of longitudinal tension, the matrix and fibres are connected through the fibre–matrix interface in parallel and most of the applied load is borne by the fibres. Therefore, as far as the mechanism of load distribution is concerned, the fibre–matrix adhesion should not be expected to play a dominant role in the longitudinal tensile behaviour. However, changes in the failure modes resulting from the change in fibre–matrix adhesion may have an effect on the longitudinal tensile strength. On the other hand, in the case of transverse tension, the matrix and fibres are connected through the fibre–matrix interface in series and all the three components, i.e. fibre, matrix, and interface/interphase carry equal load. In such a case, the fibre–matrix adhesion should be expected to have a dominant effect on the composite properties. In the following sections the structure–property relationship establishing the causal linkage between fibre–matrix adhesion and composite properties, is discussed.

4.2.1. On-axis properties

Average values of the on-axis properties for the three composite systems are listed in Table IV. The compressive results are averages of properties obtained from 12 specimens each for the three composites systems, whereas the other properties are the average of 10 specimens each. Thus, Table IV summarizes the results from 96 specimens. A discussion on the average results is provided below.

4.2.1.1. $[O]_{12}$ tension. The longitudinal stress–strain curves for each specimen, generated using strain gauges, for all the cases were non-linear in all the strain ranges, i.e. the longitudinal tensile modulus, E_{11}, was a function of axial strain, ε_1, Fig. 10. In all cases, the modulus increased with axial strain until the point when the applied load began to drop due to damage progression. All the specimens showed some perturbation in E_{11} near zero strain levels. The modulus of carbon fibres has also been reported to show perturbations at low strains [17]. As the strain increases the perturbations disappear and E_{11} increases almost linearly with strain until about 0.3% strain. This behaviour of the 0° tensile stress–strain curves of carbon/epoxy composites is the result of the non-Hookean behaviour of carbon fibres. The increase in the modulus of carbon fibres with axial strain results from the "unwrinkling" of graphitic layers during the applied axial loading [18]. To calculate the longitudinal tensile modulus of composites, the initial points

TABLE IV Summary of on-axis property results for carbon/epoxy composites

Test	AU-4/Epoxy	AS-4/Epoxy	AS-4C/Epoxy
$[0]_{12}$ tensile modulus, E_{11} (GPa)	130 ± 9	138 ± 5	150 ± 9
$[0]_{12}$ tensile strength, σ_1^f (MPa)	1403 ± 107	1890 ± 143	2044 ± 256
$[0]_{12}$ compressive modulus, E_{1C} (GPa)	131 ± 8	126 ± 9	153 ± 8
$[0]_{12}$ compressive strength, σ_{1C}^f (MPa)	679 ± 116	911 ± 180	1174 ± 207
$[0]_{12}$ three-point flexural modulus, E_{1B} (GPa)	154 ± 6	136 ± 11	147 ± 5
$[0]_{12}$ three-point flexural strength, σ_{1B}^f (MPa)	1662 ± 92	1557 ± 102	1827 ± 52

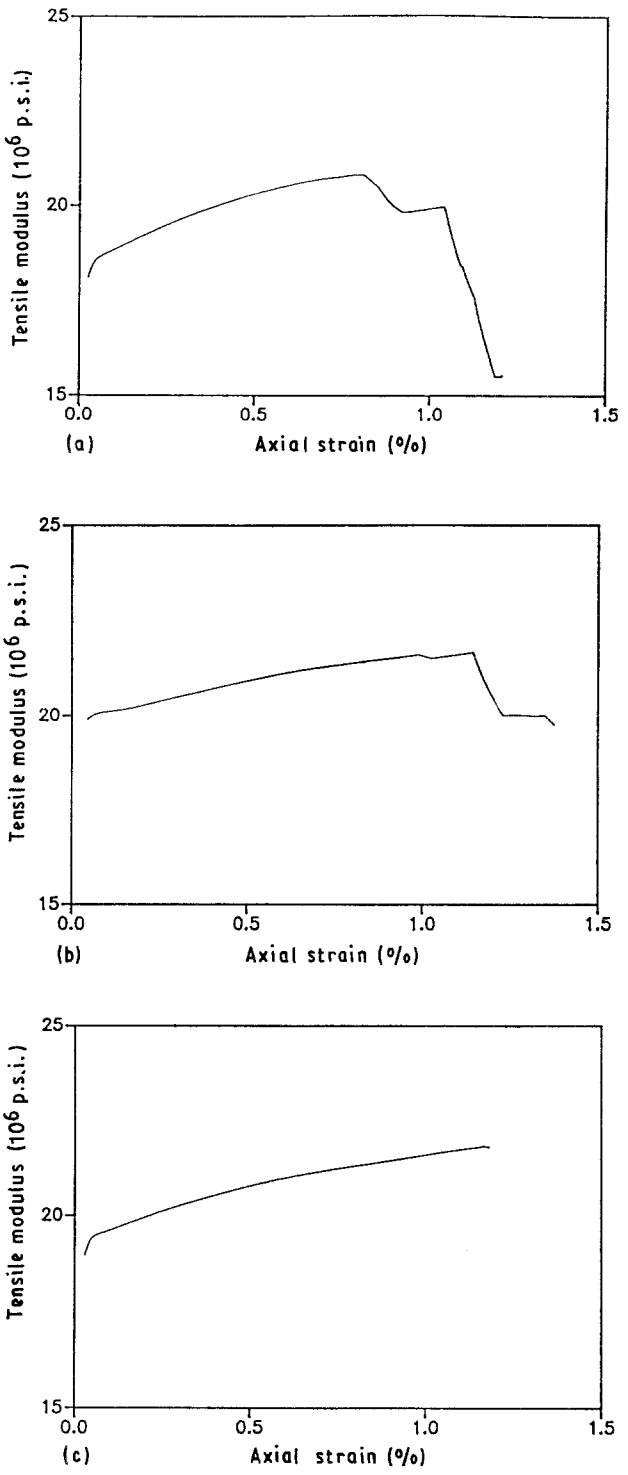

Figure 10 Variation of longitudinal tensile modulus with applied strain for (a) AU-4/Epoxy, (b) AS-4/Epoxy, and (c) AS-4C/Epoxy. The modulus increases with applied strain in all the three cases.

that included perturbation in E_{11} were removed and a linear regression analysis was performed on the remaining points below the strain of 0.3%. The linear regression lines were then extrapolated to $\varepsilon_1 = 0$ to yield the values of E_{11}(at $\varepsilon_1 = 0$). The average values of modulus thus obtained are listed in Table IV.

It should be noted that the fibre volume fractions of different panels are not identical (see Table I). Therefore, for the comparison purposes the values of the longitudinal tensile modulus and tensile strength were linearly scaled to the average fibre volume fraction of 67.7%. This is the average fibre volume fraction of all the panels from which the specimens for 0° tension tests were taken. A comparison among the average longitudinal moduli of the three composite systems shows little difference of statistical significance, Fig. 11. The insensitivity of the E_{11} to fibre–matrix adhesion should be expected, considering that in 0° tension specimens, fibre and matrix are connected through the interface in parallel. Most of the applied load is carried by the longitudinal fibres. The role of interface (and matrix) is limited to transferring stress from highly stressed fibres to the neighbouring fibres carrying relatively low stress, so as to result in a uniform stress distribution in the composite. Within the elastic range, the interface can meet this role effectively for all the three composite systems. Therefore, fibre–matrix adhesion has little effect, if any, on the elastic modulus, even when the adhesion is increased by more than a factor of two. In such a case, the rule-of-mixture (ROM), Equation 5, can be applied to predict the tensile modulus

$$E_{11} = V_f E_f + (1 - V_f - V_v)E_m \qquad (5)$$

where E_{11}, E_f and E_m are tensile moduli of composite, fibre, and matrix, respectively, and V_f and V_v are the volume fractions of fibres and voids, respectively. Using the data given in Tables I and III, Equation 5 can be applied to predict the values of the longitudinal tensile modulus for the three different composite materials. These values are listed in Table V. Note that the V_f and V_v of panels from which the tensile specimens were machined are slightly different from the values listed in Table I. The values listed in Table I are the average from all the panels.

For all the three composite systems, the ROM predictions are about 13%–18% higher than the experimental values. The ROM equation is a theoretical upper bound of tensile modulus that assumes perfect fibre–matrix bonding and ignores the variations resulting from imperfect fibre alignment, non-uniform fibre distribution, local non-homogeneities, void content, etc. In addition, the transverse deformations resulting from Poisson's effect are not considered in the ROM equation. In practical situations all of these factors are present and, therefore, the measured value of the modulus is always smaller than that predicted by the ROM.

The average longitudinal tensile strengths, σ_1^f, of the three composite materials are shown in Fig. 12. It is interesting to note that when the ISS is increased from the low to the intermediate values (i.e. an increase in the ISS of about 83%) the strength increases by about 25%. However, when the ISS is further increased to the high level (i.e. additional increase in the ISS by about 19%), the strength shows no increase (within the error band). The change in the tensile strength as a function of fibre–matrix adhesion is attributed to the change in the failure modes and failure processes.

Photographs of the failed specimens of the three composite materials are shown in Fig. 13. The AU-4/Epoxy composites, which have the lowest value of ISS, do not show much surface damage. However, extensive internal damage, primarily in the form of delamination that extended deep into the end-tabs, can be seen. Because of the weak interface, the damage starts occurring early (at about 50%–60% ultimate load) in

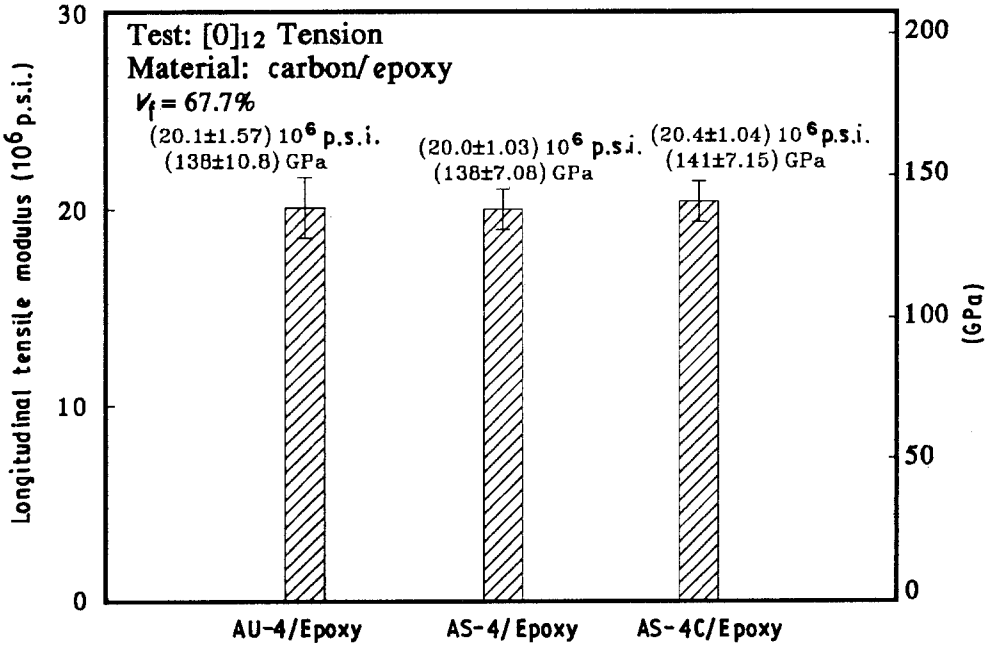

Figure 11 Comparison of the longitudinal tensile modulus of the three composite materials. All three composite materials yield similar values.

TABLE V Comparison between experimental and predicted longitudinal tensile modulus from ROM values

	AU-4/Epoxy	AS-4/Epoxy	AS-4C/Epoxy
ROM (GPa)	150	163	169
Experimental (GPa)	130	138	150

the AU-4/Epoxy specimens. The progression of damage could also be heard. Audio emissions are heard continuously indicating cumulative damage progression in the specimens with increasing applied load. At these loads (50%–60% ultimate load) the fibres may not have broken. However, because the weakened interface is not able to transfer efficiently the load from critically stressed fibres to the lower-stressed neighbouring regions, the composite is cumulatively weakened. Because of the cumulative damage progression in AU-4/Epoxy specimens, the stored strain energy does not build up to levels that are large enough to cause extensive fibre–matrix splitting during the final fracture process.

The AS-4/Epoxy composites, where the interface is stronger than that in AU-4/Epoxy, show extensive fibre–matrix splitting. This type of failure is described as "brush-like". From the visual observation of the

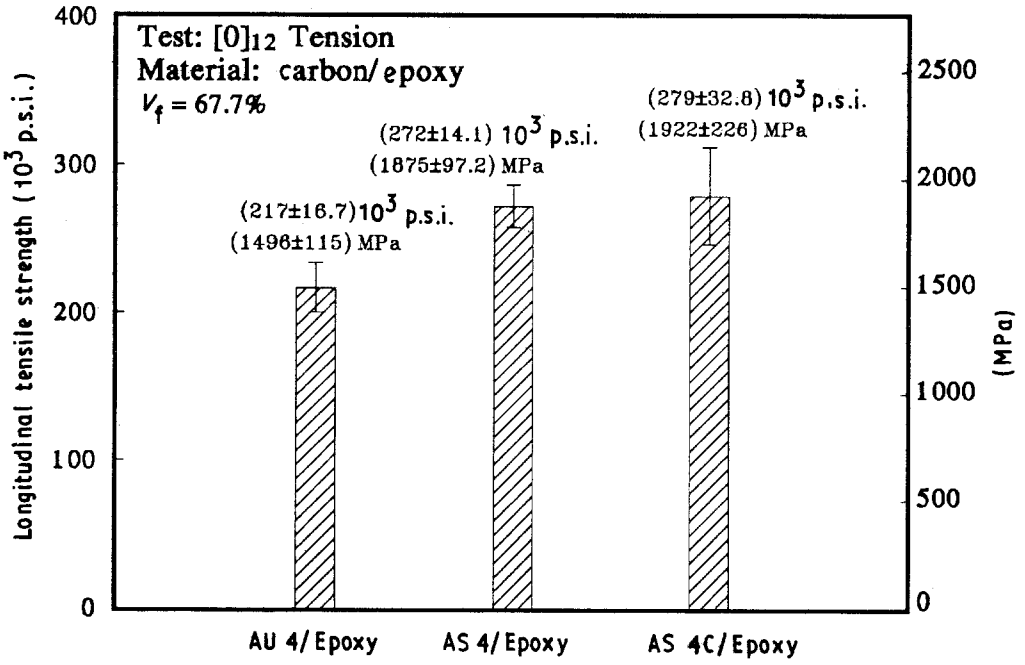

Figure 12 Comparison of the longitudinal tensile strength of the three composite materials. The strength of AS-4/Epoxy is about 25% higher than that of AU-4/Epoxy. However, the strength of AS-4C/Epoxy is similar to that of AS-4/Epoxy.

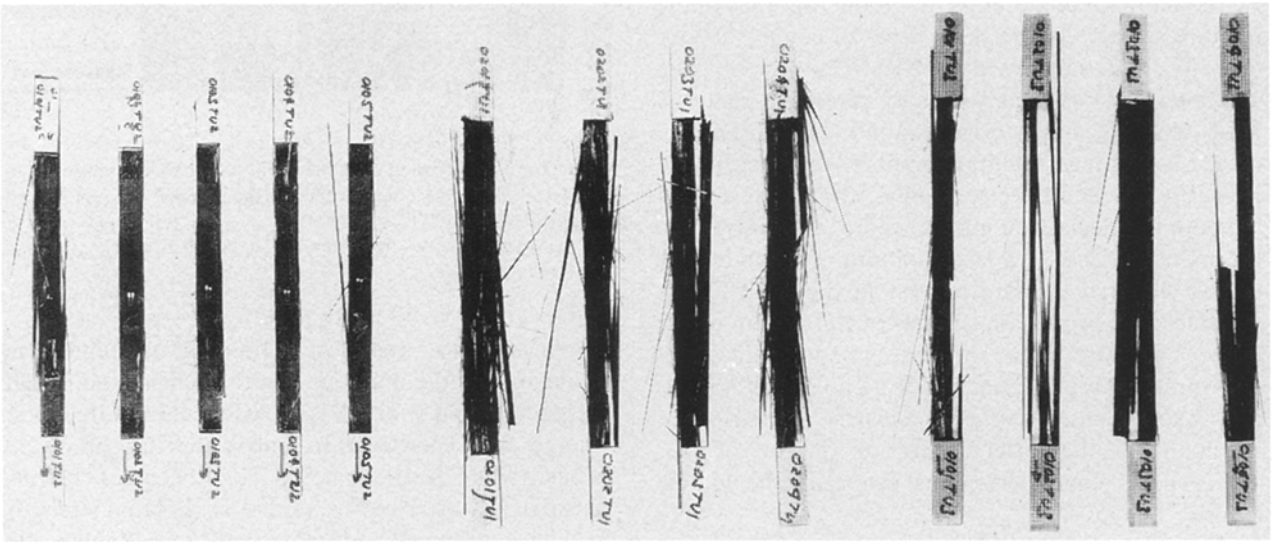

Figure 13 Effect of the ISS on the external appearances of the fractured $[0]_{12}$ carbon/epoxy tensile specimens. The AU-4/Epoxy specimens do not show much surface damage. The AS-4/Epoxy and AS-4C/Epoxy show "brush-like" and "brittle" failure, respectively.

specimen surface during the loading process some splitting was seen (and heard) to initiate from specimen edges at approximately 70% of the maximum load. At such applied loads the interface fails at sporadic locations where the stresses are the highest. An interfacial crack grows parallel to the fibres and acts as a "crack-arrester" thereby relieving the stresses from the critically stressed regions. In such a case the stresses in the composite are distributed more uniformly. Therefore, instead of cumulative damage progression, the failure of 0° AS-4/Epoxy is like an "explosion" resulting in a "brush-like" appearance of the fractured specimens. The widespread splitting seen in the failed specimens of AS-4/Epoxy composite, Fig. 13, takes place instantaneously during the final fracture process when suddenly a large amount of strain energy is released.

In the AS-4C/Epoxy specimens where the interfacial shear strength has been noted to be highest, cracks have cut across the specimen section with little fibre–matrix splitting, Fig. 13. Some splitting occurs as a result of an "explosion" caused by a sudden release of a large amount of strain energy during the final fracture process. The strong interface in AS-4C/Epoxy specimens is able to sustain larger loads. Thus, the "crack-blunting" mechanism that was active in AS-4/Epoxy specimens is not operative in AS-4C/Epoxy specimens. When fibres start breaking the strong interface at the broken ends of the fibres does not fail and a crack propagates perpendicular to the fibre axis. Therefore, any gain in the strength due to the higher ISS is offset by the increased "notch-sensitivity" of the material. As a result the crack propagates in a "self-similar" manner across the specimen and the load-carrying capacity of the composite is reduced. This type of failure is described a "brittle" fracture.

To determine the effect of fibre surface treatment on the micro-failure modes, fracture surface morphologies of representative samples were examined by SEM. Fig. 14 shows representative photomicrographs of the fracture surfaces of the three types of composite systems. The fibre surfaces in the AU-4/Epoxy composite specimen are completely devoid of matrix material indicating extensive interfacial failure. In addition, the matrix is no longer holding the fibres together. In the AS-4/Epoxy composite specimens, the failure modes are both interfacial and matrix failure. Also, in spite of the sudden release of a large amount of strain energy during the final fracture process in the AS-4/Epoxy specimen, the broken matrix pieces still adhere to the fibres. There are minor differences between the fracture surface morphologies of AS-4/Epoxy and AS-4C/Epoxy specimens. However, the matrix failure is more dominant in the latter. Thus, the failure of AS-4C/Epoxy is characterized as primarily the matrix failure.

From these failure modes it can be concluded that the tensile strength increases with increasing interfacial shear strength only as long as the failure is primarily interfacial. In such a situation damage zones are easily "decoupled" by fibre–matrix splitting. However, if the interfacial strength is too weak, the composite fails prematurely because of cumulative weakening of the material. On the other hand, when interfacial bond strength is excessive, the failure mode changes from interfacial to matrix and the composite behaves like a brittle material, i.e. it becomes "notch-sensitive". Thus, excessive fibre–matrix bond strength may have detrimental effect on the longitudinal tensile strength of the composite.

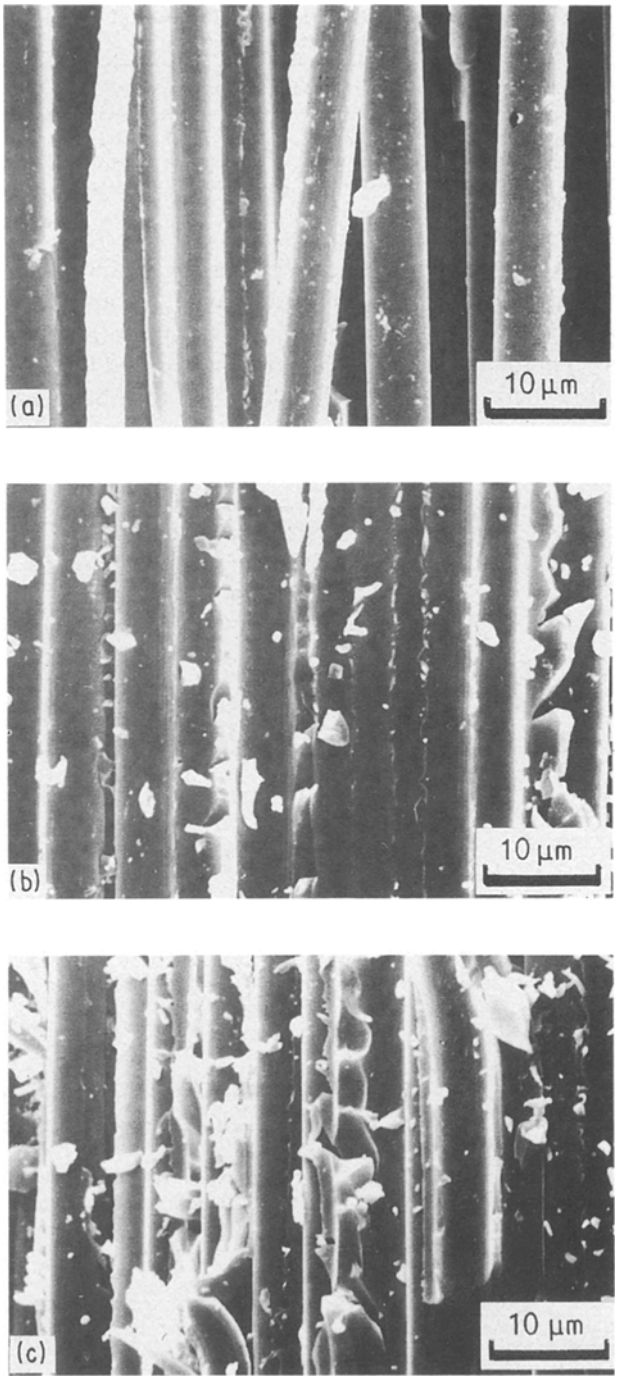

Figure 14 Effect of the ISS on the major failure modes in carbon/epoxy $[0]_{12}$ tension specimens. The failure mode changes from interfacial to matrix failure as the ISS is increased from the low to the high values. (a) AU-4/828 mPDA, spec. no. DIO 4TU2, (b) AS-4/828 mPDA, spec. no. 0303TUI, (c) AS-4C/828 mPDA, spec. no. 0104 TU3.

4.2.1.2. $[O]_{12}$ Compression. Representative examples of longitudinal compressive stress–strain curves obtained from the back-to-back strain gauges are

shown in Fig. 15 for the three material systems. Generally the curves from the two strain gauges are similar; however, in some cases strain divergence is seen at higher loads indicating possible instability (buckling) effects. The compressive modulus for each specimen was determined by averaging the slopes of the stress–strain curves between the strain range of 0.1% –0.3% from the readings of both the strain gauges. The average (of 12 specimens each) compressive modulus for the three different composite materials is listed in Table IV.

For the purpose of comparison among the three composite materials, the average compressive modulus and strength values were linearly scaled to the average fibre volume fraction of 66.1%. This is the average fibre volume fraction of all the panels from which the specimens for 0° compression tests were taken. These average values of the compressive moduli for the three composite systems are shown in Fig. 16. There is little change (within the experimental error) in the compressive modulus between AU-4/Epoxy and AS-4/Epoxy, even though the ISS of the latter is about

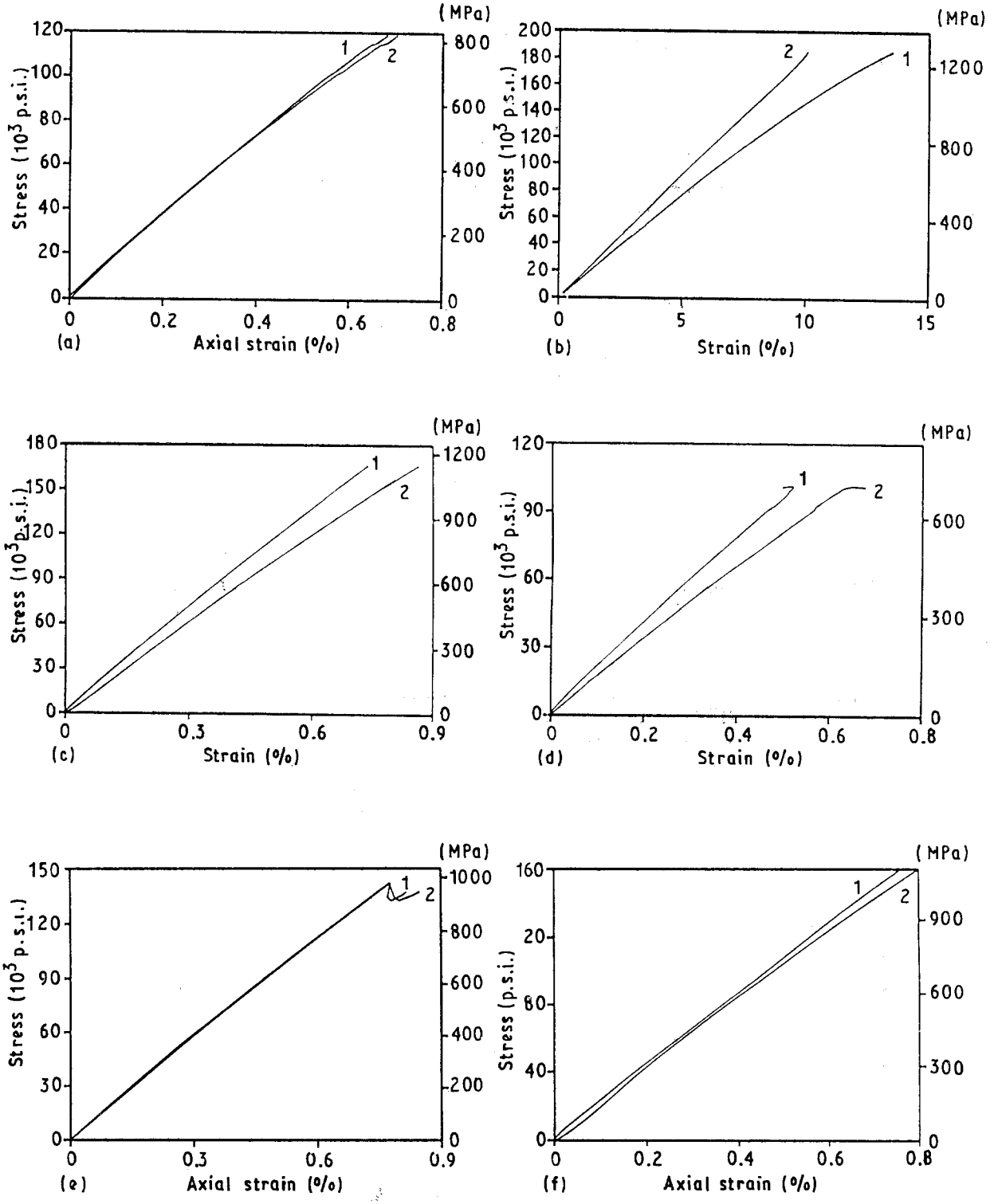

Figure 15 Representative longitudinal compressive stress–strain curves obtained from the back-to-back strain gauges for the three types of carbon/epoxy composite materials. Both the strain gauges yield similar curves; however, in some cases the two curves diverge at higher loads indicating specimen bending. 1, Front strain gauge; 2, back strain gauge.

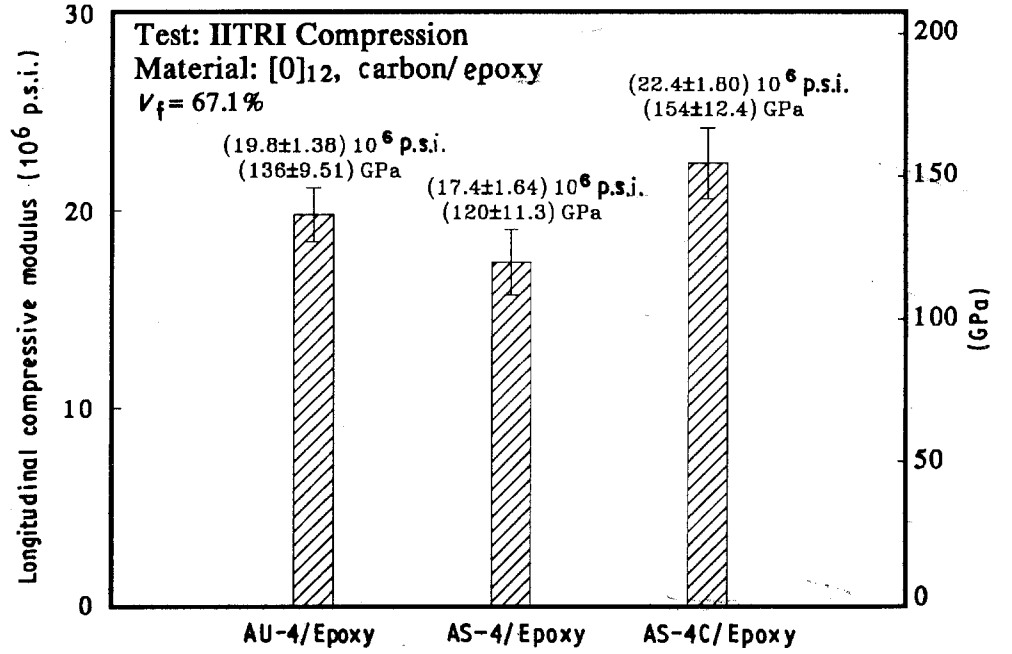

Figure 16 Comparison of the average compressive modulus of the three carbon/epoxy composite materials. The moduli of AU-4/Epoxy and AS-4/Epoxy are similar and they are higher than that of the AS-4C/Epoxy.

83% higher than that of the former. Between the AS-4/Epoxy and AS-4C/Epoxy, there is an increase in the compressive modulus of about 29% for a corresponding increase in the ISS of about 19%. The comparison between the AU-4/Epoxy and AS-4/Epoxy suggests that the increased adhesion between fibre and matrix has little effect on the elastic compressive properties of unidirectional graphite/epoxy composites. It implies, therefore, that the increase in the compressive modulus of the AS-4C/Epoxy is not because of the increased adhesion between fibre and matrix, but it is due to the presence of the high-modulus brittle interphase around the AS-4C graphite fibres. A common deformation mode in unidirectional composites subjected to compressive loading is the shear mode of fibre buckling [19]. In this mode fibres tend to buckle in-phase and, thus, the matrix is subjected to shear loads. In the case of AS-4C/Epoxy composites, the high-modulus brittle interphase around fibres [15] provides additional flexural rigidity and resists the fibre bending, thereby increasing the compressive modulus of the composite.

The average compressive strength values for the three composite materials are shown in Fig. 17. In spite of the large scatter in the experimental data, the increasing trend in the compressive strength with increasing ISS is clearly indicated. It is interesting to note that the strength increases more rapidly when the

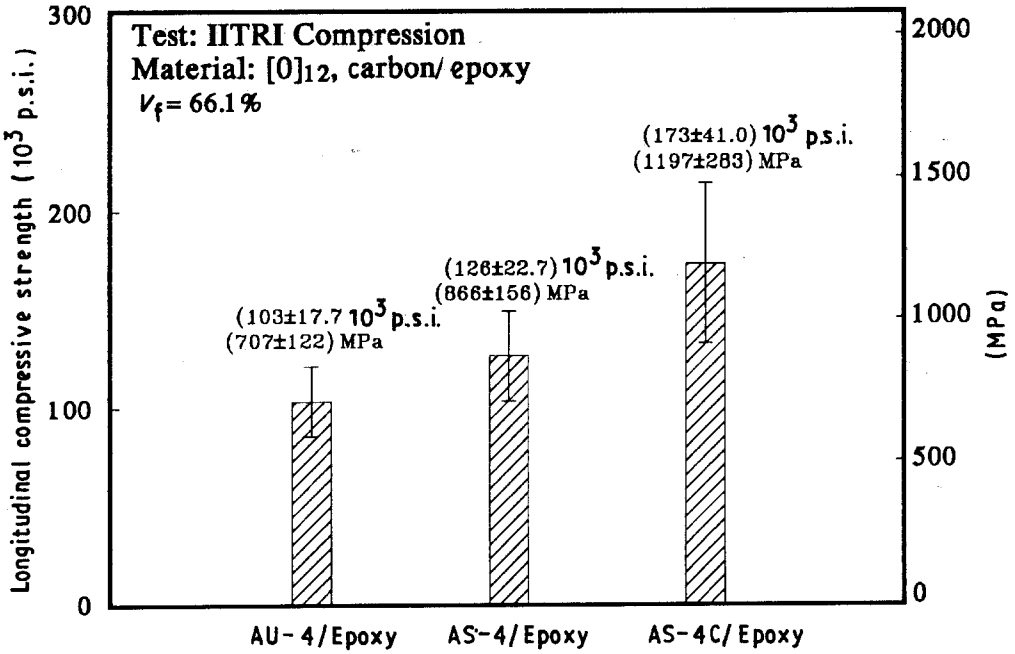

Figure 17 Comparison of the average longitudinal compressive strength of the three types of carbon/epoxy composites. The composite having the stronger fibre–matrix adhesion yields higher compressive strength.

ISS is increased from the intermediate to the highest values. This is because the composite having the highest level of the fibre–matrix adhesion also has the brittle interphase around the graphite fibres. This interphase provides additional flexural rigidity to the composite, improving the compressive strength. Also, during the uniaxial compressive loading, transverse tensile stresses develop in the composite due to Poisson's effect. These transverse tensile stresses may cause local interfacial or matrix failure in the composites having poor transverse tensile strength, and, therefore reduce the local transverse constraint on the fibres. Experimental results obtained on the same three groups of composites (to be discussed later) have shown that the transverse tensile strength increases significantly when the fibre–matrix adhesion is increased (see Table VI). In addition to the other factors, the higher transverse tensile strength of composites having better fibre–matrix adhesion should also be responsible for the increase in the compressive strength of these composites.

In summary, therefore, the increase in the compressive strength corresponding to the increase in the ISS from the low to the intermediate values, and then the subsequent more rapid increase in the strength corresponding to the increase in the ISS from intermediate to the highest values suggest that both the improved shear strength between fibre and matrix coupled with the presence of the high-modulus brittle interphase around the graphite fibres, and the improved transverse tensile strength of the composite contribute to the greater compressive strength of these composites.

The mechanisms by which the ISS affects the compressive strength of a unidirectional composite can be better understood by examining the effect of the ISS on failure processes and failure modes of these composites. Photographs of representative fractured specimens are shown in Fig. 18. The following observations can be made from these photographs. In the case of AU-4/Epoxy composite specimens, the fracture occurred near the end-tab. However, the specimens did not separate into two pieces. Extensive delamination near the end-tabs is noticed in all the AU-4/Epoxy specimens. Observation of the specimen surface during the testing indicated that delamination occurred first, and with increasing applied compressive load, this delamination buckled. Extensive fibre debonding also occurred resulting in "fibre brooming". Partial end-tab debonding (about 5–7 mm deep) could be seen in these specimens. This end-tab debonding might have an effect on simultaneously increasing the effective specimen gauge length and reducing the end-constraint factor. The AS-4/Epoxy composite specimens fractured near the end-tabs. In most of the specimens fracture occurred at an angle suggesting shear failure. Limited delamination near the specimen edges also occurred. Delamination planes are flat, i.e. delamination buckling did not occur. Partial end-tab debonding (about 3 mm deep) near the specimen edges is also seen. The AS-4C/Epoxy composite specimens also fractured near the end-tabs. However, unlike the AS-4/Epoxy composites where the crack propagated along an angle suggesting the shear failure, the fracture plane in the AS-4C/Epoxy composites was along a line perpendicular to the loading axis. This suggests that the compressive fracture of the AS-4C/Epoxy composites was not caused by the shear failure of the material.

TABLE VI Effect of fibre–matrix ISS on the transverse tensile strength of graphite/epoxy composites

	AU-4/Epoxy	AS-4/Epoxy	AS-4C/Epoxy
Fibre–matrix interfacial shear strength (MPa)	37.2	68.3	81.4
Composite transverse strength (MPa)	18.0	34.2	41.2

The scanning electron micrographs of the fracture surfaces of the three types of composites are shown in Figs 19 and 20. The curvature in the fibres in the fracture surface of AU-4/Epoxy specimen is the result of delamination buckling. Random fibre breaks seen in the AU-4/Epoxy specimen in Fig. 19 may have occurred due to excessive bending of fibres during delamination buckling. An enlarged view of the fracture surface of an AU-4/Epoxy specimen shows clean fibre surfaces indicating extensive fibre–matrix interfacial failure, Fig. 20. The failure modes in AU-4/Epoxy composites are characterized as delamination, delamination buckling, and interfacial failure.

The fracture surface of AS-4/Epoxy specimen shows multiple fibre breaks and localized rotation of broken fibres. Unlike the AU-4/Epoxy, the fibre breaks in AS-4/Epoxy have not occurred randomly. Instead the broken ends are aligned. In addition, the broken fibres are of uniform lengths, Fig. 19. This type of failure is induced by fibre microbuckling such as found in the compressive failure of E-glass bundles embedded in Epon 815 epoxy matrix [20]. The failure pattern shown in Fig. 19 suggests that the microbuckling of fibres may start with the buckling of a single fibre and progressively involve adjacent fibres as damage propagates. Because the fibre microbuckling propagated along a line oriented approximately 45° to the loading axis, it suggests that the failure occurred along the line of maximum shear stress. An enlarged view of the fibre surface of the AS-4/Epoxy specimen shows portions of fibre surfaces that are devoid of matrix indicating interfacial failure, Fig. 20. However, the broken fibre pieces are still held together by the matrix material indicating matrix failure as well. Therefore, the compressive failure modes in AS-4/Epoxy are fibre microbuckling, interfacial failure, and matrix failure.

The fracture surface of AS-4C/Epoxy specimen shows significantly different features than those shown by AU-4/Epoxy and AS-4/Epoxy specimens, Figs 19 and 20. Globally the fracture appears to have taken place along one single plane that is perpendicular to the loading axis, Fig. 18. However, a closer look indicates "stepped" surfaces, Fig. 19. The broken fibre ends in the fracture surfaces at the higher steps are smooth, whereas the fracture surfaces at the lower steps are much more rugged and they show fibre debris and fibre pull-out. The "stepped" fracture surface was noted also on the compression side of the

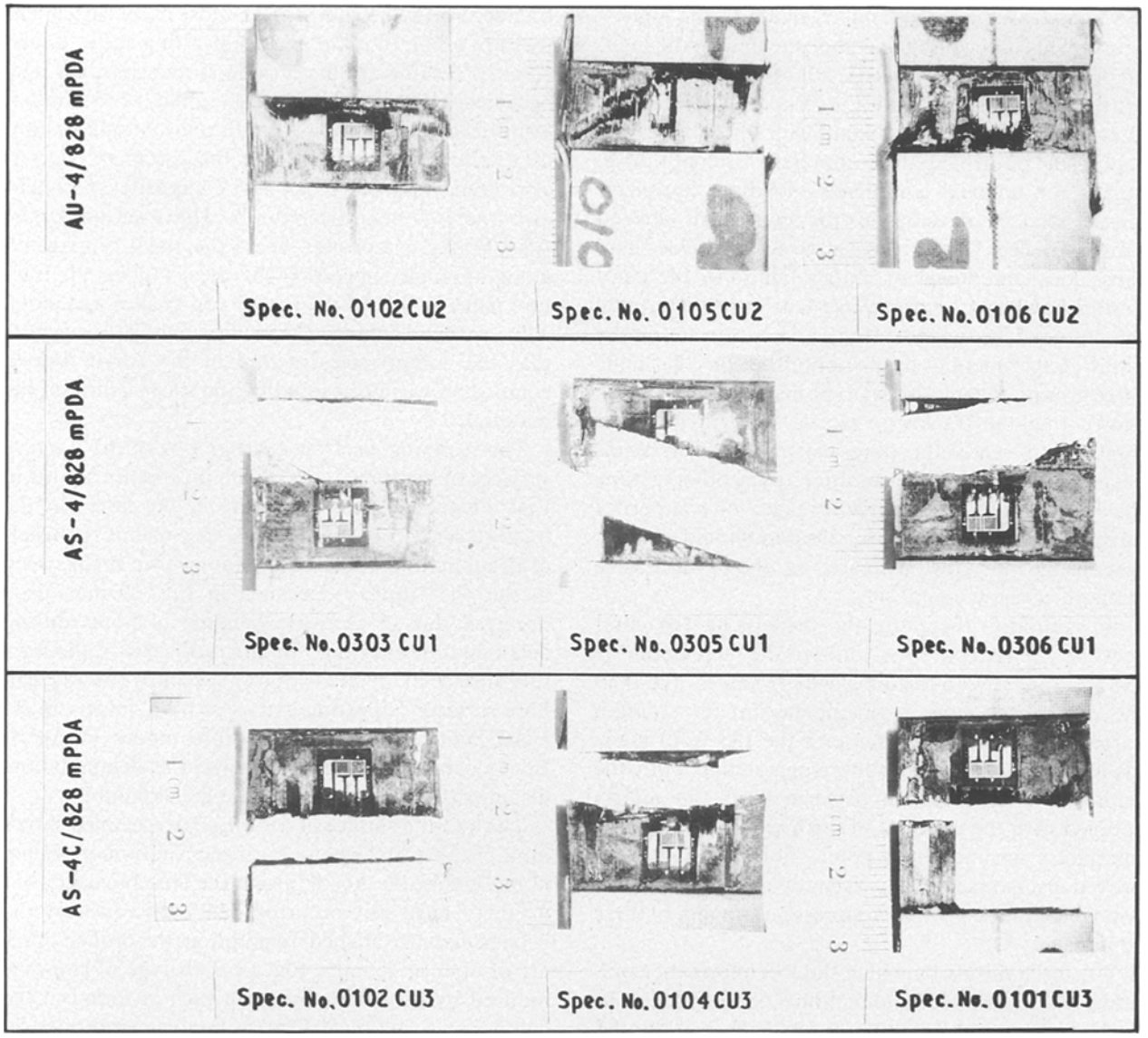

Figure 18 Photographs of the representative fractured specimens showing global delamination buckling for the AU-4/Epoxy, fracture planes oriented at an angle to the loading axis for the AS-4/Epoxy, and fracture planes perpendicular to the loading axis for the AS-4C/Epoxy. $[0]_{12}$ compression.

three-point flexure tests of the AS-4C/Epoxy specimens (to be shown later). The mechanism that caused the "stepped" fracture surface is believed to be the following. The compressive failure of fibres is initiated at one plane. At certain locations of this plane, longitudinal matrix cracking or interfacial failure occurs. As a result, the side constraints around fibres are reduced and the failure path is diverted from one plane to the other and thus the compressive failure of fibres occurs in a different plane resulting in a "stepped" fracture surface. The enlarged view of the fracture surface of the AS-4C/Epoxy specimen shows fibre debris at the broken fibre ends, Fig. 20. The fibres are closely held by the matrix and the fibre surfaces are coated with the matrix material indicating strong adhesion between fibre and matrix. The major failure modes in the AS-4C/Epoxy composite are characterized as compressive failure of fibres and matrix failure.

The major failure modes identified for the three types of graphite/epoxy composites are summarized schematically in Fig. 21. The schematic diagram shows delamination and global delamination buckling for the composite having the untreated AU-4 fibres. In the composite having the surface-treated AS-4 fibres, the failure is initiated by local fibre microbuckling that propagates along the line of maximum shear stress. In the case of composite having the surface-treated and coated AS-4C fibres, the failure is caused by the compressive failure of fibres that occurs in several planes resulting in a "stepped" fracture surface.

In correlating the effect of fibre surface treatment on compressive strength with the observed failure modes, the following is suggested. The fibres surrounded by matrix material in a unidirectional composite subjected to compressive load are like beam columns that are laterally supported on an elastic foundation. The integrity of the fibre–matrix interface will determine the effectiveness of the surrounding elastic foundation that will, in turn, affect the compressive properties of a unidirectional composite. In the composites having the lowest value of ISS (i.e. AU-4/Epoxy), the failure is governed by delamination. Because of the poor fibre–matrix adhesion the fibres in the delaminated regions are easily separated from the matrix resulting

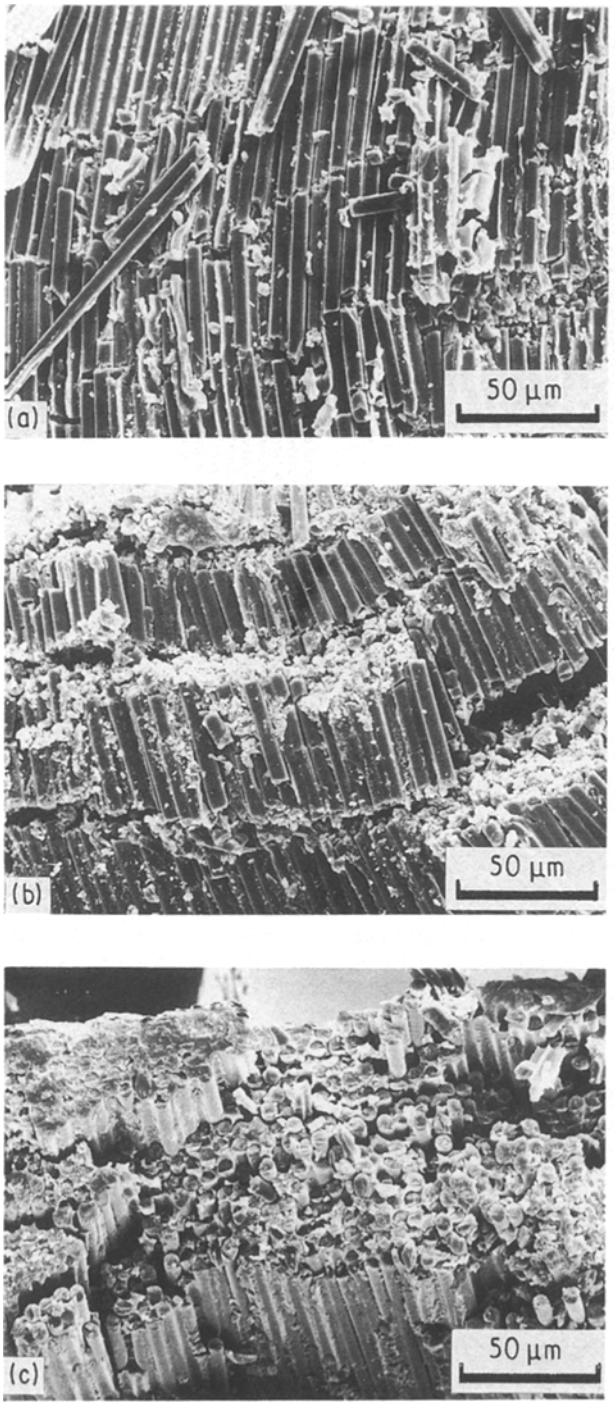

Figure 19 Scanning electron micrographs of fracture surfaces showing the global delamination buckling indicated by (a) the broken fibres lying along an arc in the AU-4/Epoxy, (b) local microbuckling of fibres in AS-4/Epoxy, and (c) compressive failure of fibres resulting in a "stepped" fracture surface in the AS-4C/Epoxy specimens. $[0]_{12}$ compression.

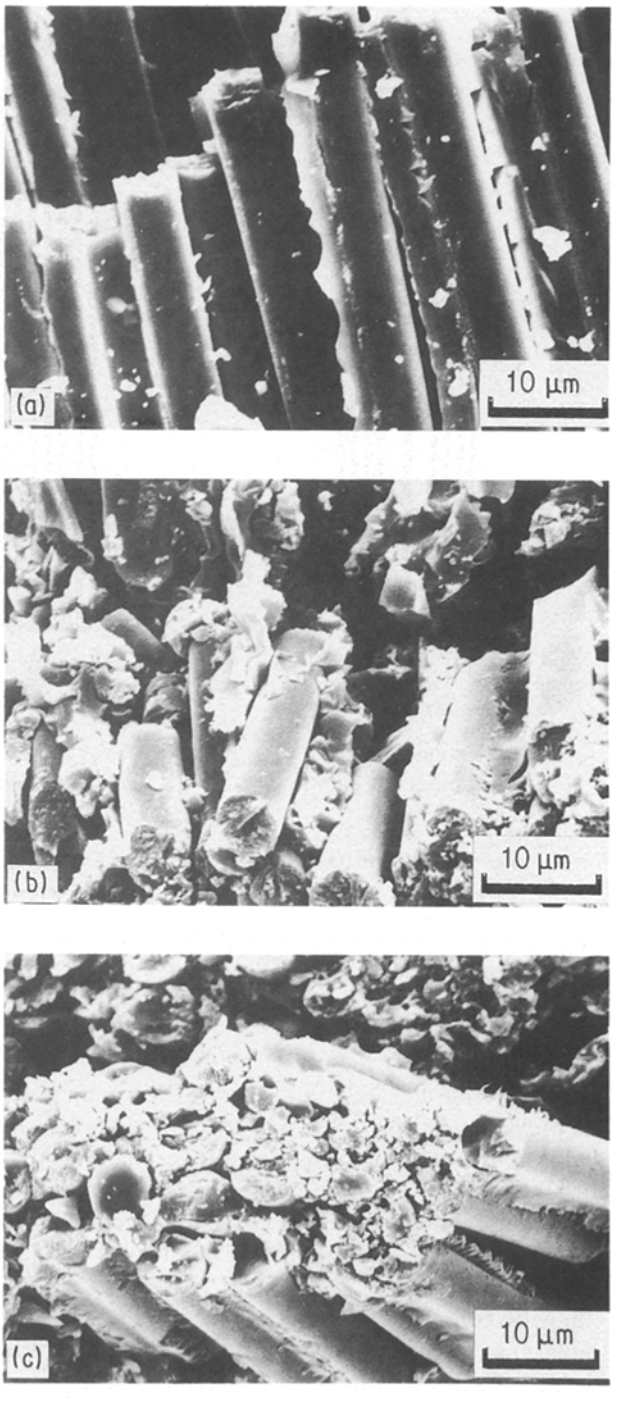

Figure 20 Scanning electron micrographs of fracture surfaces showing (a) significant interfacial failure in the AU-4/Epoxy, (b) both interfacial and matrix failure in the AS-4/Epoxy, and (c) primarily the matrix failure in the AS-4C/Epoxy specimens. $[0]_{12}$ compression.

in global delamination buckling under in-plane compressive loading. In addition, the extensive end-tab debonding induces Euler column buckling, reducing the compressive strength even further. In the composites with the intermediate values of ISS (i.e. AS-4/Epoxy), because of the improved fibre–matrix adhesion, delamination is contained only near the specimen edges and end-tab debonding is much reduced. Local interfacial failure, however, does take place and in such a case the fibre columns may locally behave like beam columns resting in matrix tunnels. With increasing applied load, local microbuckling may start in this fibre column and propagate in the adjacent fibre columns resulting in final failure of the specimen. Therefore, the reasons for the improved compressive strength of AS-4/Epoxy composites are two-fold, namely, (a) failure is governed by microbuckling of fibres rather than delamination failure and (b) end-tab debonding is reduced, thus, the gauge length and end constraints are not much affected. In the AS-4C/Epoxy composites where the ISS is the highest, the delamination, interfacial failure, end-tab debonding,

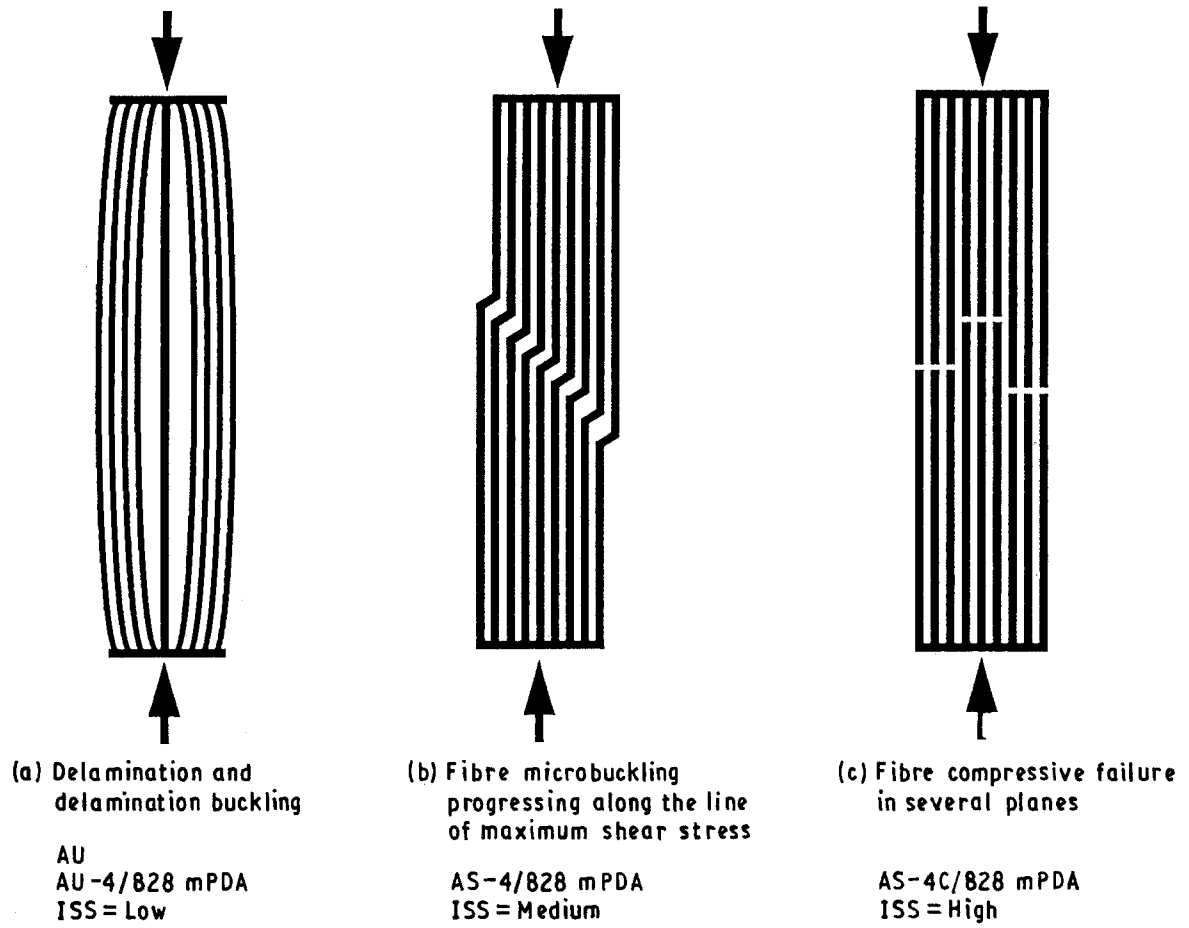

Figure 21 Schematic diagrams of the major failure modes detected for the three types of carbon/epoxy composite materials. These failure modes are (a) global delamination buckling, (b) local fibre microbuckling, and (c) fibre compressive failure for the composites having the poor, intermediate, and the highest levels of fibre–matrix adhesion, respectively.

and transverse tensile failure due to Poisson's effect are prevented by the strong fibre–matrix adhesion. In addition, the high-modulus strong interphase around carbon fibres in AS-4C/Epoxy composites provides strong lateral support to the graphite fibre columns. Thus, the fibres can be compressively loaded to their maximum capacity.

Fig. 22 compares the longitudinal compressive and longitudinal tensile properties of the three composite systems. The tensile modulus is relatively insensitive to the change in the fibre–matrix adhesion level. However, the compressive modulus shows a moderate increase when the ISS is increased from the intermediate to the highest level. The reason for this was attributed to the presence of the brittle interphase around the AS-4C fibres that provides additional flexural rigidity to the fibres during the compressive loading. While the compressive modulus is similar to the tensile modulus, the compressive strength differs significantly from the tensile strength for all three composite materials. The tensile strength is higher than the compressive strength by about 107%, 111%, and 57% for composites having the low, medium, and the highest ISS, respectively. Note that the difference between the tensile and compressive strengths is much smaller in the AS-4C/Epoxy composite compared to that in the other two composites. In the AU-4/Epoxy composites where the fibre–matrix bonding is poor, the global delamination occurs early and causes the specimen instability during the compressive loading, yielding low compressive strength of the composite. The stronger fibre–matrix adhesion in the AS-4/Epoxy composites prevents the global delamination. However, the local interfacial failure causes local instability resulting in fibre microbuckling. This microbuckling propagates to the neighbouring fibres resulting in a failure of the composite. In the tensile test, on the other hand, the interfacial failure decouples the failure modes and helps alleviate the local stress concentration, thus, improving the load-carrying capacity of the composite. During the compressive loading of the AS-4C/Epoxy composites, the interfacial failure is further prevented by even stronger fibre–matrix adhesion. Also, the high-modulus brittle interphase around the AS-4C graphite fibres provides additional flexural rigidity to the load-carrying fibres. Whereas, in the tensile test, the improvements in the strength resulting from the high ISS are offset by the increased notch sensitivity of the material because of the presence of the brittle interphase. In such a case, a smaller difference between the tensile and compressive values for the AS-4C/Epoxy composites should be expected.

4.2.1.3. $[O]_{12}$ three-point flexure. For the purpose of comparison between different composite systems, all the flexural modulus and strength values were linearly

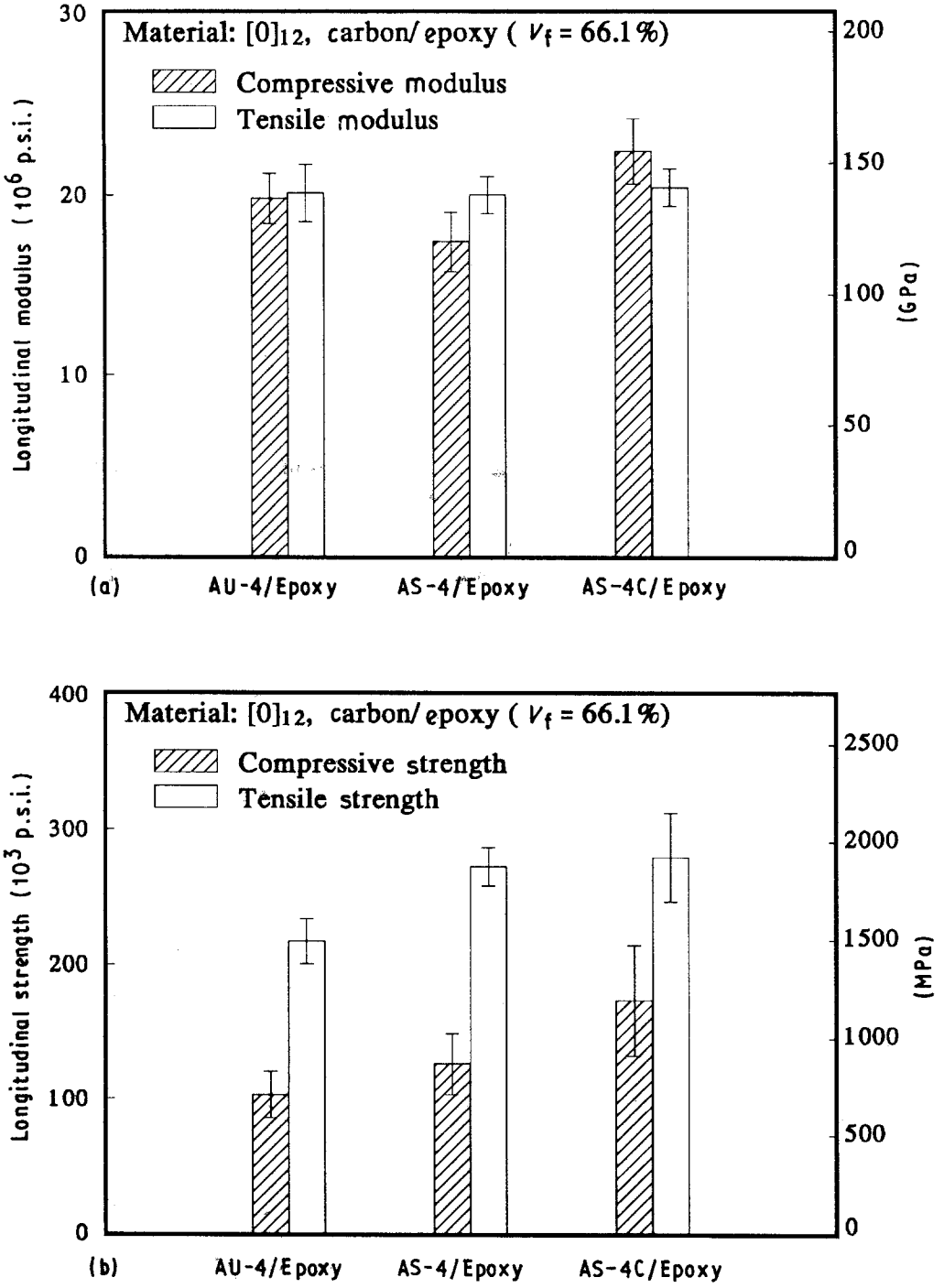

Figure 22 (a, b) Comparison between the compressive and tensile properties of the three types of $[0]_{12}$ carbon/epoxy composites. The modulus values are similar in both the loading modes. The compression test yields much smaller strength than tensile strength. Also the compressive strength is more sensitive than the tensile strength to fibre–matrix adhesion.

scaled to the average V_f(= 67.7%). These scaled values of the flexural modulus for the three composite systems are shown in Fig. 23. The composite having the lowest and the highest levels of fibre–matrix adhesion have the higher flexural moduli than that of composite having the intermediate level of adhesion. The higher modulus of composites having poor adhesion (i.e. AU-4/Epoxy) is believed to be due to "interlaminar sliding" among different layers caused by interlaminar shear stresses. Several interlaminar cracks were observed prior to failure in these specimens. This "sliding" reduces the axial strain in the outer fibres resulting in higher slopes of the flexural stress–strain curves. Some interlaminar cracks were also observed in the AS-4/Epoxy specimens. However, these cracks appeared only at the instant of specimen failure. No interlaminar cracks were observed in the AS-4C/Epoxy specimens. Because the AS-4/Epoxy and the AS-4C/Epoxy composites have much higher ISS compared to that in the AU-4/Epoxy composites, it is unlikely that the "interlaminar sliding" occurred in the former two composites. In such a situation, the only factor responsible for the increased flexural stiffness of AS-4C/Epoxy composite compared to that of AS-4/Epoxy is the presence of high-modulus brittle interphase around the AS-4C graphite fibres. It can be assumed that the shear modulus of this brittle interphase will also be higher than that of the bulk epoxy. It is likely, therefore, that the higher shear and axial moduli of the interphase region contribute to the

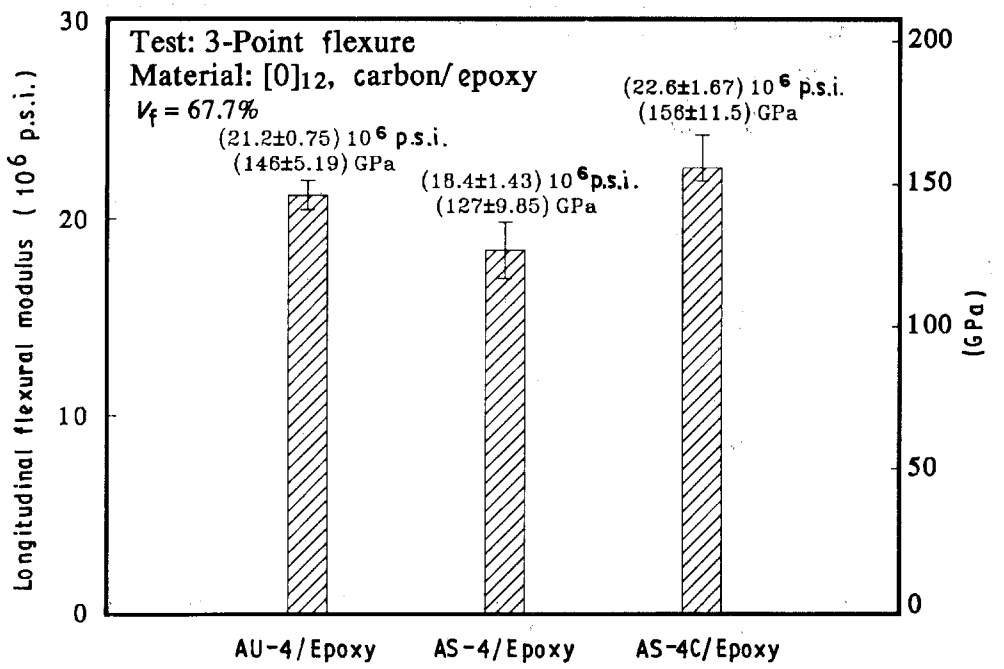

Figure 23 Longitudinal flexural moduli of the three carbon/epoxy composite materials. The higher modulus of the AU-4/Epoxy composite is due to "interlaminar sliding". The higher modulus of the AS-4C/Epoxy is due to the presence of the brittle interphase around the AS-4C fibres.

flexural stiffness of the AS-4C/Epoxy composite. It should be noted that such an effect of the interphase was not as dominant in the longitudinal tensile modulus, Fig. 11. It is because in the tensile tests the interlaminar shear stresses are not present, thus the increased shear modulus of the interphase is of little significance. Also, because the modulus of the fibre is much higher (about 65 times) than that of the matrix, then according to the ROM, the increased axial modulus of the interphase should cause only marginal increase in the longitudinal tensile modulus.

The average longitudinal flexural strengths for the three composite systems are shown in Fig. 24. There is little difference (within the scatter band) between flexural strengths of AU-4/Epoxy and AS-4/Epoxy composites. However, the strength of AS-4C/Epoxy is about 33% higher than that of AS-4/Epoxy. Because the interlaminar cracks were observed both in the AU-4/Epoxy and AS-4/Epoxy composites, it suggests that in these specimens even at large aspect ratios (= 60), the longitudinal flexural failure was still initiated by the interlaminar failure of the specimens. When the ISS is at its highest level (such as in the AS-4C/Epoxy), the interlaminar failure is suppressed and the fracture occurs due to tensile (or compressive failure) of the specimens. As a result, the flexural strength of the AS-4C/Epoxy composite is higher than that of the other two composites.

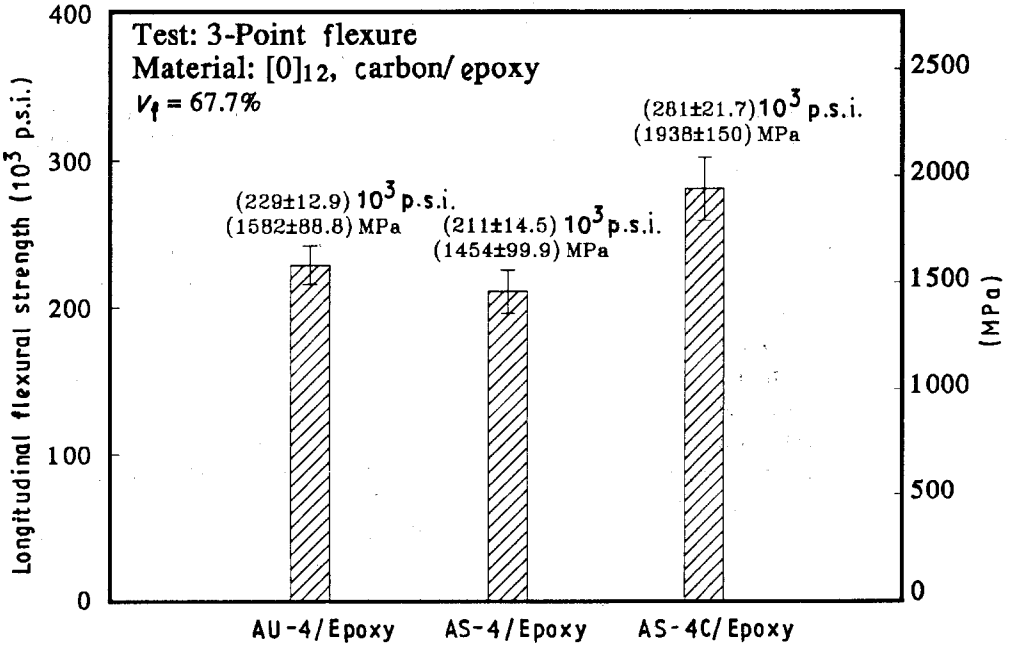

Figure 24 Longitudinal flexural strengths of the three types of carbon/epoxy composite materials. There is insignificant change in the flexural strength for the three composite materials.

The fracture surface morphologies of the longitudinal flexure specimens were examined under the SEM. The specimens from the AU-4/Epoxy composites did not separate into two pieces after their fracture. In order to look at the fracture surfaces, representative specimens from the AU-4/Epoxy composites were continued to be loaded until the specimen separation occurred. The specimens from the AS-4/Epoxy and AS-4C/Epoxy composites, however, did break into two pieces at the maximum load. The tensile and compressive sides of the fracture surfaces of the three groups of composite specimens are shown in Figs 25 and 26, respectively. The tension side of the

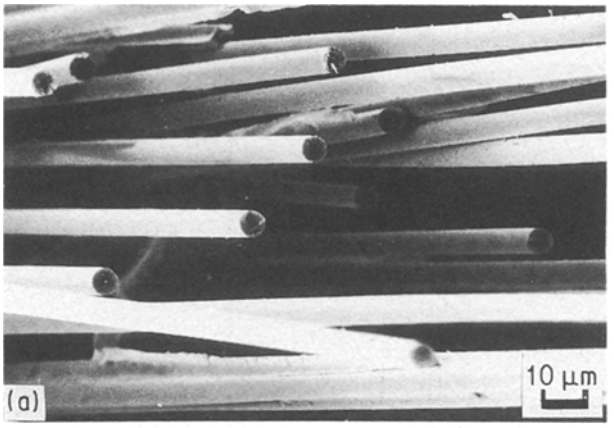

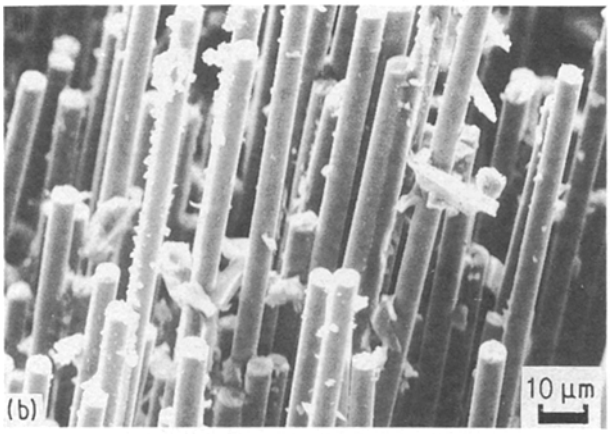

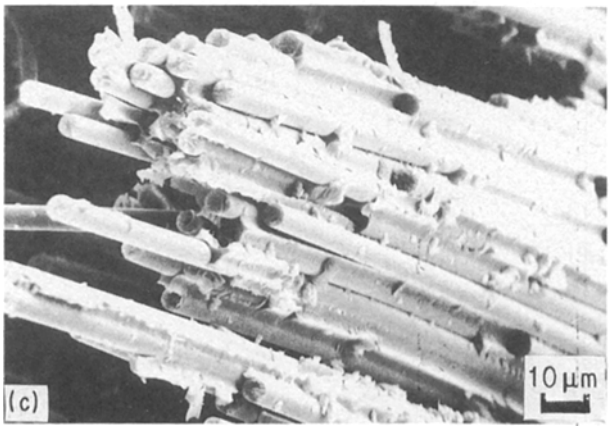

Figure 25 Effect of the ISS on the major failure modes on the tensile side of the three-point flexural $[0]_{12}$ specimens. The failure mode changes from interfacial to matrix when the ISS is increased from the low to the high values. (a) AU-4/828 mPDA, spec. no. 0607FL2; (b) AS-4/828 mPDA, spec. no. 0903FL1; (c) AS-4C/828, spec. no. 0302FL3.

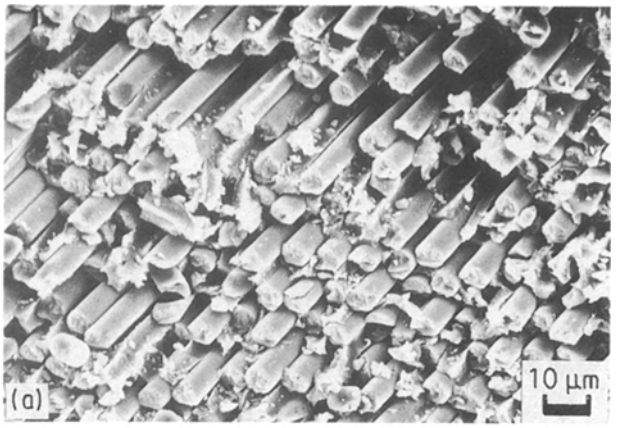

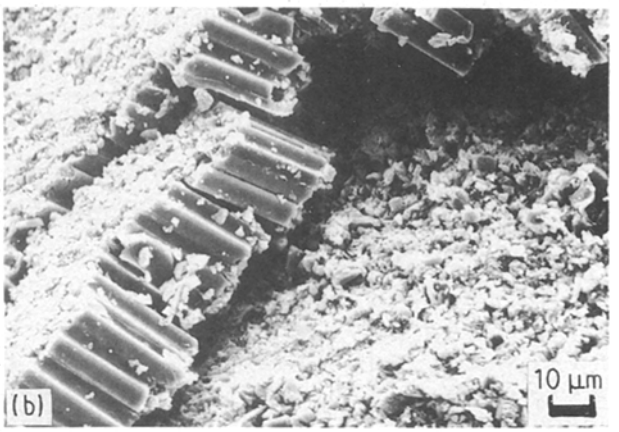

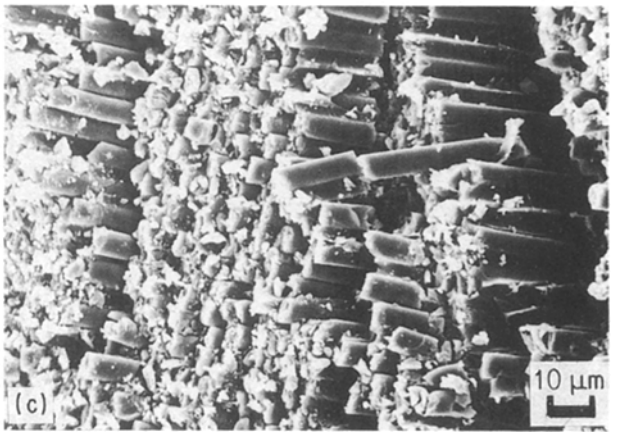

Figure 26 Effect of the ISS on the major failure modes on the compression side of the three-point flexure $[0]_{12}$ specimens. "Stepped" fracture surfaces occur in specimens having the intermediate and the high values of the ISS. (a–c) As Fig. 25.

AU-4/Epoxy specimen only shows interfacial failure. There is no trace of matrix material both between and around the graphite fibres. The AS-4/Epoxy specimen also shows significant interfacial failure. However, some fibres are still coated with matrix material, i.e. the failure mode is a combination of both interfacial and matrix failure. In the AS-4C/Epoxy specimen, the dominant failure mode is the matrix failure. In contrast with the other two cases, the fibres in the AS-4C/Epoxy specimen are closely held together by the matrix, Fig. 25.

On the compression side also, the AU-4/Epoxy specimen shows extensive interfacial failure, Fig. 26. The broken fibres are loosely held by the matrix. The

compression side fracture surfaces of the AS-4/Epoxy and AS-4C/Epoxy specimens are quite similar. Both show "stepped" fracture surfaces, i.e. the fibres are broken in several planes perpendicular to the fibre axis. Interfacial failure is seen in both the AS-4/Epoxy and AS-4C/Epoxy specimens, however, the broken fibre pieces are closely held by the matrix material.

In summary, therefore, it has been shown that there was little change in the longitudinal flexural properties when the ISS was increased from the low to the intermediate values. Some improvement was noticed in both the flexural stiffness and strength when the ISS was increased from the intermediate to the highest levels. The improvement in the stiffness is attributed to the presence of the high-modulus interphase and that in the strength is attributed to the ability of the strong interface to suppress the interlaminar failure. The widespread interfacial failure evident in the fracture surfaces of the AU-4/Epoxy and AS-4/Epoxy specimens suggests the likelihood of the fracture initiated by the interlaminar failure in these specimens.

A comparison between the longitudinal tensile and longitudinal flexural properties is shown in Fig. 27. Both the tensile and flexural properties are similar and they show similar effects of the ISS, i.e. insignificant change in the properties due to change in fibre–matrix adhesion.

4.2.2 Off-axis properties

Average values of the off-axis properties for the three composite systems are listed in Table VII. Each entry in the table is an average from ten specimens.

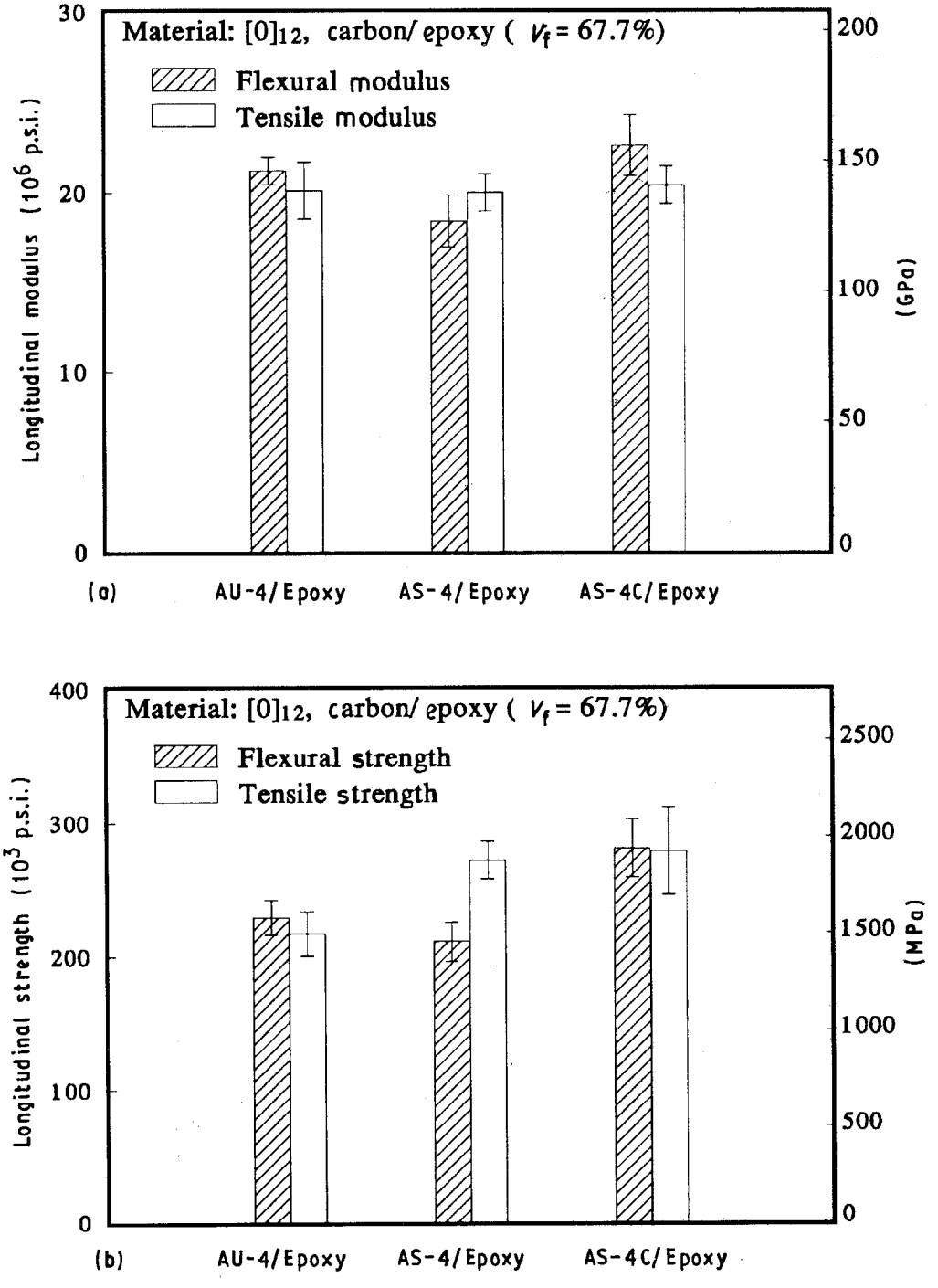

Figure 27 Comparison between the longitudinal tensile and flexural properties of the three types of carbon/epoxy composites: (a) longitudinal modulus and (b) longitudinal strength. Both methods yield similar values.

TABLE VII Summary of off-axis property results for carbon fibre/epoxy composites

Measurement	AU-4/Epoxy	AS-4/Epoxy	AS-4C/Epoxy
$[90]_{12}$ tensile modulus, E_{22} (GPa)	8.9 ± 0.6	9.8 ± 0.6	10.3 ± 0.6
$[90]_{12}$ tensile strength, σ^f_2 (MPa)	18.0 ± 3.9	34.2 ± 6.2	41.2 ± 4.7
$[90]_{12}$ flexural modulus, E_{2B} (GPa)	10.2 ± 1.5	9.9 ± 0.5	10.7 ± 0.6
$[90]_{12}$ flexural strength, σ^f_{2B} (MPa)	21.4 ± 5.8	50.2 ± 3.4	75.6 ± 14.0
$[\pm 45]_{3S}$ in-plane shear modulus, G_{12} (GPa)	9.1 ± 1.5	6.2 ± 0.5	6.0 ± 0.2
$[\pm 45]_{3S}$ in-plane shear strength, τ^f_{12} (MPa)	37.2 ± 1.8	72.2 ± 12.4	97.5 ± 7.4
Iosipescu in-plane shear modulus, G_{12} (GPa)	7.2 ± 0.5	6.4 ± 1.0	7.9 ± 0.4
Iosipescu in-plane shear strength, τ^f_{12} (MPa)	55.0 ± 3.0	95.6 ± 5.1	93.8 ± 3.3
Short-beam interlaminar shear strength, τ^f_{13} (MPa)	47.5 ± 5.4	84.0 ± 7.0	93.2 ± 3.8

4.2.2.1. $[90]_{12}$ tension. The transverse tensile moduli, E_{22}, were calculated from the slopes of the stress–strain curves between the strain range from 0.01% –0.2%. A comparison of the average transverse tensile moduli of the three types of composite systems is shown in Fig. 28. Like the longitudinal tensile modulus, the transverse tensile modulus is also relatively insensitive to the ISS. Only an increase of about 15% in the E_{22} corresponding to a 118% increase in the ISS is noted. Within the experimental scatter, this increase is insignificant.

Comparisons of average transverse tensile strength, σ^f_2, of the three types of composites is shown in Fig. 29. In spite of the large scatter in the transverse tensile data, a strong sensitivity of the ISS to the transverse tensile strength is seen. When the ISS is increased by about 83%, the transverse tensile strength increases by about 72%. For an additional increase in the ISS by about 19%, the strength is increased by 20%, Fig. 29. The mechanisms responsible for these changes are better understood from the failure modes and failure process that are examined below.

The photographs of the failed specimens, Fig. 30, show fairly clean fracture surfaces for the AS-4/Epoxy and AS-4C/Epoxy specimens. However, the fracture surfaces of AU-4/Epoxy specimens show extensive fibre–matrix separation. Examination of these fracture surfaces under the SEM shows different microfailure modes for these composites, Fig. 31. In the AU-4/Epoxy composite, the clean fibre surfaces indicate extensive interfacial failure. In addition, there is little matrix material between the fibres, i.e. the fibres are loosely held by the matrix material. The fracture surface of AS-4/Epoxy specimen shows bare fibres as well as fibres coated with matrix material. Unlike the AU-4/Epoxy specimen, the fibres in the AS-4/Epoxy specimen are held together by the matrix material, Fig. 31. Scattered fibre breaks are also seen in the fracture surfaces. The fibre breaks may have resulted when fibres were transversely pulled during the separation of the specimen. The fibre pulling was noticed in the AU-4/Epoxy specimens as well; however, the fibre breaks did not occur because the fibres were separated from the matrix before they could be broken. Because the matrix failure also occurs in addition to the interfacial failure in AS-4/Epoxy composites, it can be assumed that the interfacial strength has reached close to its optimum value beyond which

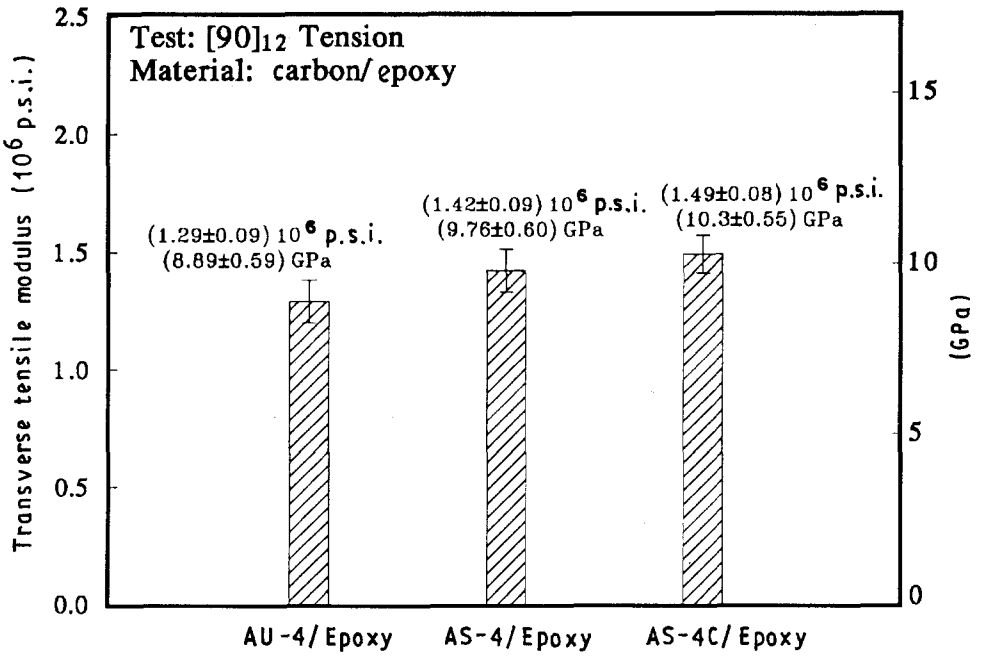

Figure 28 Comparison among the transverse tensile moduli of the three types of carbon/epoxy composites. All the three composite materials yield similar values.

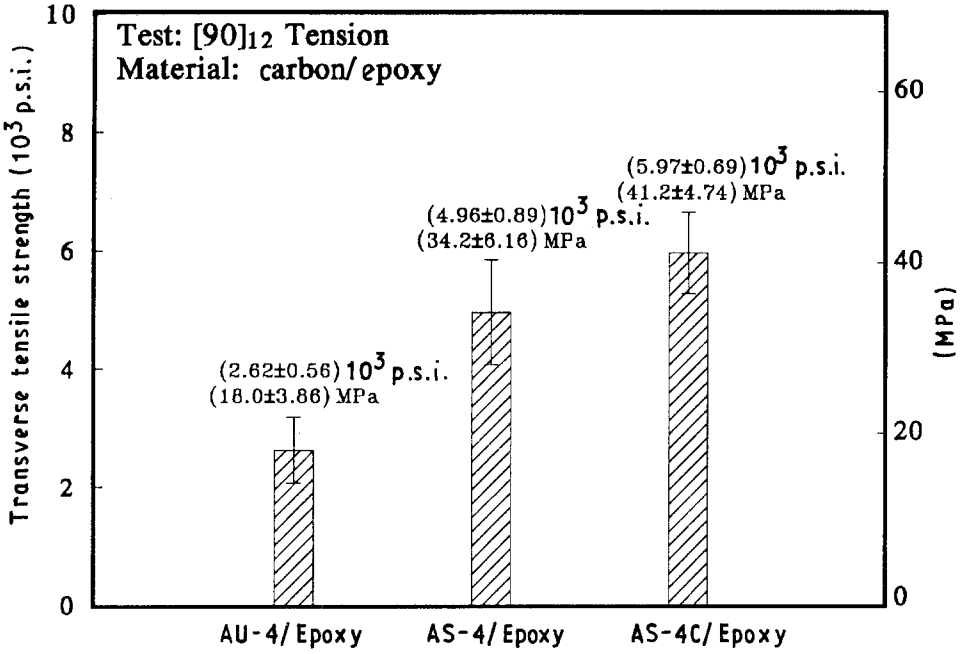

Figure 29 Transverse tensile strength of the three composite materials. In spite of the large scatter in the experimental data, a strong sensitivity of the ISS on the transverse strength can be seen.

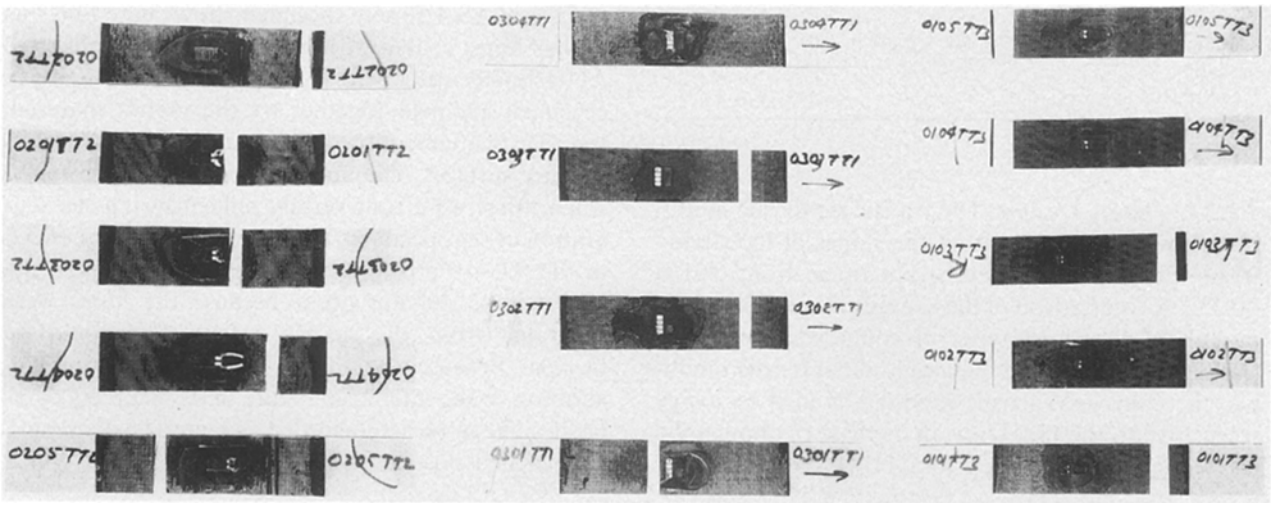

Figure 30 Effect of the ISS on the external appearances of the fractured carbon/epoxy $[90]_{12}$ tension specimens. Fibre–matrix separation is more evident in the composite having the low ISS (i.e. AU-4/Epoxy).

primarily matrix failure would be expected. For example, in the AS-4C/Epoxy composites, where the ISS is greater than that in the AS-4/Epoxy, the fracture surface shows significantly more matrix failure. Except at a few locations where fibres are bare, almost all the fibres are coated with matrix material. Fibre breaks also seem to occur more frequently. During the separation of each specimen, some fibres that are bridged between the two pieces of the specimen tend to be pulled by each broken piece of the specimen. Because of the strong interfacial bond, fibres are more easily broken than separated from the matrix.

4.2.2.2. $[90]_{12}$ three-point flexure. A comparison of the average transverse flexural moduli, E_{2B}, of the three types of composite systems is shown in Fig. 32. All three material systems yield similar values indicating little effect of the ISS on the transverse flexural modulus. The transverse flexural strength σ^f_{2B}, on the other hand, is highly sensitive to the ISS, Fig. 33. The percentage increase in the strength is even higher than the corresponding increase in the ISS. A 118% increase in the ISS yields about a 253% increase in the transverse flexural strength. The mechanisms causing these changes in the transverse flexural properties are explained from the fracture surface morphologies of the specimens from the three groups of composite materials.

The fracture surfaces of representative specimens from the three groups of composite materials are shown in Fig. 34. The tensile and the compressive sides

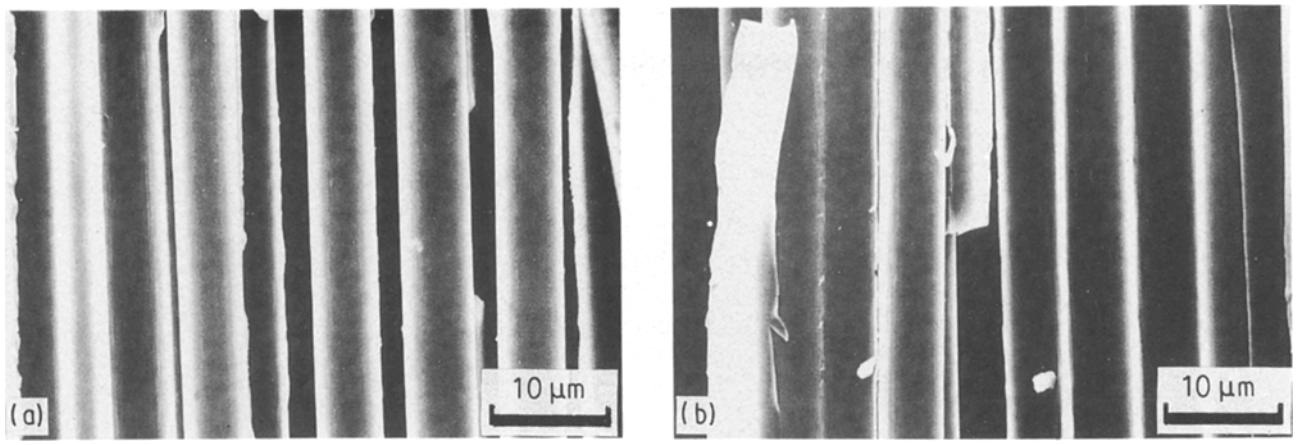

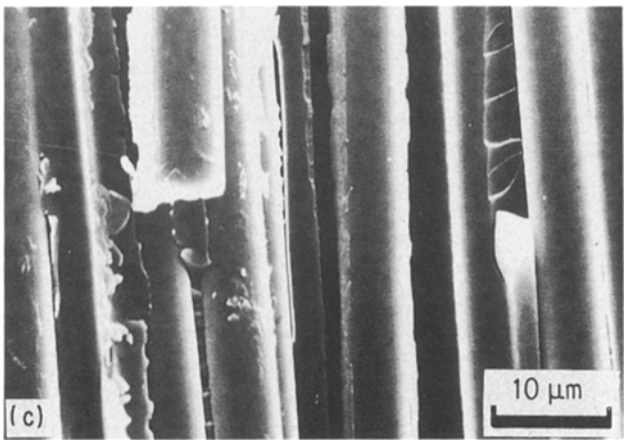

Figure 31 Effect of the ISS on the major failure modes of $[90]_{12}$ tension carbon/epoxy composites. The failure mode changes from interfacial to matrix when the ISS is increased from the low to the high values. (a) AU-4/828 mPDA, (b) AS-4/828 mPDA, (c) AS-4C/828 mPDA.

of these specimens showed little difference in their fracture surface morphologies. The AU-4/Epoxy specimen fractured entirely along the interface. Fibres are separated from each other with no matrix material around them. The AS-4/Epoxy specimen also shows significant interfacial failure. However, in addition to the interfacial failure, matrix failure is seen as well. In the AS-4C/Epoxy specimen, where the ISS is the highest, the primary failure mode is the matrix failure. Some interfacial failure can also be seen.

A strong sensitivity of the ISS on the transverse flexural strength should be expected because the bending stresses are directly borne by the interface and the specimen failure occurs either due to tensile (or compressive) failure of the interface or matrix or a combination of the two. The single-fibre fragmentation tests have indicated that the fibre surface treatment can have a strong influence on the interfacial shear strength. The transverse flexural test results indicate that the same surface treatment has even a stronger influence on the tensile (or compressive) strength of the interface. Therefore, the transverse flexural strength can be used as a much more sensitive indicator of the interfacial strength.

A comparison between transverse flexural and transverse tensile modulus and strength is shown in

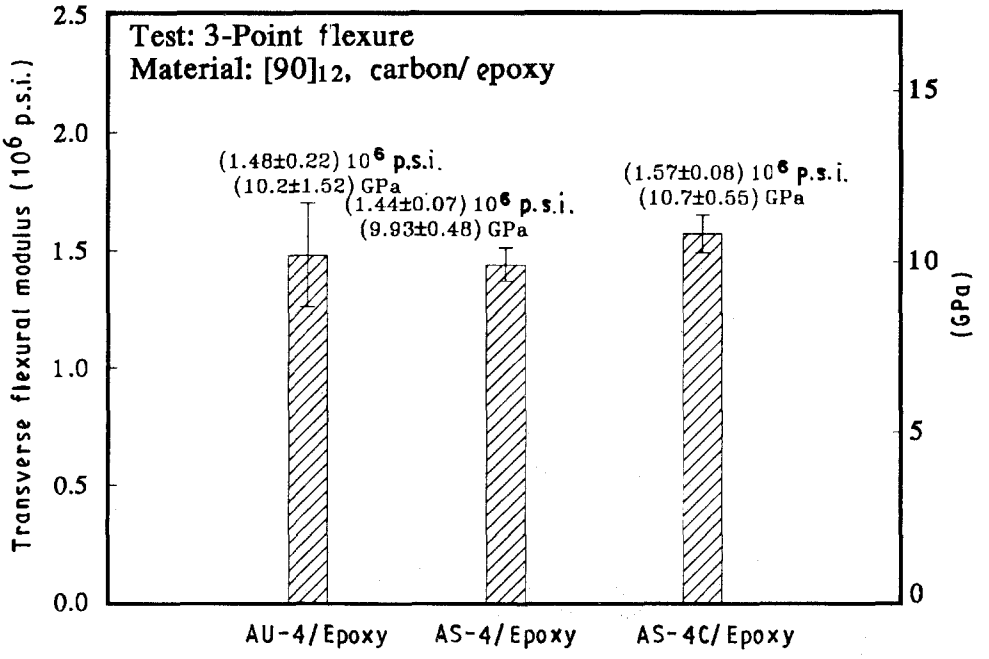

Figure 32 Transverse flexural modulus of the three types of carbon/epoxy composite materials. All the three materials yield similar values.

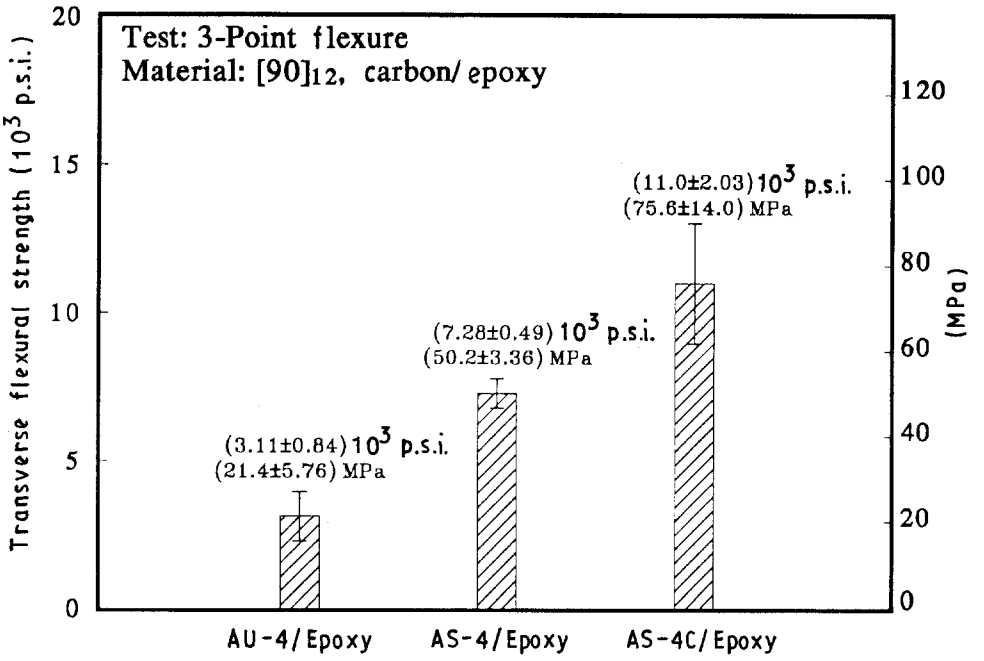

Figure 33 Transverse flexural strength of the three types of carbon/epoxy composite materials. The strength increases significantly with the ISS.

Fig. 35. While both the tensile and flexural moduli are similar to each other and are insensitive to fibre–matrix adhesion, there is a significant difference between transverse flexural and transverse tensile strengths. Not only that the transverse flexural strength is more sensitive than the transverse tensile strength to the ISS, it is much higher than the transverse tensile strength. The higher values and higher sensitivity of the transverse flexural strength compared to the transverse tensile strength can be explained by the non-uniformity of stress in the three-point flexure test. The maximum tensile stress exists only in the outer fibres at the mid-span of the beam in a three-point flexural test. While in a tensile test, the whole gauge section of the beam is subjected to a uniform tension. Because of the scatter in the strength, the probability of failure in a small volume of material at a given stress is lower than that in a large volume. Clearly, therefore, if the failure is governed by the probability of finding a critical flaw, the strength determined from a tension test where a much larger volume is critically stressed should be lower than the strength determined from a three-point flexure test. It should be noted, however, that in the case of longitudinal specimens (0°), both the tensile and flexural strengths were similar, Fig. 27. In the 0° case, the

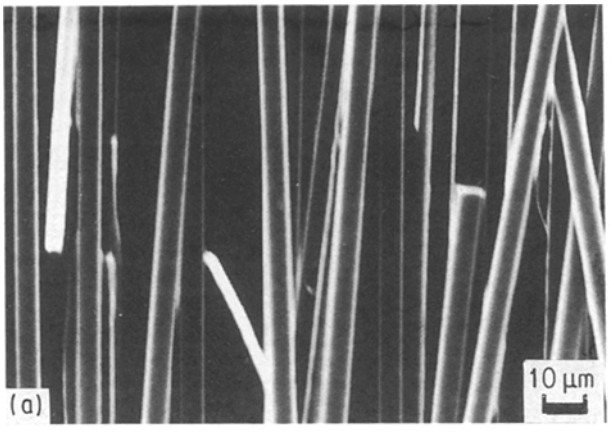

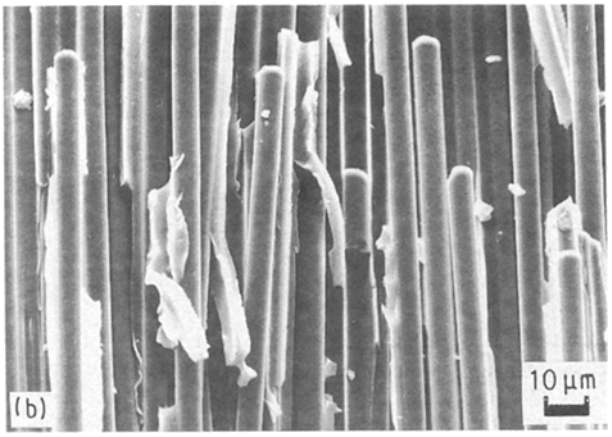

Figure 34 Effect of the ISS on the major failure modes of $[90]_{12}$, three-point flexure carbon/epoxy specimens. When the ISS is low, the failure mode is entirely interfacial. The higher values of the ISS yield matrix failure in addition to the interfacial failure. (a) AU-4/828 mPDA, spec. no. 0804FLT2, (b) AS-4/828 mPDA, spec. no. 1004FLT1, (c) AS-4C/828 mPDA, spec. no. 0304FLT3.

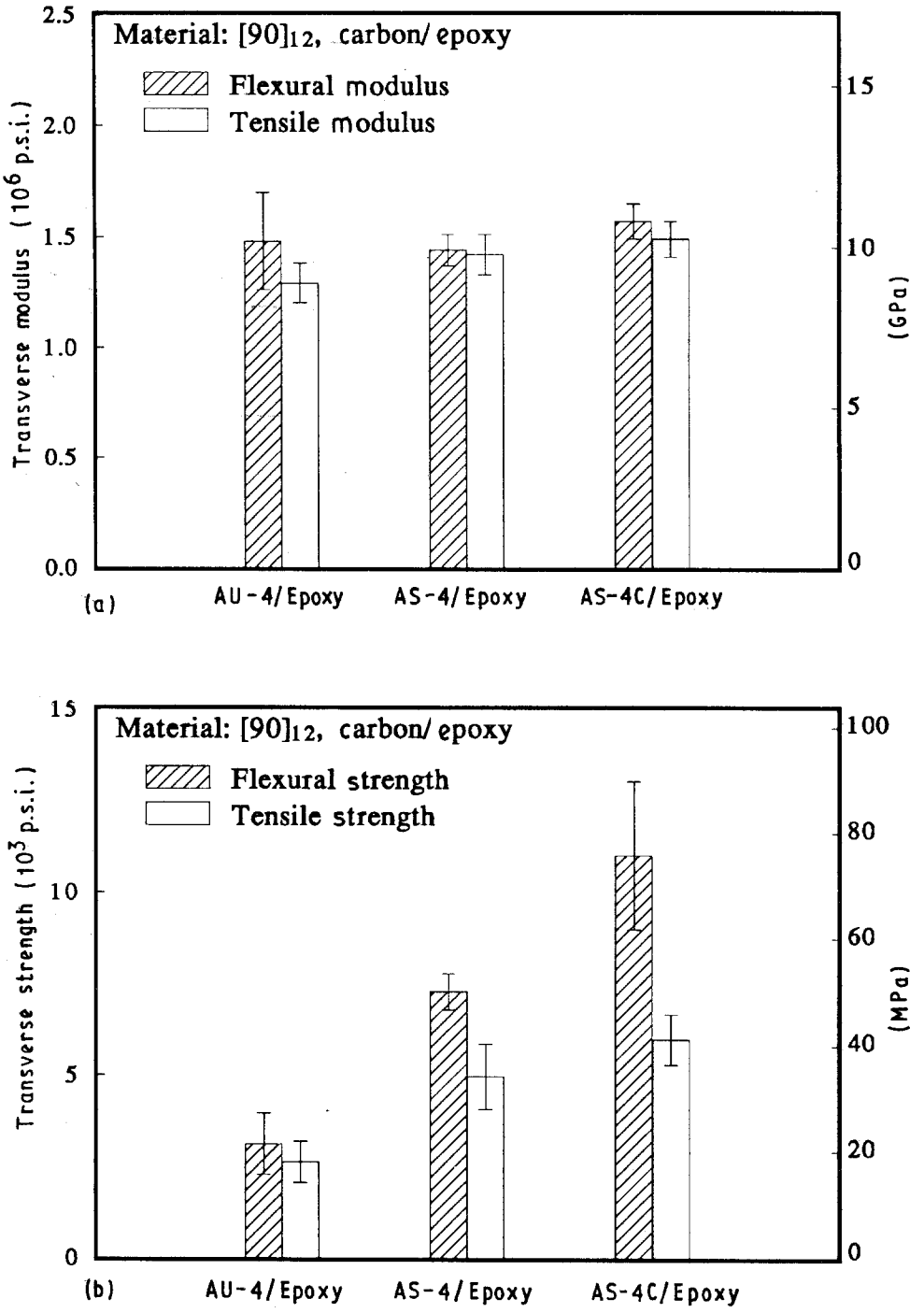

Figure 35 Comparison between the transverse tensile and flexural properties for $[90]_{12}$ carbon/epoxy composites: (a) transverse modulus and (b) transverse strength. Both methods yield similar values of the modulus but the flexural strength is much higher than the tensile strength.

stress concentration around a flaw is alleviated by matrix splitting or interfacial failure. Thus, the existence of greater probability of finding a flaw in a 0° tension specimen may not cause any reduction in the longitudinal tensile strength. In addition, the longitudinal tensile failure is not localized, rather it extends over the entire specimen, Fig. 13, whereas the transverse tensile failure is highly localized. Therefore, the effect of local flaws will be more pronounced on the transverse tensile strength than on the longitudinal tensile strength.

4.2.2.3. In-plane shear response – $[\pm 45]_{3s}$ tension test. The shear modulus of each specimen was calculated from the strain gauge readings in the shear strain range of 0.01%–0.10%. The average values of G_{12} for the three material systems are listed in Table VII, and the same values are plotted in Fig. 36. Unexpectedly, the shear modulus of the composite containing the untreated fibres (AU-4) is higher than for those containing the treated fibres. Intuitively, it would seem that if the fibre and matrix properties remained the same the shear modulus should not be significantly affected by the level of fibre–matrix adhesion, and if there is any effect, the modulus should have increased with an increase in fibre–matrix ISS. After fractographic examination of the set of samples, the following explanation is proposed as being responsible for this unusual behaviour.

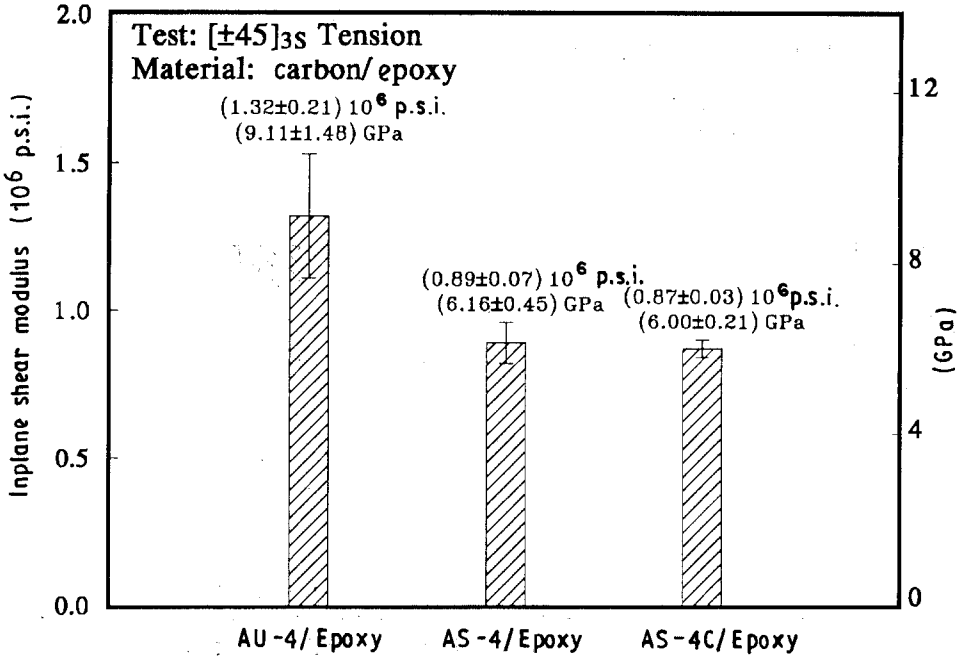

Figure 36 Inplane shear modulus determined from the $[\pm 45]_{3S}$ tension tests for the three types of carbon/epoxy composite materials. The higher modulus of the AU-4/Epoxy composite is believed to be due to the "scissoring" effect resulting in a "rigid-body" rotation of the 45° plies.

Under the uniaxial tensile stress on $\pm 45°$ specimens, each 45° ply will be under uniaxial tension. If there is poor adhesion between the adjacent plies, the moment caused by the uniaxial tensile stress will tend to cause a "scissoring" effect resulting in a "rigid-body" rotation between the plies. Therefore, in the AU-4/Epoxy specimens, which are characterized as having poor fibre–matrix ISS, there will be some rotation of different plies relative to each other at small applied tensile loads. Because the "rigid-body" rotation does not induce axial strain, due to the interply failure the measured strain values from the strain gauges applied at the outer plies will be smaller than for the case when there is no "rigid-body" rotation. Although this phenomenon has not been verified directly, some evidence to such an effect is provided by the fractured specimens.

The fractured specimens from each of the three groups of composite were encapsulated in epoxy so that the different layers of fibres separated during the fracture process are locked at their places. Subsequently, the specimens were cut in the fractured region and the surfaces perpendicular to the loading axis were exposed, polished and then examined under a microscope. The micrographs of these fractured surfaces of the representative specimens from three groups of composites are shown in Fig. 37. The different fibre layers in AU-4/Epoxy are distinctly separated, whereas in the AS-4/Epoxy and AS-4C/Epoxy specimens the different fibre layers show much less separation. Because, the fracture of $\pm 45°$ tension specimens is not a high-energy event, i.e. large strain energy is not released during the final fracture (such as that during the fracture of 0° tension of carbon/epoxy), the separation of plies could not have happened during the final fracture. Because of the poor fibre–matrix adhesion in the AU-4/Epoxy specimens, the individual $\pm 45°$ plies may separate at relatively low applied loads causing a "rigid-body" rotation between adjacent plies. The evidence for poor fibre–matrix adhesion in AU-4/Epoxy will be further revealed by the fracture surface examination by the SEM (to be discussed later).

In light of these arguments it is believed that the $\pm 45°$ tension test method for calculating the inplane shear modulus of composite having poor fibre–matrix adhesion may not be an appropriate test method. When different plies are separated due to poor ISS, the assumption used, that the shear stress along the $\pm 45°$ fibres is constant through the thickness may not be valid.

A comparison of the average in-plane shear strengths, τ_{12}^{f}, among the three composite systems is shown in Fig. 38. The in-plane shear strength is highly sensitive to the fibre–matrix ISS. For an increase of 118% in the ISS, the corresponding increase in the in-plane shear strength is 162%. It should be noted that separation of different plies in $\pm 45°$ tension test due to interply failure during the loading will not only affect the local strain measurements on the outer plies (such as in AU-4/Epoxy specimens), it will also reduce the load-carrying capacity of the composite. For such composites (AU-4/Epoxy) the $\pm 45°$ tension tests may yield lower values of in-plane shear strength.

The increase in the in-plane shear strength with the ISS is the result of different failure modes occurring in the three different groups of composites. The photograph of all the failed specimens is shown in Fig. 39. Most of the AS-4/Epoxy and AS-4C/Epoxy specimens failed near the end-tabs whereas the AU-4/Epoxy specimens failed away from the end-tabs. This observation once again reinforces the earlier finding that the poor bonding between the $+45°$ and $-45°$ plies in the AU-4/Epoxy specimens promotes a "rigid-body" rotation among different plies under uniaxial tensile loading. The end-tabs restrict this rotation in

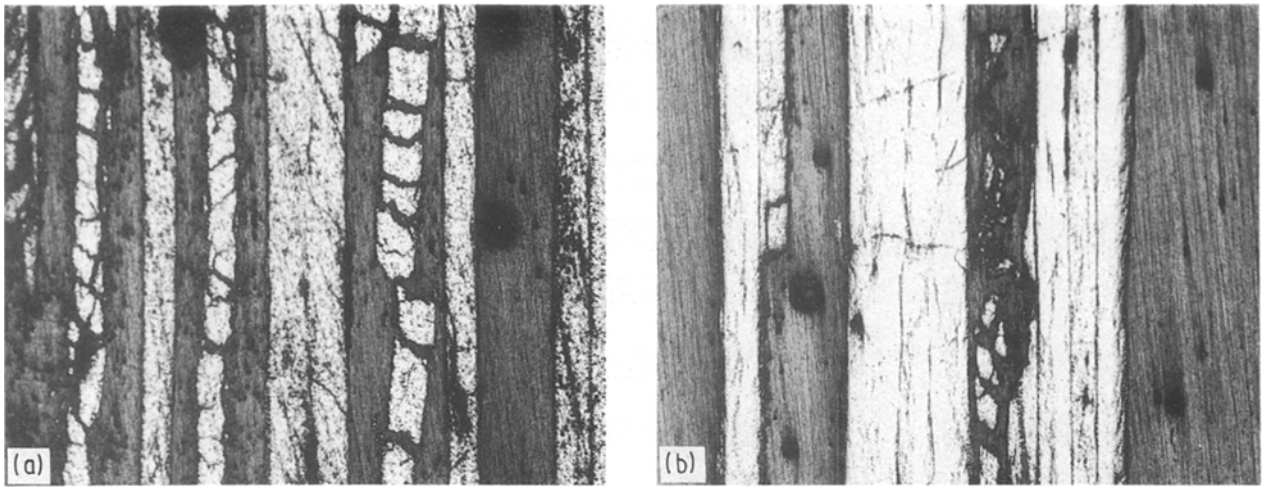

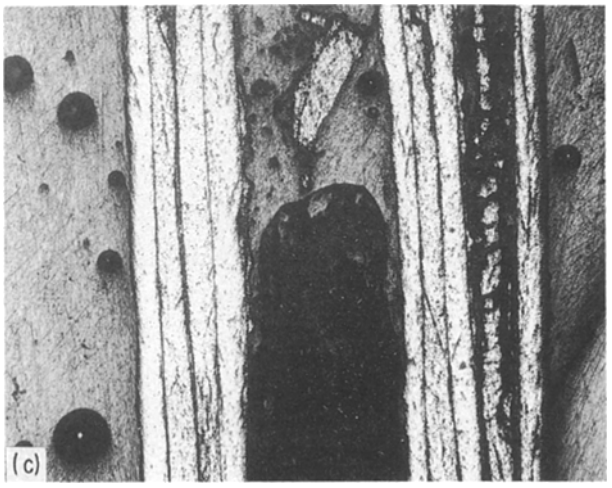

Figure 37 Micrographs of cross-sections of failed $[\pm 45]_{3S}$ tension specimens. Individual plies in the composite having low ISS (AU-4/Epoxy) are all separated indicating extensive interply failure, whereas in the other two cases the interply failure is not extensive. (a) AU-4/828 mPDA, spec. no. 1001TG2; (b) AS-4/828 mPDA, spec. no. 1103TG1; (c) AS-4C/828 mPDA, spec. no. 0504TG3.

their vicinity. However, in the regions away from the end-tabs where there is no additional support to the plies, the rotation of plies occur. With increasing applied load, these plies are pulled apart causing the failure of specimen, whereas in the AS-4/Epoxy and AS-4C/Epoxy specimens the strong level of adhesion prohibits the "rigid-body" rotation and, as a result, the specimens deform more uniformly across their length away from the end-tabs. In the vicinity of the end-tabs there are local stress concentrations causing the specimen failure to occur near the end-tabs.

The scanning electron micrographs of the fracture surfaces of the three types of composites are shown in Fig. 40. In the AU-4/Epoxy specimens where the fibres are untreated, the failure mode is entirely interfacial. The fibres are almost completely devoid of matrix. A "sheet" of matrix material with impressions of adjacent layers of fibres which can be seen at the upper right-hand side of photograph of the AU-4/Epoxy specimen indicates that a whole ply has been separ-

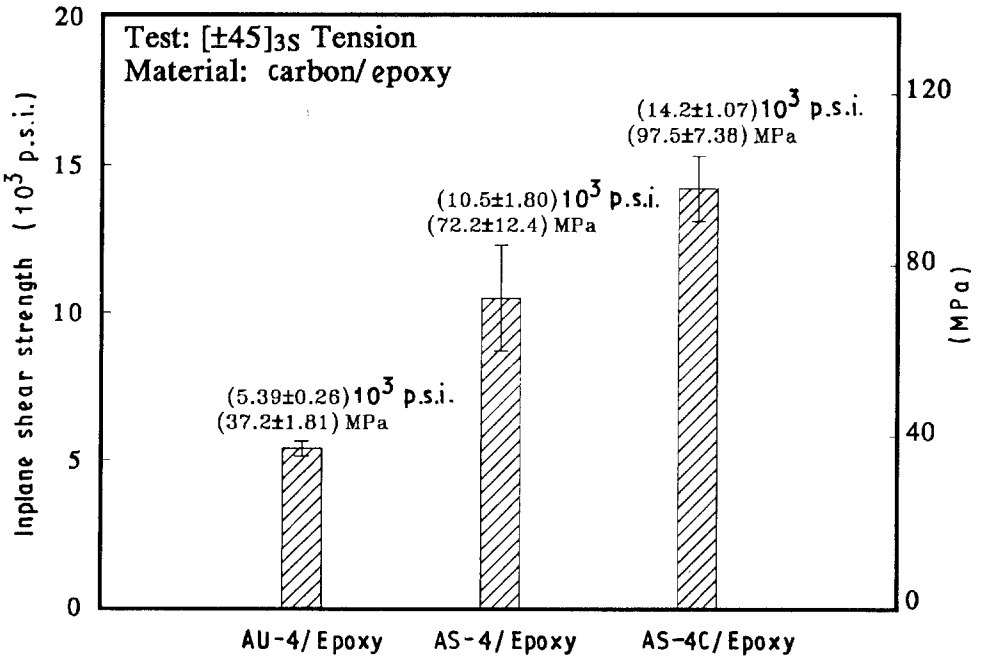

Figure 38 Average in-plane shear strength of the three types of carbon/epoxy composites. The shear strength is much higher for composite having higher ISS.

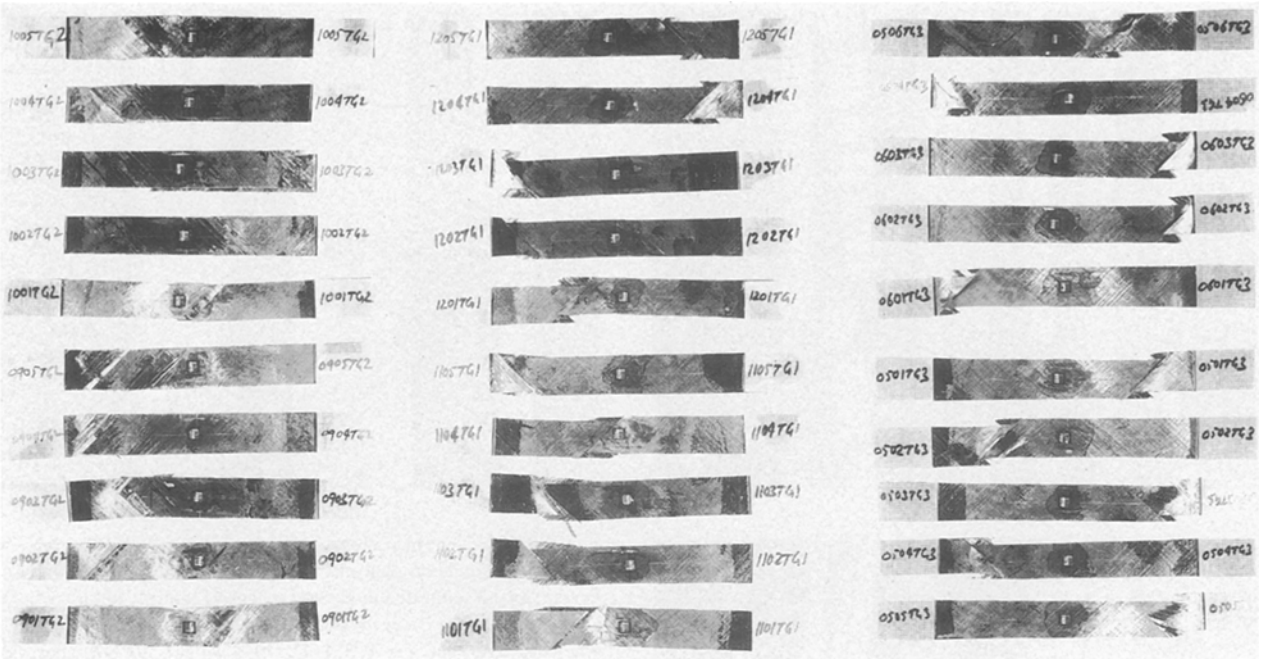

Figure 39 Photographs of the failed $[\pm 45]_{3s}$ tension specimens. Generally, the composites having high ISS (i.e. AS-4/Epoxy and AS-4C/Epoxy) fail near end-tabs whereas those having poor ISS (i.e. AU-4/Epoxy) fail away from end-tabs.

ated from the adjacent ply along the interface. The low ISS causes the interply failure along the interface resulting in a low shear strength of the composite. In the AS-4/Epoxy specimens where the fibres are surface treated, the major failure modes are interfacial and matrix failure; however, the interfacial failure is still more dominant. Because the ISS in the AS-4/Epoxy system is approaching the matrix shear strength [15], a combination of the interfacial and matrix failure modes is expected. Unlike in the AU-4/Epoxy specimens, the fibres in AS-4/Epoxy specimens are still held together by the matrix. In the AS-4/Epoxy specimens where the ISS is about twice as large as in the AU-4/Epoxy specimens, not only that the rotation between the adjacent plies is prevented by strong fibre–matrix adhesion, it also helps achieve a more

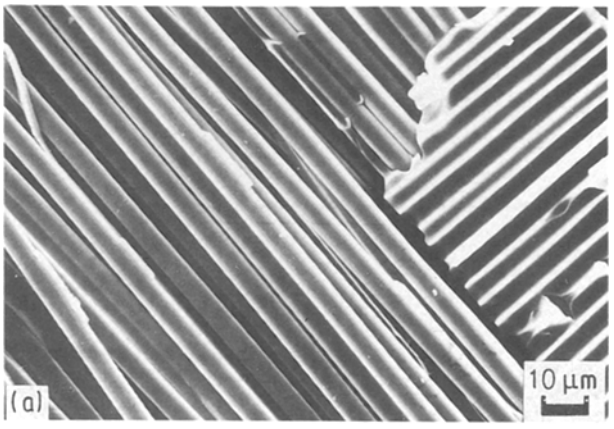

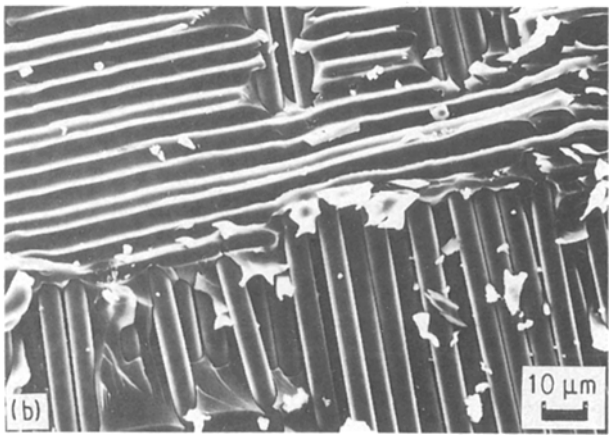

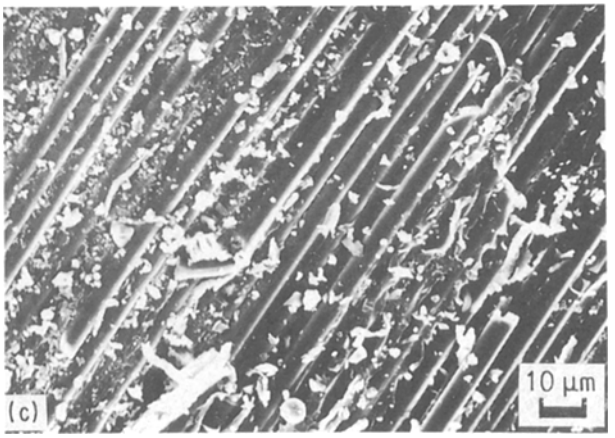

Figure 40 Effect of ISS on the fracture surface morphologies of the $[\pm 45]_{3s}$ tension specimens. As the ISS is increased from low to the intermediate to the high values, the failure modes change from interfacial to a combination of interfacial and matrix to primarily matrix failure, respectively. (a) AU-4/828 mPDA, spec. no. 0904TG2; (b) AS-4/828 mPDA, spec. no. 1105TG1; (c) AS-4C/828 mPDA, spec. no. 0505TG3.

uniform stress field. The high in-plane shear strength of AS-4/Epoxy composites is attributed to these two factors. In the AS-4C/Epoxy composites where the ISS is the highest, the dominant failure mode is the matrix failure. This should be expected because the ISS in AS-4C/Epoxy is larger than the matrix shear strength. In addition to the factors that are responsible for improving the in-plane shear strength of AS-4/Epoxy composites, the brittle interphase that is present around the AS-4C fibres [15] further helps in achieving more uniform stress transfer between adjacent fibres and between adjacent plies.

4.2.2.4. In-plane shear response – Iosipescu shear test. A summary of the results from the Iosipescu shear test is given in Table VII. The average inplane shear moduli for the three composite systems are shown in Fig. 41. Within the scatter band there is an insignificant effect of fibre–matrix ISS on the inplane shear modulus of graphite/epoxy composites. Considering that fibre and matrix properties remain unchanged, Table III, and assuming that interface quality is the same in all the three composite systems, i.e. there is complete adhesion between fibre and matrix in the three cases, and further assuming that there is no damage taking place within the shear strain range (0.01%–0.1%) used here to calculate the shear modulus, the strength of interfacial bond should not affect the elastic shear properties of the composite.

The average in-plane shear strengths of the three material systems are shown in Fig. 42. A sharp increase in the shear strength when going from

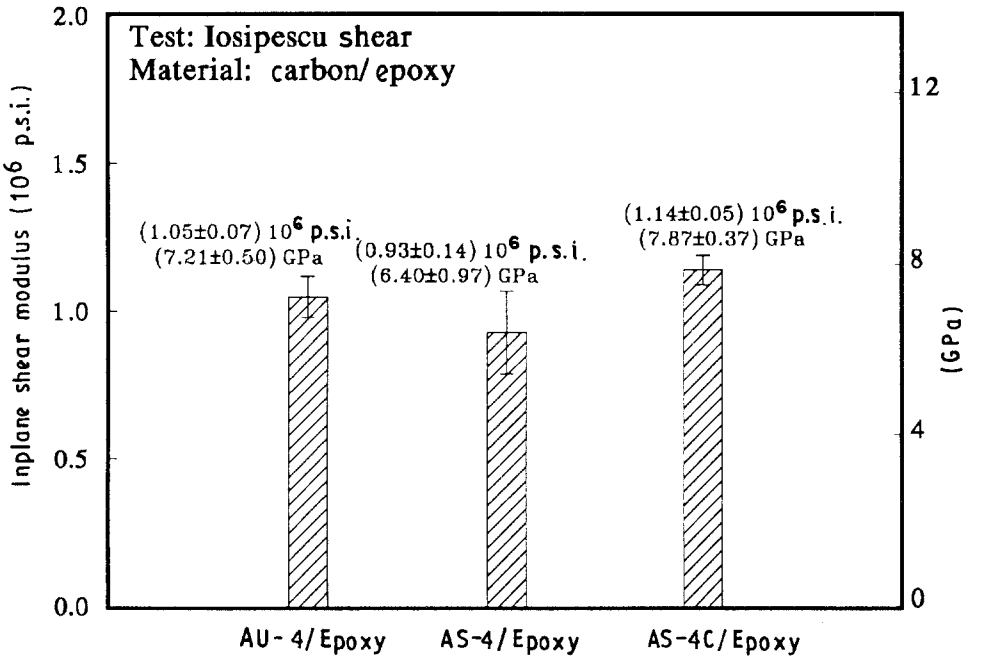

Figure 41 Average in-plane shear modulus determined from the Iosipescu shear test for the three types of carbon/epoxy composite materials. Within the scatter band the values of the shear modulus for all the three composite materials are similar.

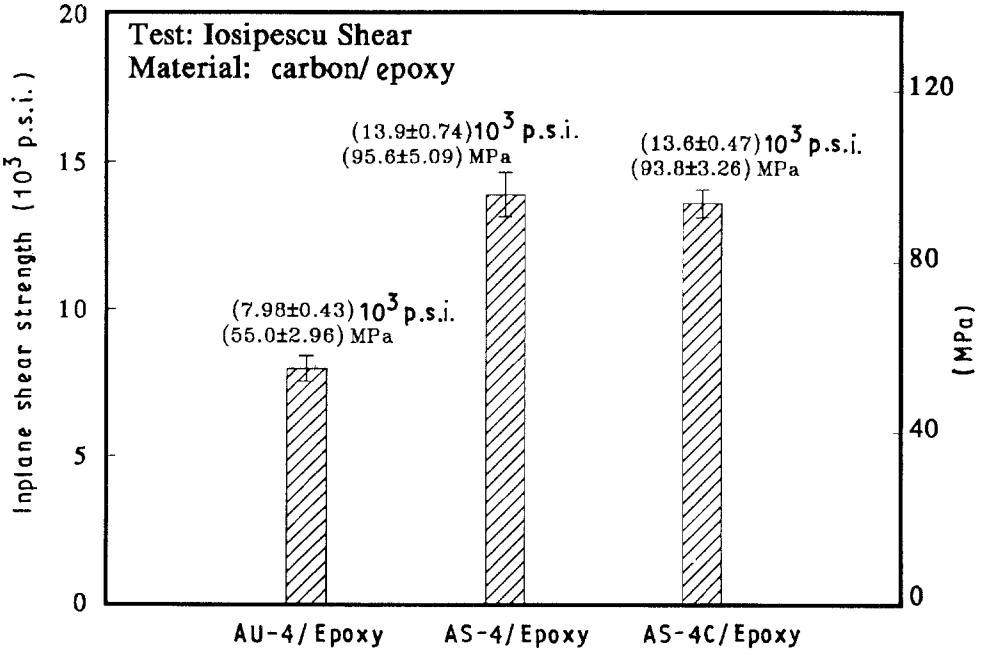

Figure 42 Average inplane shear strength determined from the Iosipescu shear test. The shear strength of the AS-4/Epoxy is much higher than that of AU-4/Epoxy; however, between AS-4/Epoxy and AS-4C/Epoxy there is not much difference in the strength.

AU-4/Epoxy to AS-4/Epoxy composites is evident. However, unlike as 45° tension tests, the in-plane shear strength calculated from Iosipescu shear test method does not register any further increase in going from AS-4/Epoxy to AS-4C/Epoxy composites. This difference between the results of two different test methods, both measuring the in-plane shear properties, is explained below from the examination of the failure modes occurring in these tests.

The failure of the Iosipescu shear test specimen occurs when a crack initiating at the notch root propagates parallel to the fibre axis and away from the notches resulting in a drop of the applied load. Representative specimens from each of the three groups of composite were carefully cut to expose the cracked surfaces. These cracked surfaces were examined under the SEM. The results are shown in Fig. 43. In the AU-4/Epoxy specimen the crack propagated almost entirely along the fibre–matrix interface. The interfacial failure can be seen in AS-4/Epoxy specimen as well; however, the significant amount of matrix debris indicates that failure mode is a combination of interfacial and matrix failures. In the AS-4C/Epoxy specimen there is almost no evidence of interfacial failure and the failure surface is relatively featureless (as typically seen in a brittle failure of materials) i.e. there is little matrix debris. Therefore, the failure mode in AS-4C/Epoxy specimen can be characterized as the brittle fracture of the interphase.

The sharp increase in the shear strength in going from AU-4/Epoxy to AS-4/Epoxy is obvious. The weak interface in the former does not provide much resistance to the crack front. The crack can easily propagate along the weak interface and as a result the composite exhibits poor in-plane shear strength. In the AS-4/Epoxy composites the interface is much stronger and the fibre matrix ISS is almost equal to the matrix shear strength. Clearly, therefore, both the failure modes (interfacial and matrix failure) should be expected and the composite's in-plane shear strength should increase approximately in the same ratio as the increase in the ISS (the in-plane shear strength increases by 74% for a corresponding increase in the ISS of 83%, Fig. 42). In the case of AS-4C/Epoxy composites the ISS is even higher but at the same time there exists a brittle interphase around AS-4C graphite fibres [15]. The additional increase in the ISS is not translated into the additional gain in the shear strength because the local stress concentration around the machined notch can cause a premature brittle failure of the interphase. As a result, the shear failure of the composite occurs prior to the full realization of the fibre–matrix ISS. In the case of $\pm 45°$ tension specimens, however, the in-plane shear strength increased even in the presence of the brittle interphase because in the $\pm 45°$ tension test no external phenomenon causing the stress concentration was present.

4.2.2.5. Interlaminar shear response – short-beam shear test. The short beam shear (SBS) test was used as a basis for comparing the apparent interlaminar shear strength (ILSS), τ^{f}_{13}, of the carbon/epoxy composites as a function of fibre–matrix adhesion. The average ILSS for the three composite systems are listed in Table VII and they are plotted in Fig. 44. The ILSS increases by about 77% for a corresponding increase in ISS of about 83%. Further increasing the ISS by 19%, the ILSS shows an additional increase of about 11%. A slight decrease in the rate of increase of ILSS with ISS in going from AS-4/Epoxy to AS-4C/Epoxy may suggest that almost full potential of the

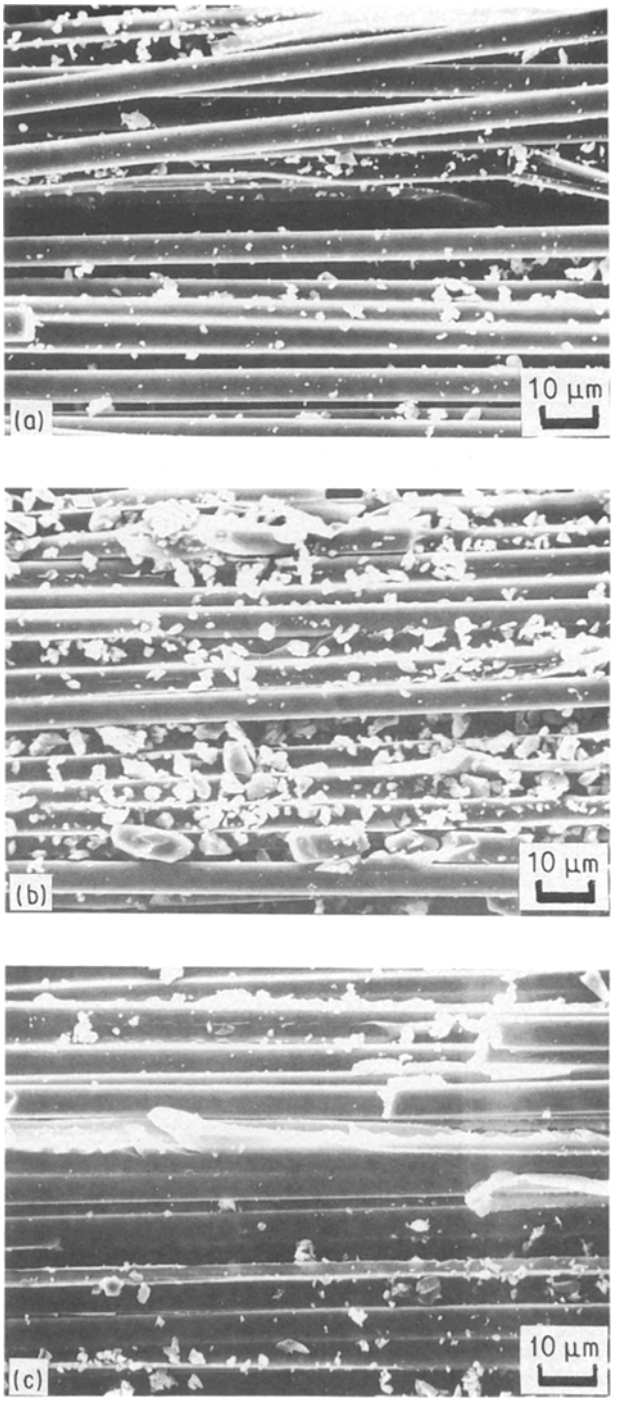

Figure 43 Effect of the ISS on the fracture surface morphologies of Iosipescu shear test specimens. As the ISS is increased from the low to the intermediate to the high values, the failure mode changes from interfacial to a combination of interfacial and matrix to failure of brittle interphase, respectively. (a) AU-4/828 mPDA, spec. no. 0802IO2; (b) AS-4/828, spec. no. 1303IO1; (c) AS-4C/828 mPDA, spec. no. 0305IO3.

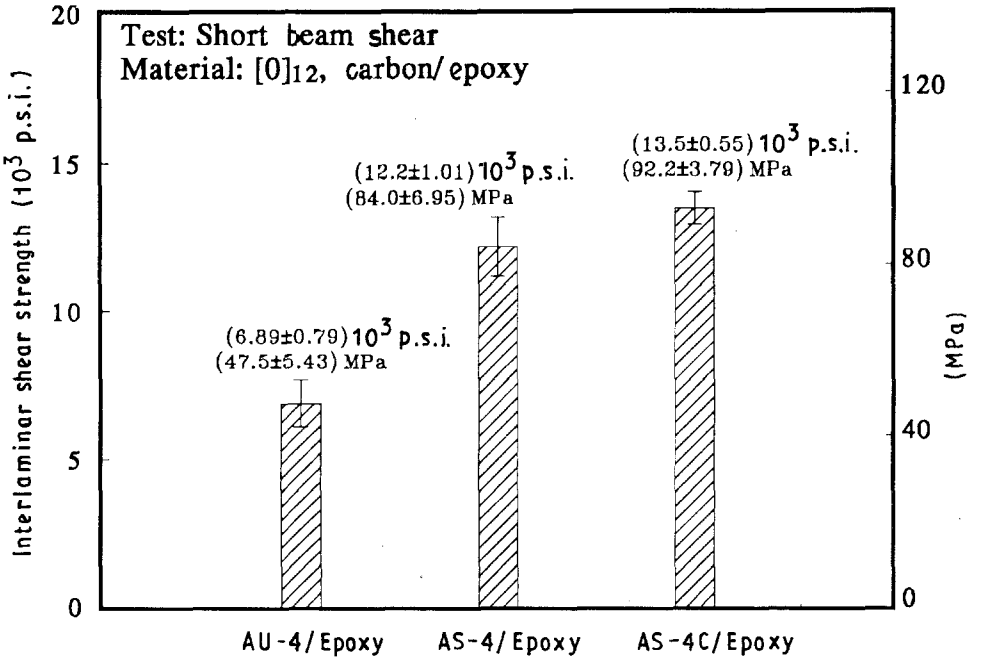

Figure 44 Average interlaminar shear strength for the three composite materials. The shear strength increases with increasing ISS.

fibre–matrix interface may have already been utilized in the AS-4/Epoxy composites and therefore further strengthening the interface (as in AS-4C/Epoxy composites) will drive the interlaminar failure to occur in the matrix resulting in only a marginal improvement in the ILSS.

A strong relationship between ISS and ILSS should be expected considering that the data from both the single-fibre test (for calculating the ISS) and the SBS test (for calculating ILSS) are a relative measure of the same component of the shear stress (i.e. τ_{13}). The absolute values of ILSS and ISS, however, do not agree very well, Table III and Table VII. This is not surprising considering the nature of differences in the two tests and the different equations and simplifying assumptions used in these two different methods. In the single-fibre test the ISS is related to the tensile strength of the embedded fibre [4] whereas in the SBS test the ILSS is determined from the maximum shear stress equation derived from the beam theory. When the midplane shear stress in the SBS specimen exceeds the interfacial shear stress or the matrix shear stress, whichever is smaller, the interlaminar failure is assumed to occur. In practical situations, however, the SBS specimens often show a combination of failure modes, such as delamination in several planes across the specimen depth, local crushing of the specimen by the loading pin, bending failure, etc. In addition, even the slight non-uniformities in the boundary conditions across the loading pin would destroy the symmetry of the deformed shape of the specimen resulting in a non-uniform state of shear stress. The ILSS values calculated from the SBS test method provide only a qualitative comparison of the interlaminar shear strengths of the three composite systems.

The results obtained from different shear test methods are compared in Figs 45 and 46. With regard to the in-plane shear modulus, whereas the Iosipescu shear test yields similar values for all the three composite systems, the $\pm 45°$ tension test yields similar values only for the composites having intermediate and high values of ISS, Fig. 45. For the case of a composite having low ISS, the $\pm 45°$ tension test gives much higher values of shear modulus. As explained earlier, the "scissoring" effect was believed to occur in the $\pm 45°$ tension tests when the adhesion between fibre and matrix was poor, thus resulting in erroneous readings of both shear modulus and shear strength. Because all the plies are oriented at the same angle in the Iosipescu shear specimens, the "scissoring" effect is not present. Therefore, the Iosipescu shear test yields similar modulus values for all three composite materials.

In the case of shear strength, the results obtained from the Iosipescu shear test method have the least scatter of the three tests, Fig. 46. Taken individually, the $\pm 45°$ tension test indicates that the composite shear strength rises with increasing ISS. Both the Iosipescu and short-beam shear tests register increasing composite shear strength rise with the intermediate level of adhesion sample in parallel with the $\pm 45°$ tension test, but level off or slightly decrease for the composite with the highest level of adhesion. This was explained earlier by the different failure mode produced by the samples with the highest level of adhesion. Both the Iosipescu and short-beam shear specimens fail prematurely under matrix-failure dominated conditions while the $\pm 45°$ tension specimen is not sensitive to this failure mode change.

Finally, with regard to the appropriateness of these different test methods for determining the shear properties, it can be said that when the level of adhesion between fibre and matrix is not known the Iosipescu shear test method should be used for the determination of shear modulus, because the $\pm 45°$ tension test can cause a "scissoring" effect in composites having

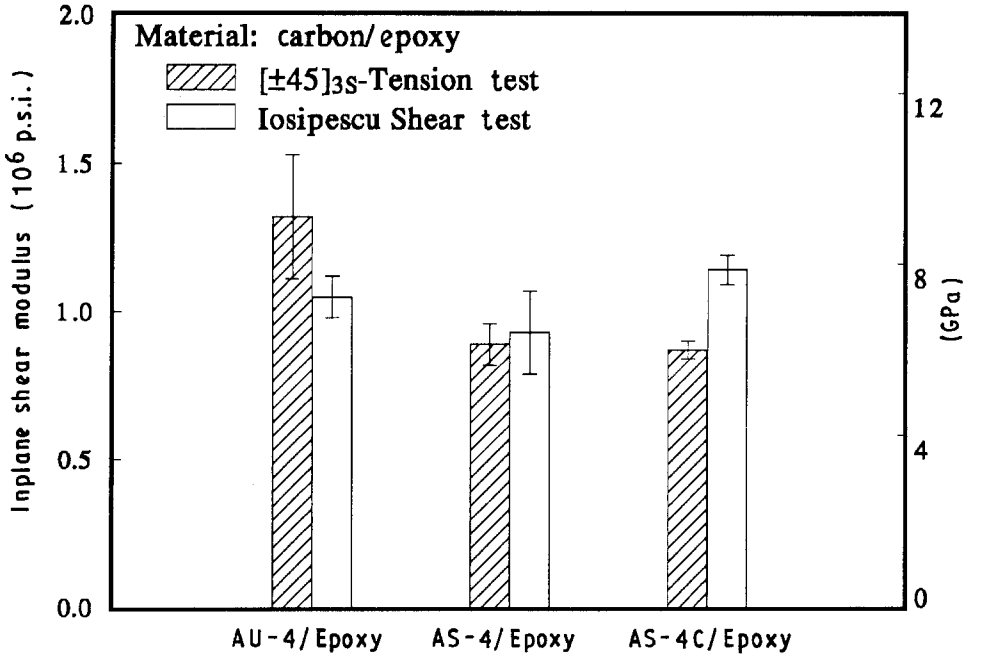

Figure 45 Comparison between the inplane shear modulus determined from the $[\pm 45]_{3S}$ tension and Iosipescu shear test methods. The results from the two methods differ significantly when the interface is either too weak or too strong (and brittle). For intermediate values of the ISS the two methods yield similar values.

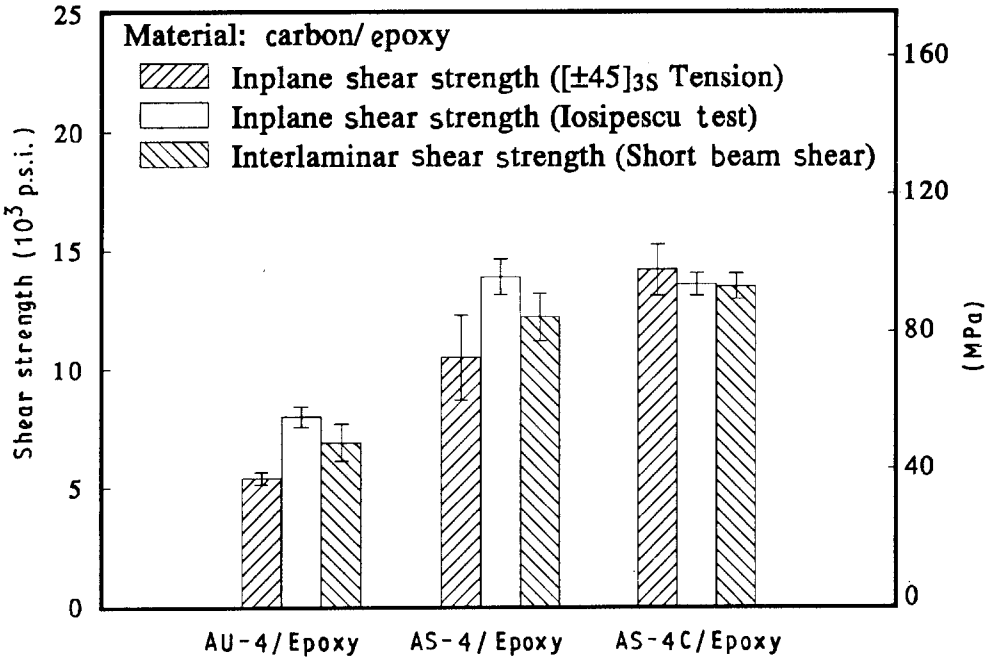

Figure 46 Comparison of the shear strengths determined from the three different test methods. When the fibre–matrix interphase is not brittle, the Iosipescu shear test yields the higher shear strength. The interlaminar shear strength is closer to the in-plane shear strength determined from the Iosipescu shear test method.

poor ISS. For the shear strength, none of the tests used give results that are clearly characteristic of composite shear strength for all values of ISS or interfacial failure mode. It is shown that the "scissoring" effect in the composites having poor ISS in the $\pm 45°$ tension tests, and the effect of stress concentration at the notch-tip of Iosipescu shear specimens of composites having a brittle interphase can result in lower in-plane shear strength values. Therefore, for a proper interpretation of the in-plane shear strength data from either of the two test methods, an understanding of the fibre–matrix adhesion level and the interfacial failure modes is essential. The interlaminar shear strength values are similar to the in-plane shear strength values, thus the short-beam shear test method can also be used as a relatively easier "screening" tool for evaluating composite adhesion properties.

4.2.3. Fracture toughness characterization

The Mode I and Mode II testing was performed using the double cantilever beam (DCB) and end-notched flexure (ENF) test methods, respectively. The geometry and dimensions of the DCB and ENF specimens are shown in Figs. 4i and j, respectively. Each

specimen consisted of 24 plies and contained a starter crack generated by the inclusion of a 38 mm (1.5 in) wide and 0.02 mm (0.79×10^{-3} in) thick Teflon-coated plain weave fibre glass fabric in the mid-plane of the composite along one edge during fabrication. The DCB specimens contained a double layer and the ENF specimens contained a single-layer Teflon-coated fabric. Insertion of the Teflon-coated fabric created a "resin-pocket" ahead of the insert. Fig. 47 shows the micrographs of these "resin-pockets" in the DCB and the ENF specimens. Metallic hinges were bonded on the cracked end of DCB specimens to allow unrestrained rotation at that end during the line load introduction. One side of each specimen was painted white to enhance observation of crack growth on a closed circuit television (CCTV) monitor via a microscope. Edges of the DCB specimens were marked at 10 mm increments for visual crack growth determinations. Whenever the crack reached one of these marks during the DCB testing, the specimen was unloaded to zero load and then reloaded until the crack extended to the next mark. All the tests were conducted in a displacement-controlled mode on a servohydraulic MTS-880 machine at a crosshead displacement rate of 2mm min^{-1}. The crack opening displacement (COD) in the DCB specimens was measured by a 50 mm (2 in) gauge length extensometer (model MTS-632.25B-20) as well as by the crosshead displacement. The mid-point deflection in the ENF specimens was monitored by means of crosshead displacement only. The summary of results is listed in Table VIII.

4.2.3.1. Mode I fracture toughness (DCB tests). The DCB test provides a direct approach for determining interlaminar Mode I fracture toughness, G_{IC}. Because the DCB test is conducted in a displacement-controlled loading, it yields a stable crack growth which makes it well suited for energy release rate measurements. The DCB test simulates the delamination growth by interlaminar normal (peel) stress. To calculate the G_{IC} for each specimen, the elastic beam analysis method was employed. The average G_{IC} for the different composite systems are listed in Table VIII. The values of the G_{IC} for the composites having the untreated AU-4 fibres could not be determined, because in all these specimens extensive "fibre-nesting" occurred during loading. Fig. 48 shows photographs of representative specimens from the three types of composite. In all the AU-4/Epoxy DCB specimens, not only is there extensive "fibre-nesting" but also the crack growth is not self-similar, Fig. 48. In addition, the crack extension did not occur smoothly in these specimens, i.e. the crack progressed in "jumps". Also, because of the extensive "fibre-nesting", the applied load continued to increase even during the crack growth process. The problem with the interpretation of the DCB test results for the composites having untreated fibres has also been reported for glass/epoxy composites. In the untreated glass/epoxy laminates, separation of adjacent plies during the DCB testing created a double delamination situation [21]. To account for this situation, the calculated values of the interlaminar fracture energy were divided by two for these untreated glass/epoxy laminates [21]. In the case of untreated AU-4/Epoxy graphite/epoxy composite, however, the problem was not because of the multiple delamination situation, but meandering of the crack through several planes. In such a case, it is not possible to account for the different energy absorbing mechanisms during the crack propagation.

Some "fibre-nesting" was noted in the AS-4/Epoxy and AS-4C/Epoxy composites as well, but the extent of it was much less and the crack growth was self-similar and stable. The average values of the G_{IC} for the AS-4/Epoxy and AS-4C/Epoxy are listed in Table VIII. The table also shows the G_{IC} for the epoxy matrix. The G_{IC} of the composites is about two to three times higher than that of epoxy itself. Similar ratios have been reported for other composite systems containing brittle matrices [22].

The average values of the G_{IC} for the AS-4/Epoxy and AS-4C/Epoxy are plotted in Fig. 49. For about 19% increase in the fibre–matrix ISS (see Table III), the G_{IC} increases by about 17%. It is interesting to note that the sensitivity of the G_{IC} is similar to that of transverse tensile strength, σ_2^f. For the 19% increase in the ISS, σ_2^f improved by about 20%. The similarity

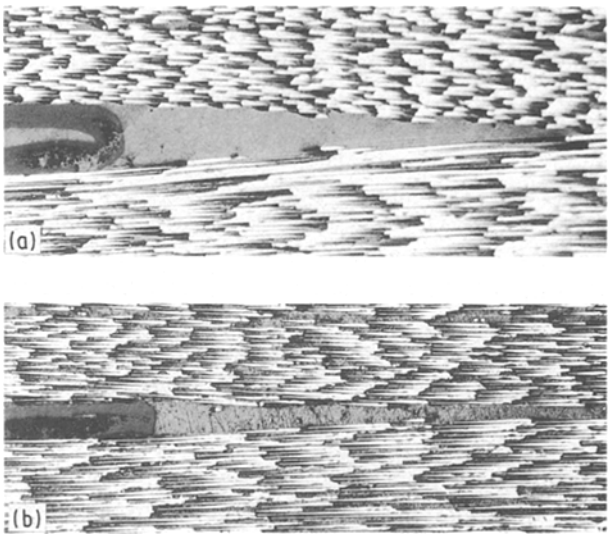

Figure 47 Photographs of the "resin-pockets" ahead of the starter cracks in the DCB and ENF specimens. (a) Mode I, (b) Mode II.

TABLE VIII Summary of Mode I and Mode II fracture toughness results for $[0]_{24}$ carbon fibre/epoxy composites

Measurement	AU-4/Epoxy	AS-4/Epoxy	AS-4C/Epoxy	Epoxy
Mode I fracture toughness, G_{IC} (kJm^{-2})	Could not be measured	0.33 ± 0.02	0.39 ± 0.03	0.13[a]
Mode II fracture toughness, G_{IIC} (kJm^{-2})	0.40 ± 0.08	1.04 ± 0.17	1.15 ± 0.13	

[a] The epoxy value was calculated from K_{IC} given in [13] $G_{IC} = K_{IC}^2(1 - \nu^2)/E$ where $E = 3.6$ GPa, $K_{IC} = 0.73$ MPa $m^{1/2}$ and $\nu = 0.35$.

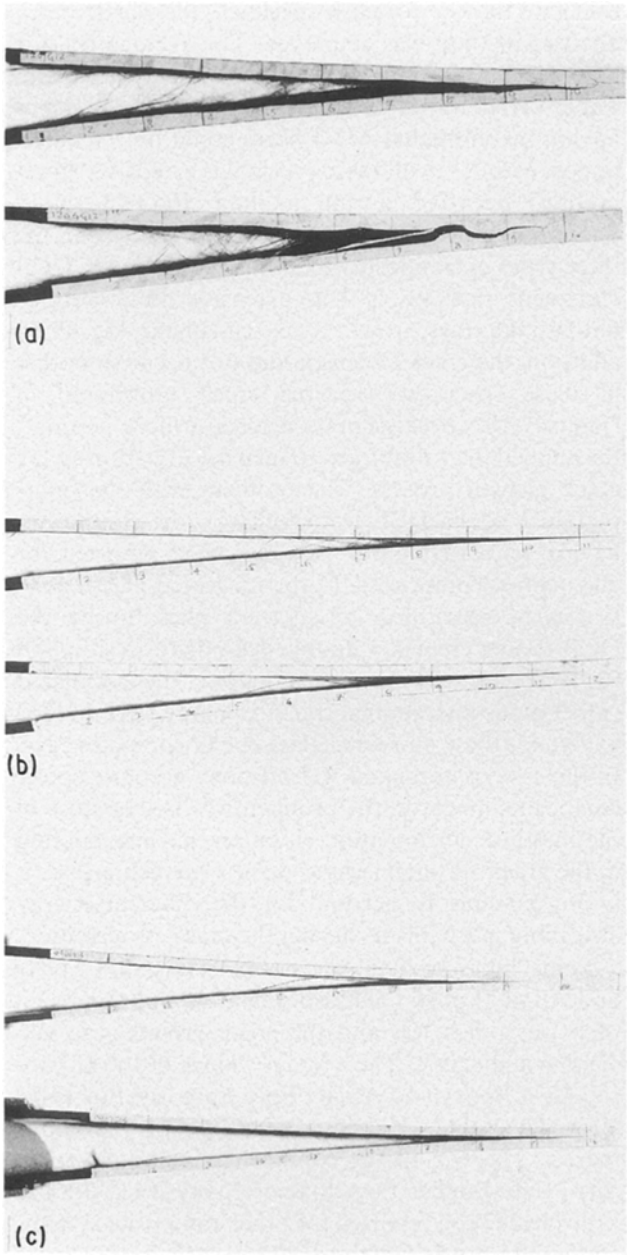

Figure 48 Photographs of the representative specimens showing significant "fibre-nesting" and crack meandering for AU-4/Epoxy specimens and only limited "fibre-nesting" in the other composite specimens. (a) AU-4/828 mPDA graphite/epoxy; (b) AS-4/828 mPDA graphite/epoxy; (c) AS-4C/828 mPDA, graphite/epoxy.

in the sensitivities of G_{IC} and σ_2^f to the ISS should be expected, considering that the peel stress (or transverse tensile stress) dominates in both the cases. The fibre–matrix ISS of the AS-4C/Epoxy is about 19% higher than that of the AS-4/Epoxy, and in addition the graphite fibres in the former are surrounded by a thin interphase that has lower fracture toughness than the bulk matrix [15]. There may be two opposing mechanisms at work in the AS-4C/Epoxy composites. The improved fibre–matrix adhesion in the AS-4C/Epoxy should provide increased resistance to delamination growth, but the presence of the brittle interphase may tend to lower the delamination fracture toughness of these composites. Because the G_{IC} of the AU-4/Epoxy could not be determined, the relative contribution due to the increased fibre–matrix adhesion alone on the G_{IC} is not known. However, because there is a net increase in the G_{IC} of AS-4C/Epoxy, the effect of increased fibre–matrix adhesion must be more dominant than that of the brittle interphase.

The fracture surface morphologies of the representative specimens from the three groups of composites were examined by the SEM. The results show substantial differences in the morphology of the fracture surfaces as a function of fibre–matrix adhesion, Figs 50 and 51. The evidence of extensive "fibre-nesting" in the composite having the lowest ISS (i.e. AU-4/Epoxy) is once again seen from the loosely held fibres that are lying in random directions. The fibres are completely devoid of matrix indicating extensive fibre–matrix interfacial failure, and there is no well-defined crack plane.

In the fracture surface of AS-4/Epoxy composites there is evidence of interfacial failure, matrix failure, fibre breaks, and fibre pull-out. Although the ISS of AS-4/Epoxy is about 1.8 times that the AU-4/Epoxy (see Table III), the interfacial failure is still significant in the former. However, some amount of resin remains on the exposed fibre surfaces indicating matrix failure as well. The matrix failure appears to be of brittle type with little features. The fibre breaks seen in the micrographs of the AS-4/Epoxy may have occurred due to breaking of the nested fibres during the opening of the two cracked faces. The micrograph also shows channels about four to five fibre diameters wide and about two to three fibre diameters deep that may have been left by fibre pull-out. The presence of these two to three fibre diameter deep channels suggests that the crack did not always remain in the mid-plane, but in some instances at certain places the adjacent plies were also involved.

In the AS-4C/Epoxy which is characterized as having the highest ISS, the relevant features in the fracture surface are the matrix fracture with hackle markings at some places, limited interfacial failure, few fibre breaks, and fibre pull-out. Because of the increased fibre–matrix adhesion in the AS-4C/Epoxy, there is only a limited amount of interfacial failure. Except at some places, most of the fibres are well coated with matrix material, indicating strong fibre–matrix adhesion. The presence of both the matrix failure and interfacial failure suggests that the interfacial shear strength has already approached its maximum value for it to be effective in increasing the fracture toughness of the composite. The hackle marks in the matrix material seem to appear on the periphery of individual fibres. The origin of these hackle marks is attributed to yielding at the periphery of individual fibres or fibre bundles during fibre pull-out [23]. The clean matrix fracture (without hackle marks) at some places suggests brittle fracture of matrix. Fibre pull-out has also taken place leaving behind clean channels of matrix material. However, unlike in the AS-4/Epoxy, the matrix channels in the AS-4C/Epoxy are only about one fibre diameter deep suggesting that the crack propagation occurred primarily in the mid-plane.

In summary, therefore, the dominant micromechanical event responsible for the increased Mode I fracture toughness of AS-4C/Epoxy compared to that of

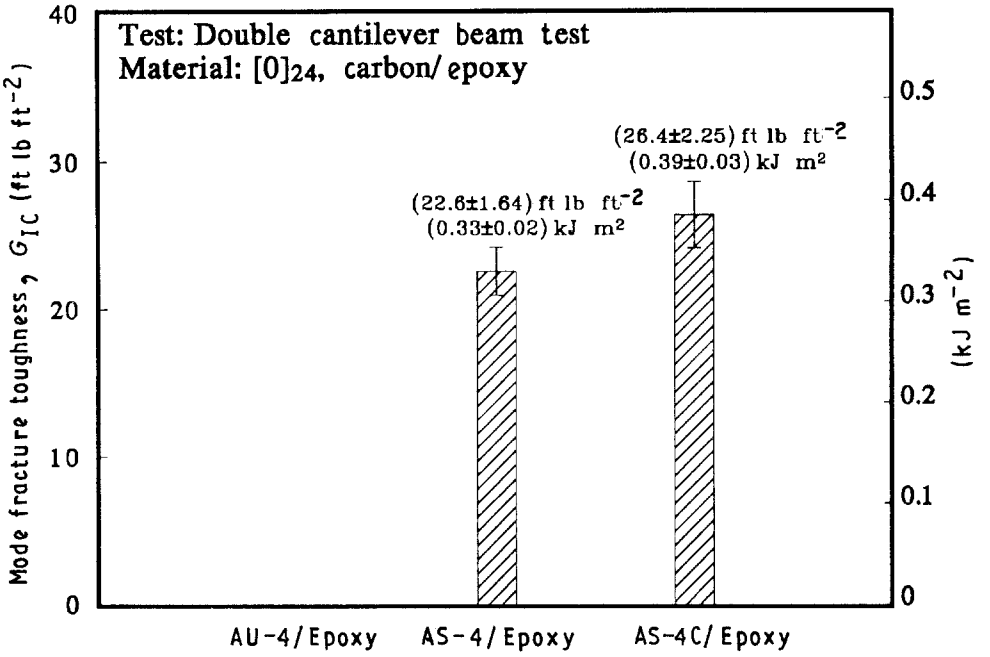

Figure 49 Mode I fracture toughness, G_{IC}, for the different composite materials. The G_{IC} for the AU-4/Epoxy could not be determined because of extensive "fibre-nesting" and crack meandering. The composite having higher ISS has higher G_{IC}.

the AS-4/Epoxy is increased matrix deformation resulting from the improved fibre–matrix adhesion. Although the AS-4C fibres are surrounded by the low fracture toughness interphase, the gain in the composite fracture toughness from the improved adhesion is larger than the loss resulting from the brittle interphase. Thus even in the composite system having highly cross-linked brittle epoxy system, the interfacial strength must be increased to a sufficiently high level in order to maximize the composite interlaminar fracture toughness.

Turning now to the correlation between composite and matrix fracture toughness, the degree of translation of matrix toughness into interlaminar fracture toughness of composite depends on matrix toughness. The G_{IC} of composite having brittle matrices (such as unmodified highly cross-linked epoxy systems) is noted to be higher than that of the bulk matrix, whereas the G_{IC} of composites having tougher matrix (such as elastomer-modified epoxies and thermoset matrices) is lower than that of the bulk matrix [22, 24–27]. In the case of composites containing brittle matrices (having the fracture toughness in the range 60–150 Jm^{-2}), the G_{IC} of the composite is about two to three times higher than that of the bulk epoxy. The data generated in this study on AS-4/Epoxy and AS-4C/Epoxy composites show a similar relationship between the fracture toughness of composite and bulk matrix (Table VIII).

This observation suggests that resin fracture toughness is fully transferred to the composite. In addition, there are several other toughening mechanisms that are present in the composite but are absent in the bulk resin specimen. For example, in the composite, if the interfacial shear strength is stronger than the matrix strength the crack will prefer to go through the weaker resin rather than breaking the stronger fibres. However, because of intermingling of fibres (resulting from high consolidation pressures during processing) and very small thickness between the plies (of the order of one fibre diameter), there is no plane containing only resin. In such a situation the crack must always go around fibres creating a much larger fracture surface area. Moreover, the resistance to crack growth will be increased by the misaligned fibres that may lie in the path of the advancing crack. All these mechanisms contribute to the composite fracture toughness. It has been suggested that the contribution of each of these toughening mechanisms to the composite fracture toughness will be highest for minimum possible thickness of the resin-rich region [26]. The fracture energy calculated for adhesive joints having varying thicknesses of brittle adhesives exhibited no bond thickness effect [27]. It should be noted, however, that the toughening mechanisms discussed above that are believed to be responsible for yielding higher fracture toughness of composites compared to that of the bulk matrix are not present in the adhesive joint test employed by Chai [27].

4.2.3.2. Mode II fracture toughness (ENF tests). The ENF test provides a method for computing the composite interlaminar fracture toughness in a forward shear mode (Mode II) [28–32]. The validity of the ENF test for inducing pure Mode II conditions at the mid-plane of specimen has been established and the effect of friction between the crack faces has been shown to be less than 4% [32]. Unlike the DCB specimens, no "fibre-nesting" was detected during the ENF testings. The average values of G_{IIC} for the three types of composites are listed in Table VIII, and the same values are shown graphically in Fig. 52. The three composite materials having different fibre–matrix ISS, yield significantly different values of the G_{IIC}. The G_{IIC} increases by about 160% for a corresponding increase in the ISS of about 83%. For a

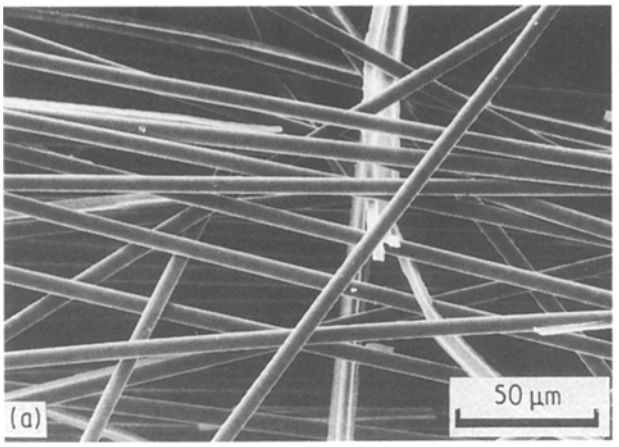

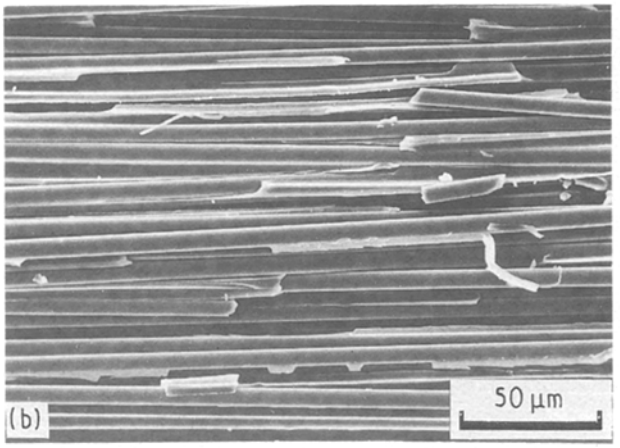

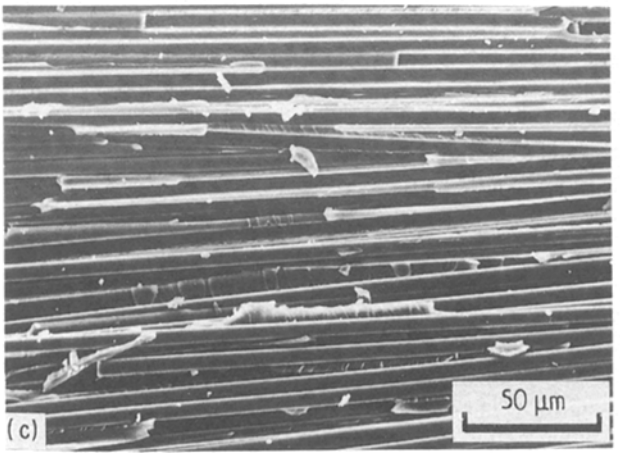

Figure 50 Scanning electron micrographs of DCB specimens showing (a) significant "fibre-nesting" and interfacial failure in AU-4/Epoxy; interfacial and matrix failure, fibre pull-out and fibre breaks in (b) AS-4/Epoxy and (c) AS-4C/Epoxy. The matrix deformation is more dominant in the AS-4C/Epoxy. Graphite/epoxy, $[0]_{24}$.

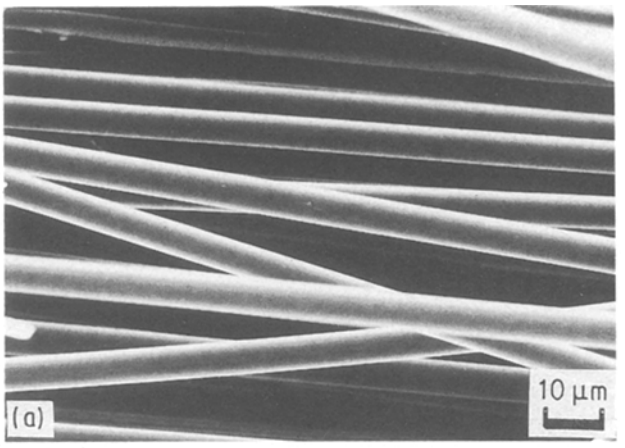

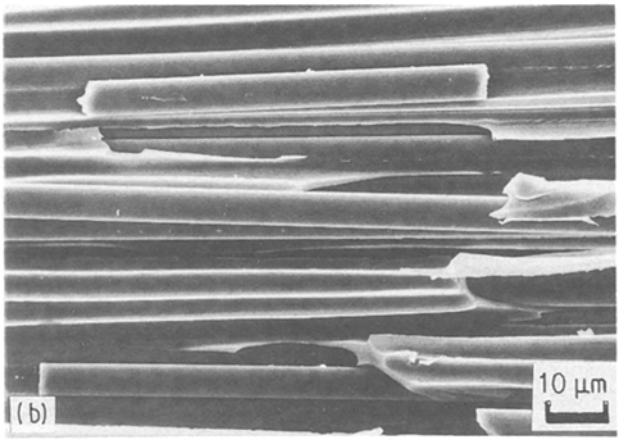

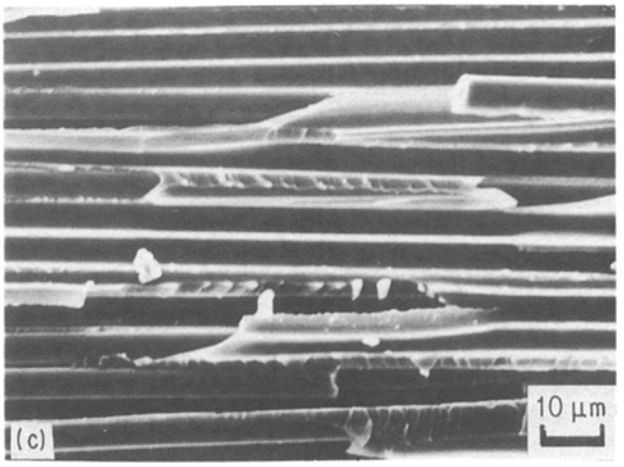

Figure 51 Scanning electron micrographs of DCB specimens showing (a) significant interfacial failure in AU-4/Epoxy; interfacial and matrix failure, fibre pull-out and fibre breaks in (b) AS-4/Epoxy and (c) AS-4C/Epoxy. The matrix deformation and hackle marks in the matrix are more dominant in the AS-4C/Epoxy. Graphite/epoxy, $[0]_{24}$.

further increase in the ISS by about 19%, the G_{IIC} registers additional increase of about 11%. Thus for a total of about 2.2-fold increase in the ISS, the G_{IIC} increased by almost 2.9 times.

The trend in the behaviour of the G_{IIC} is similar to that of the interlaminar shear strength, τ^{f}_{13}, i.e. a large increase in the G_{IIC} and τ^{f}_{13} when the ISS is increased from the low to the intermediate values, and only a moderate increase when the ISS is further increased from the intermediate to the high values. The similarity in the trends of G_{IIC} and τ^{f}_{13} is not surprising considering the similarity of the two test methods and that both of these quantities are calculated at the instant of interlaminar shear failure of composite. However, while there is almost one-to-one correlation between τ^{f}_{13} and the ISS between the low and medium values of the ISS (i.e. for the 1.8-fold increase in the ISS, the τ^{f}_{13} increases by about 1.8 times), the rate of increase in the G_{IIC} with respect to the ISS is almost twice that of the τ^{f}_{13}. This difference in the behaviour of these two quantities is the result of the way they are defined. The τ^{f}_{13} is linearly proportional to P_{max} (the

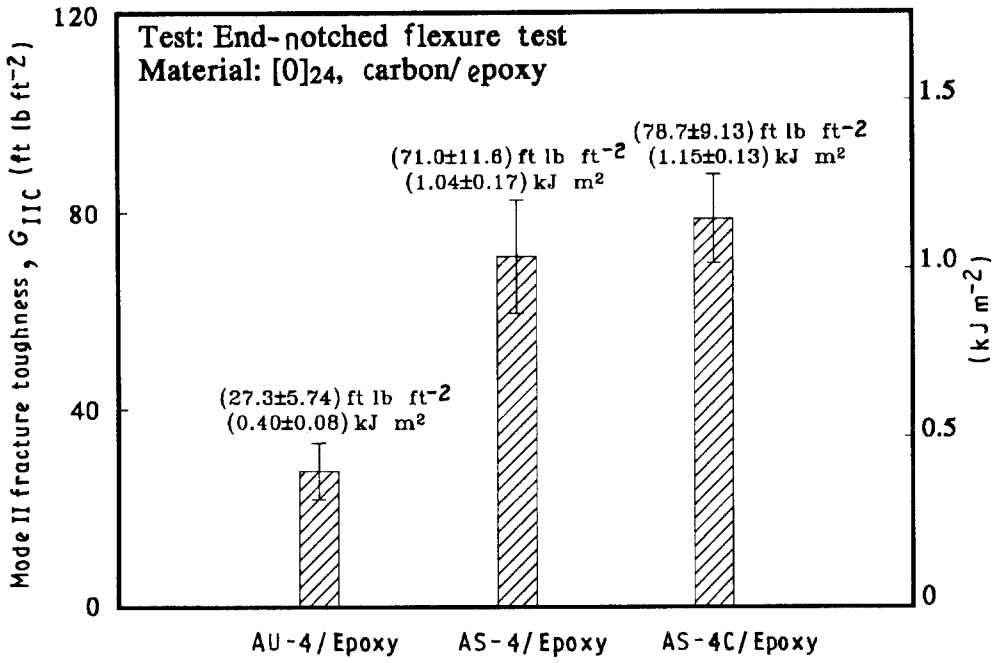

Figure 52 Mode II fracture toughness, G_{IIC}, for the three composite materials. The G_{IIC} is higher for the composite having higher ISS.

load at which interlaminar shear failure occurs in a short-beam shear test), whereas the G_{IIC} is linearly proportional to the square of P_C. Because the critical load P_C, at which the unstable delamination crack growth occurs in the ENF tests, increases with the increase in fibre–matrix adhesion, the G_{IIC} should be expected to increase more rapidly.

When the ISS is increased to the highest level (i.e. in the AS-4C/Epoxy composite), however, the increase in the G_{IIC} is not as significant. As it was mentioned earlier that there are two opposing mechanisms take place in AS-4C/Epoxy composites. The improved fibre–matrix adhesion will tend to increase and the brittle interphase around the AS-4C graphite fibres will tend to reduce the fracture toughness of these composites. In the presence of a stress concentration (such as ahead of the starter crack in the ENF specimens), the effect of the brittle interphase around the graphite fibres should be more significant. Furthermore, almost the full potential of fibre–matrix interface is already utilized in the AS-4/Epoxy composites (i.e. the fibre–matrix ISS approaches matrix shear strength). When the ISS exceeds the matrix shear strength the crack will propagate through the matrix, and thus the G_{IIC} will tend to reach a plateau. These observations will be further clarified by the fracture surface analysis (explained below) of these specimens.

The fracture surfaces of representative specimens from the three groups of composites were examined by SEM. The micrographs of these fracture surfaces are shown in Figs 53 and 54. The fracture surfaces show remarkable differences resulting from the change in fibre–matrix adhesion. The AU-4/Epoxy shows almost entirely interfacial failure. The exposed fibres are completely stripped of matrix material. The fracture surfaces of AS-4/Epoxy and AS-4C/Epoxy are similar, but they are significantly different from the fracture surface of the AU-4/Epoxy. Both the AS-4/Epoxy and AS-4C/Epoxy show extensive matrix failure, a limited interfacial failure, and some fibre pull-out. Because of the increased adhesion between fibre and matrix, the dominant failure mode is matrix deformation rather than interfacial failure. The matrix material also shows zipper-like artefacts in both AS-4/Epoxy and AS-4C/Epoxy which are more pronounced in the former, Fig. 53. These artefacts in the Mode II loading conditions have been suggested to be formed by the coalescence of a series of sigmoidal-shaped microcracks [33]. Fibre pull-out is indicated by the clean matrix channels in both cases. The differences between the fracture surface morphologies of the AS-4/Epoxy and AS-4C/Epoxy are the larger extent of interfacial failure in the former, and the presence of matrix tearing in the latter (seen at the lower right-hand corner of Fig. 54). Also, there is evidence of brittle matrix failure in the AS-4C/Epoxy. This brittle failure may have been initiated in the interphase region. The epoxy matrix in the interphase region that surrounds the AS-4C fibres has lower than the stoichiometric amount of curing agent [15]. The decrease in the amount of curing agent makes the epoxy more brittle and reduces its strain to failure [15, 34]. Therefore, the matrix tearing seen in the fracture surface of the AS-4C/Epoxy may be the result of the failure of the brittle interphase.

In correlating the effect of fibre–matrix adhesion on the G_{IIC} and the observed failure modes, it is shown that by improving the adhesion the primary failure mode changes from interfacial failure to the matrix failure. The work required to cause matrix fracture is significantly larger than that to cause the failure of the interface having low ISS. When the fibre–matrix adhesion is strong, several energy-absorbing phenomena, such as, matrix deformation, matrix cracking, fibre pull-out, interfacial failure, etc., take place. As a result, the G_{IIC} of the composites shows significant improvement when fibre–matrix adhesion is increased. At a certain level when the interfacial strength approaches

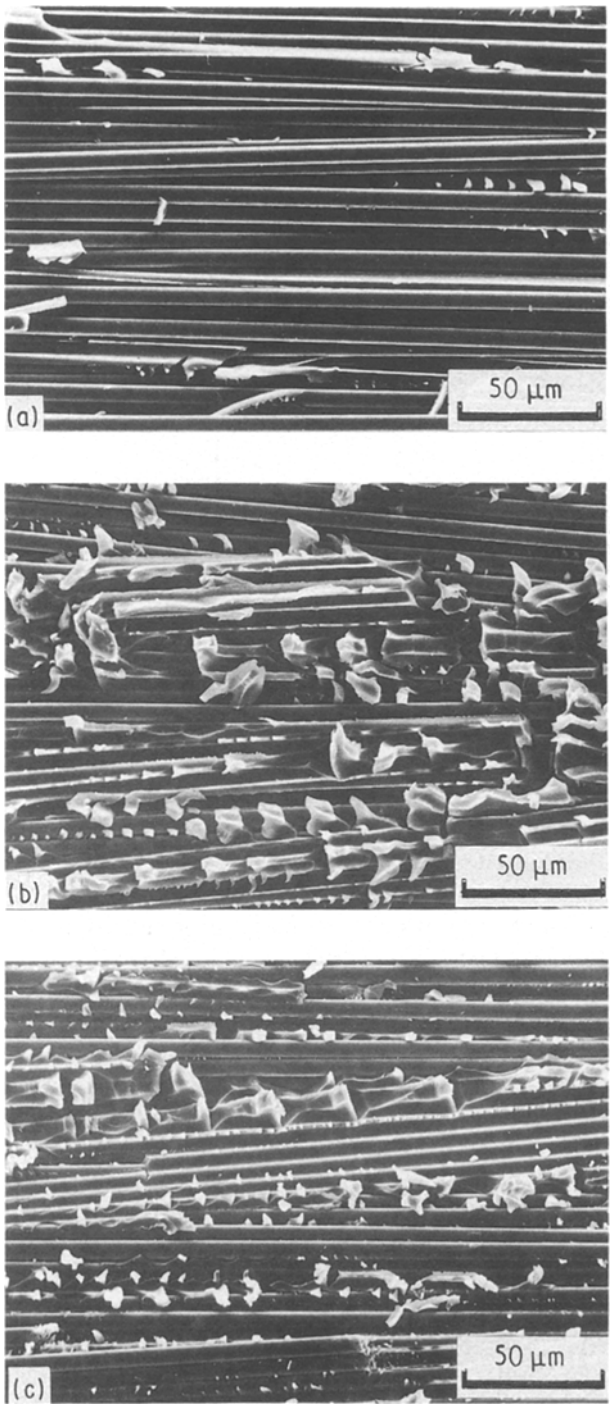

Figure 53 Scanning electron micrographs of ENF specimens showing (a) primarily interfacial failure in AU-4/Epoxy, and significant matrix failure in (b) AS-4/Epoxy and (c) AS-4C/Epoxy. Zipper-like patterns are more evident in the AS-4/Epoxy. Graphite/epoxy, $[0]_{24}$.

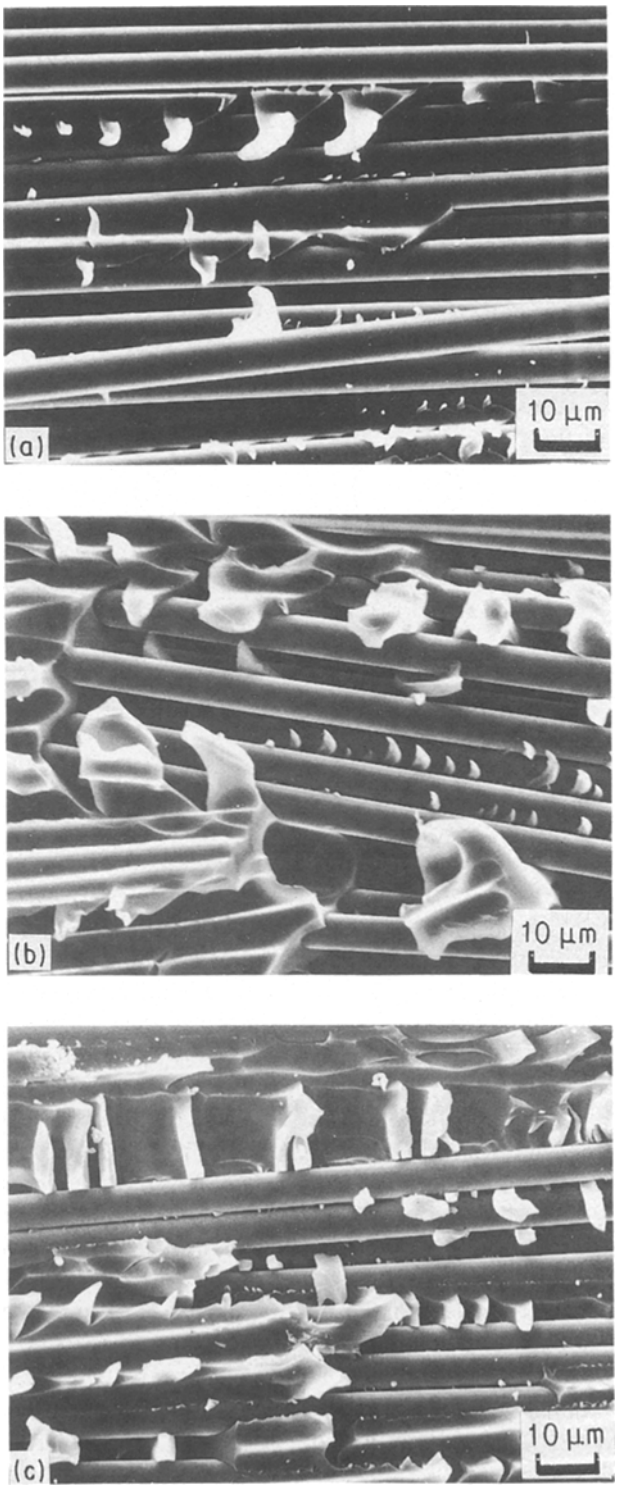

Figure 54 Scanning electron micrographs of ENF specimens showing (a) primarily interfacial failure in AU-4/Epoxy; (b) interfacial and matrix failure in AS-4/Epoxy; and (c) primarily matrix failure, some interfacial failure in AS-4C/Epoxy. Graphite/epoxy, $[0]_{24}$.

the matrix strength, the additional increase in the ISS may not yield much improvement in the fracture toughness of the composite. The similarities in the fracture surface morphologies of the AS-4/Epoxy and AS-4C/Epoxy suggest that almost the full potential of the interface has already been realized in the AS-4/Epoxy composites. Therefore, the percentage increase in the G_{IIC} corresponding the increase in the ISS from the medium to the highest levels is much smaller than that corresponding to the increase in the ISS from the low to the medium levels. The brittle matrix failure that was believed to be due to the presence of the brittle interphase around the AS-4C fibres may have also cancelled part of the gain in the G_{IIC} resulting from the increase in fibre–matrix adhesion.

Finally, a comparison between the G_{IC} and G_{IIC} for the three material systems is shown in Fig. 55. The G_{IC} for the AU-4/Epoxy composite could not be determined because of the extensive "fibre-nesting" and non-self-similar crack propagation. For the other two composite systems, the G_{IIC} values are about three times higher than the G_{IC}. Similar ratios of G_{IIC}/G_{IC}

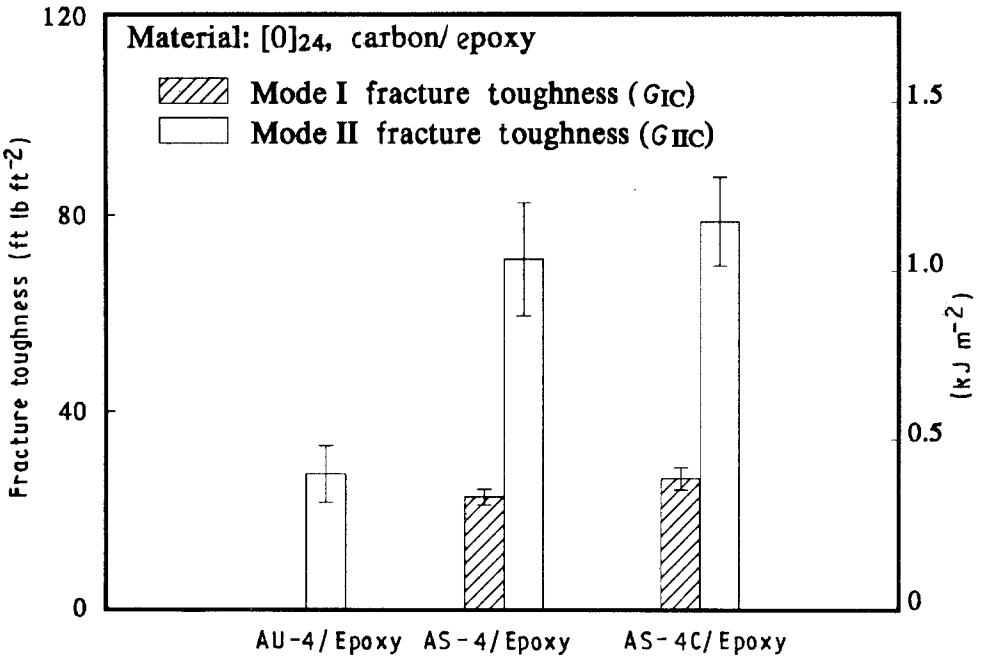

Figure 55 Comparison between the Mode I and Mode II fracture toughness of the three composite materials. The Mode II fracture toughness is about three times higher than the Mode I fracture toughness.

for composites having brittle epoxy matrices have also been reported for a variety of graphite/epoxy systems [22, 33]. The reason for the lower G_{IC} compared to the G_{IIC} is attributed to the inability of the unmodified brittle epoxies to undergo volume expansion (dilatation) under the plane strain tensile loading conditions that exist ahead of the crack-tip in the DCB test [35]. Because the polymer need not dilate under the shear deformation of Mode II loading, a highly cross-linked brittle epoxy may have a much higher Mode II toughness than Mode I toughness.

5. Conclusions

As a result of this study, the following conclusions can be drawn.

The embedded single-fibre fragmentation test has been shown to be both a predictor of changes in composite properties brought about by changes in fibre–matrix adhesion and a useful research tool which not only quantitatively measures fibre–matrix interfacial shear strength but also identifies failure modes.

Comparison between results from the single-fibre and composite tests indicate that two key parameters must be obtained from single-fibre tests in order to explain composite property data. They are the level of adhesion and the failure mode, i.e. interfacial or matrix.

Fibre–matrix adhesion affects composite properties in different ways depending on the state of stress created at the fibre–matrix interphase.

1. On-axis properties

(a) Composite 0° tensile strength. The tensile strength increases with increasing interfacial shear strength only as long as the failure is interfacial. If the interfacial strength is too weak, the composite fails prematurely because of cumulative weakening of the material. When interfacial bond strength is excessive, the failure mode changes from interfacial to matrix and the composite behaves like a brittle material, i.e. it becomes "notch-sensitive" which may have a detrimental effect on the longitudinal tensile strength of the composite.

(b) Composite 0° compressive strength. Increasing fibre–matrix adhesion increases composite compressive strength by increasing the load necessary to cause transverse tensile failure of the interface due to Poisson's effect. Delamination failure is reduced in favour of microbuckling of fibres. Further increase in the adhesion yields more rapid increase in the compressive strength. Three sources are believed to be contributing to this rapid increase in the compressive strength, namely (i) high adhesion prevents local microbuckling, (ii) the presence of the brittle interphase provides additional lateral support to the graphite fibres, and (iii) high transverse strength prevents local delamination resulting from Poisson's effect.

(c) Composite 0° flexural strength. There was little change in the longitudinal flexural properties when the ISS was increased from the low to the intermediate values. Improvement was noticed in both the flexural stiffness and strength when the ISS was increased from the intermediate to the highest levels due to the presence of the high modulus interphase and its ability to suppress the interlaminar failure.

2. Off-axis properties

(a) Composite 90° transverse tensile and flexural strength. The transverse tensile strength increases with increasing fibre–matrix adhesion. The transverse flexural test results indicate that fibre–matrix adhesion has a stronger influence on the transverse flexural strength than on the transverse tensile strength. The

transverse flexural strength can be a very sensitive indicator of the interfacial strength.

(b) Composite in-plane shear strength. For a proper interpretation of the in-plane shear strength data from any of the three test methods, an understanding of the fibre–matrix adhesion level and the interfacial failure modes is essential. The Iosipescu method showed the least scatter and tracked changes in fibre–matrix adhesion. The $\pm 45°$ specimen also tracked changes in fibre–matrix adhesion. For the highest levels of adhesion with matrix-dominated failure, the $\pm 45°$ specimen showed a greater value than the Iosipescu specimen because of the lack of sensitivity to matrix cracking. The short-beam shear specimen also paralleled the single-fibre results as long as the failure mode was interfacial. At high levels of adhesion with matrix failure the specimen failed prematurely under these matrix dominated conditions.

(c) Composite fracture properties. The dominant micromechanical event responsible for the increased Mode I fracture toughness is increased matrix deformation resulting from the improved fibre–matrix adhesion. Even the low fracture toughness interphase surrounding the AS-4C fibres increases the composite fracture toughness as a result of improved adhesion.

The effect of fibre–matrix adhesion on the G_{IIC} and the observed failure modes is shown to be a primary failure mode change from interfacial failure to the matrix failure. When the interfacial strength approaches the matrix strength, the additional increase in the ISS may not yield much improvement in the fracture toughness of the composite.

References

1. L. T. DRZAL and P. J. HERRERA-FRANCO, "Composite Fiber–Matrix Bond Tests", "Engineered Materials Handbook: Adhesives and Sealants", Vol. 3 (ASM International, Metals Park, OH, 1990).
2. B. MILLER, P. MURI and L. REBENFIELD, *Compos. Sci. Technol.* **28** (1987) 17.
3. M. NARKIS, E. J. H. CHEN, and R. B. PIPES, *Polym. Compos.* **9** (1988) 245.
4. A. KELLY, and W. R. TYSON, *J. Mech. Phys. Solids* **13** (1965) 329.
5. A. N. NETRAVALI, L. T. T. TOPOLESKI, W. H. SACHSE and S. L. PHOENIX, *Compos. Sci. Technol.* **35** (1989) 13.
6. D. L. CALDWELL, and F. M. CORTEZ, *Modern Plastics* September (1988) 132.
7. "Engineered Materials Handbook: Composites", Vol. 1 (ASM International, Metals Park, OH, 1988).
8. L. B. DONNET and R. C. BANSAL, "Carbon Fibers" (Marcel Dekker, New York, 1984).
9. M. C. WATERBURY and L. T. DRZAL, *J. Rein. Plast. Compos.* **8** (1989) 627.
10. C. ZWEBEN, W. S. SMITH and M. W. WARDLE, in "Composite Materials Testing and Design" (Fifth Conference), ASTM STP 674, edited by S. W. Tsai, (American Society for Testing and Materials, Philadelphia, PA, 1979) pp. 228–62.
11. D. F. ADAMS and D. E. WALRATH, "Composite Materials Testing and Design" (Sixth Conference), ASTM STP 787, edited by I. M. Daniel (American Society for Testing and Materials, Philadelphia, PA, 1982) pp. 19–33.
12. L. A. CARLSSON and R. B. PIPES, "Experimental Characterization of Composite Materials" (Prentice Hall, Englewood Cliffs, NJ 1987).
13. L. T. DRZAL and M. J. RICH, "Effect of Graphite Fibre-Epoxy Adhesion on Composite Fracture Behavior", Research Advances in Composites in the United States and Japan, ASTM STP 864 (American Society for Testing and Materials, Philadelphia, PA, 1985) pp 16–26.
14. L. T. DRZAL, *SAMPE J.* **19** (1983) 7.
15. L. T. DRZAL, M. J. RICH, M. F. KOENIG, and P. F. LLOYD, *J. Adhesion* **16** (1983) 133.
16. K. HOOK, R. AGRAWAL, and L. T. DRZAL, *J. Adhesion*, **32** (1990) 157.
17. J. D. H. HUGHES, *Carbon* **24** (1986) 551.
18. M. S. DRESSELHAUS, G. DRESSELHAUS, K. SUGIHARA, I. L. SPAIN and H. A. GOLDBERG, "Graphite Fibers and Filaments", Springer Series in Materials Science, edited by M. Cardona, (1988) Ch. 6, pp. 120–48.
19. R. M. JONES, "Mechanics of Composite Materials" (McGraw-Hill, New York, 1975).
20. H. T. HAHN and M. M. SOHI *Compos. Sci. Technol.* **27** (1986) 25.
21. P. YEUNG and L. J. BROUTMAN, *Polym. Engng Sci.* **18** (1978) 62.
22. N. SELA and O. ISHAI, *Composites* **20** (1989) 423.
23. W. D. BASCOM, D. J. BOLL, D. L. HUNSTON, B. FULLER and P. J. PHILLIPS, "Fractographic Analysis of Interlaminar Fracture", in "Toughened Composites", ASTM STP 937, edited by N. J. Johnston (American Society for Testing and Materials, Philadelphia, PA, 1987) pp. 131–49.
24. D. L. HUNSTON, R. J. MOULTON, N. J. JOHNSTON and W. D. BASCOM, "Matrix Resin Effects in Composite Delamination Mode I Fracture Aspects", *ibid.*, pp. 74–94.
25. A. J. RUSSELL and K. N. STREET, "The Effect of Matrix Toughness on Delamination Static and Fatigue Fracture Under Mode II Shear Loading of Graphite Fiber Composites", *ibid.* pp. 275–94.
26. W. L. BRADLEY and R. N. COHEN, "Matrix Deformation and Fracture in Graphite-Reinforced Epoxies", in Delamination and Debonding of Materials, ASTM STP 876, edited by W. S. Johnson (American Society for Testing and Materials, Philadelphia, PA, 1985) pp. 389–410.
27. H. CHAI, *Engng Fract. Mech.* **24** (1986) 413.
28. A. J. RUSSELL and K. N. STREET, "Moisture and Temperature Effects on the Mixed Mode Delamination Fracture of Graphite/Epoxy", in Delamination and Debonding of Materials, ASTM STP 876, edited by W. S. Johnson (American Society for Testing and Materials, Philadelphia, PA, 1985) pp. 349–70.
29. A. J. SMILEY and R. B. PIPES, in "Proceedings of the American Society for Composites, First Technical Conference", Dayton, OH (Technomic, Lancaster, PA, 1986) pp. 439–49.
30. H. CHAI, in "Proceedings of the American Society for Composites, Fourth Technical Conference", Blacksburg, VA (Technomic, Lancaster, PA, 1989) pp. 815–25.
31. W. M. JORDAN, in "Proceedings of the American Society for Composites, Third Technical Conference", Seattle, WA (Technomic, Lancaster, PA, 1988) pp. 495–504.
32. L. A. CARLSSON, J. W. GILLESPIE and R. B. PIPES, *J. Compos. Mater.* **20** (1986) 594.
33. W. M. JORDAN and W. L. BRADLEY, "Micromechanisms of Fracture in Toughened Graphite-Epoxy Laminates", in Toughened Composites, ASTM STP 937, edited by N. J. Johnston (American Society for Testing and Materials, Philadelphia, PA, 1987) pp. 95–114.
34. V. B. GUPTA, L. T. DRZAL, C. Y. C. LEE and M. J. RICH, *J. Macromol. Sci. Phys.* **B23** (1985) 435.
35. W. S. JOHNSON and P. D. MANGALGIRI, "Influence of the Resin on Interlaminar Mixed-Mode Fracture", in Toughened Composites, ASTM STP 937, edited by N. J. Johnston (American Society for Testing and Materials, Philadelphia, PA, 1987) pp. 295–315.

Received 16 January
and accepted 17 October 1991